Paleoceanographic Reconstruction of Nitrate Consumption in the Atlantic Ocean

Lukas Oesch

Dissertation ETH No: 24175

DISS. ETH NO. 24175

PALEOCEANOGRAPHIC RECONSTRUCTION OF NITRATE CONSUMPTION IN THE ATLANTIC OCEAN USING FORAMINIFERA-BOUND NITROGEN ISOTOPES

A thesis submitted to attain the degree of

DOCTOR OF SCIENCES of ETH ZÜRICH

(Dr. Sc. ETH Zürich)

presented by

LUKAS EMANUEL OESCH

MSc ETH in Atmospheric and Climate Sciences, ETH Zürich

born on 09.08.1984

citizen of Oberlangenegg (BE)

accepted on the recommendation of

Prof. Dr. Gerald H. Haug	– ETH Zürich	– examiner
Prof. Dr. Daniel M. Sigman	– Princeton University	– co-examiner
Prof. Dr. Timothy I. Eglinton	– ETH Zürich	– co-examiner
Prof. Dr. Peter B. de Menocal	– Columbia University	– co-examiner

2017

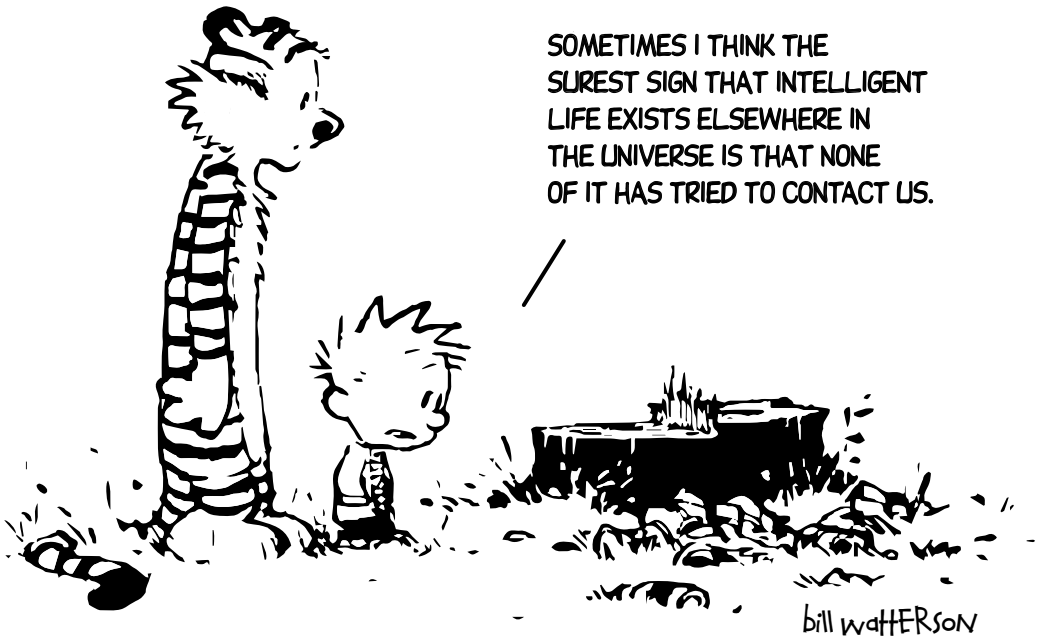
SOMETIMES I THINK THE SUREST SIGN THAT INTELLIGENT LIFE EXISTS ELSEWHERE IN THE UNIVERSE IS THAT NONE OF IT HAS TRIED TO CONTACT US.
bill watterson

Abstract

Within the last few decades, evidences emerged that the marine biological production is one of the factors controlling Earth's climate. Changes in the efficiency of the marine biological pump are able to alter the interaction between the large deep ocean carbon reservoir and the atmosphere, affecting the climate within the past 2.7 Million years. With respect to the current anthropogenic CO_2 emissions and its implications on the global climate, it is vital to understand the nature of such climate transitions. Studying the nutrient cycling in the oceans and its link to the carbon cycle helps to improve the understanding of feedback effects and dynamic processes in a rapidly changing biogeochemical system.

Biological available nitrogen, the limiting nutrient in vast parts of the surface ocean, features substantial variations in the net-budget and internal cycling during Earth's recent past. In this thesis, the sedimentary archives of planktonic foraminifera and deep-sea corals are used to reconstruct changes in the ratio of stable nitrogen isotopes (δ^{15}N) of thermocline nitrate in the Atlantic. The processes affecting the nitrate δ^{15}N include preferred assimilation of the lighter isotope by phytoplankton in regions with incomplete nutrient consumption. Thus, the assessment of δ^{15}N reveals information about the efficiency of carbon sequestration by the biological pump.

The aim of this thesis is to reconstruct nutrient cycling in the Atlantic high productive regions and to assess the high latitude influence on low latitude biogeochemistry. For this, foraminifera-bound δ^{15}N was measured on the sediment of the tropical Atlantic core ODP 662 throughout the last two glacial cycles (160 kyr BP - today) and around the Plio-Pleistocene transition (2.9 - 2.4 Myr BP). Further, deep-sea coral-bound δ^{15}N (CB-δ^{15}N) was measured on corals from the Reykjanes Ridge located on a transect through the North Atlantic Subpolar Gyre.

We found that the nitrate regime in the low latitude Atlantic of the last two glacial cycles was substantially different than across the Plio-Pleistocene transition. Thermocline nitrate δ^{15}N during the last 160 kyr was mainly influenced by nutrient cycling processes in the Southern Ocean. The proposed mechanism shows that low latitude nitrate δ^{15}N is most likely governed by an interaction between the preformed nitrate δ^{15}N and the nitrate concentration within Subantarctic Mode Water. In the course of the Plio-Pleistocene transition we observe an onset of 41 kyr cycles in FB-δ^{15}N at 2.65 Myr BP, paced by Earth's obliquity. The FB-δ^{15}N cycles are interpreted as periods with incomplete nitrate consumption in the equatorial Atlantic coinciding with very high productivity, which indicates that the nutrient supply to Site 662 was greatly enhanced compared to modern values. Further, we explain the generally lower δ^{15}N during the early Pleistocene to result from the lower Southern Ocean productivity during this time.

The CB-δ^{15}N data from the North Atlantic reflect well the predicted δ^{15}N export through the area of incomplete nitrate consumption within the Subpolar Gyre. They confirm the potential of CB-δ^{15}N to be used as a proxy for the level of surface nitrate consumption. According to our observations, it is possible to reconstruct the position of the Subpolar Gyre in the course of the North Atlantic Oscillation by the means of CB-δ^{15} throughout the Holocene.

The results of this thesis reveal the high degree of interdependences between the different latitudes. Low latitude nitrogen cycling in the Atlantic is highly linked to the Southern Ocean through the northwards flow of Subantarctic Mode Water. With regard to the known extent of Subantarctic Mode Water on nearly the entire global intermediate depths, possible teleconnections to equatorial upwelling systems in the Pacific and coastal upwelling systems off South America and Africa emerge.

Zusammenfassung

In den letzten Jahrzehnten verdichteten sich die Hinweise darauf, dass Nährstoffkreisläufe einen erheblichen Einfluss auf die Zusammensetzung der Atmosphäre und das globale Klima der letzten 3 Mio. Jahre hatten. Die Effizienz, mit der die biologische Primärproduktion CO_2 aus der Atmosphäre bindet und in die Tiefsee transportiert, ist hauptverantwortlich für die eiszeitlichen Schwankungen der CO_2 Konzentration in der Atmosphäre. Im Hinblick auf die aktuellen anthropogenen CO_2 Emissionen und deren Auswirkungen auf das Klima, ist es von grossem Interesse dieses System und dessen Rückkopplungsmechanismen zwischen dem marinen Nährstoffkreislauf und dem Kohlenstoffkreislauf zu untersuchen um die dynamischen Prozessen in einem sich schnell verändernden biogeochemischen System zu verstehen.

Biologisch verfügbarer Stickstoff ist in grossen Teilen des Ozeans der limitierende Nährstoff. Die Zu- und Abnahme dieser Stickstoffwerte sowie die Prozesse dieses Kreislaufs können durch die Analyse des Verhältnisses zwischen den stabilen Isotopen (δ^{15}N) rekonstruiert werden. Die direkte δ^{15}N Messung im Sediment wird jedoch erschwert durch terrigenes Material und diagenetische Prozesse, welche das δ^{15}N im Sediment beeinflussen können. Die vorliegende Arbeit untersucht das δ^{15}N von organischer Materie, welche in den Kalkschalen von planktischen Foraminiferen eingebaut wurde (Foraminifera-Bound δ^{15}N, δ^{15}N) und hermetisch versiegelt am Meeresboden sedimentierte. Weiter haben wir δ^{15}N an organischer Materie gemessen, welche in die Skelettstruktur von Tiefseekorallen eingelagert wurde. Das Ziel dieser Arbeit ist es, den Nährstoffkreislauf in der Region der atlantischen äquatorialen Auftriebsregion zu untersuchen und den Einfluss des subpolaren und polaren biologischen Systems auf die Tropen zu bestimmen. Wir haben für die letzten zwei Glazialzyklen (160'000 Jahre vor Heute) und während des Plio-Pleistozän Übergangs (2.9 - 2.4 Millionen Jahre) FB-δ^{15}N im Sediment des tropischen atlantischen Bohrkerns ODP662 gemessen. Des Weitern wurde Coral-Bound δ^{15}N (CB-δ^{15}N) an 43 Tiefseekorallen auf dem Reykjanes-Ridge südlich von Island auf einem Transekt durch den subpolaren Wirbel gemessen, um so die Nutzung von Tiefseekorallen zur Rekonstruktion der kurzzeitigen Schwankungen (10-100 Jahre) der biologischen Produktion an der Oberfläche zu validieren.

Unsere Resultate zeigen, dass das Nitrat-Regime im tropischen Atlantik in den letzten 160'000 Jahre signifikant variiert hat vom Regime während des Plio-Pleistozän-Übergangs. Während der letzten zwei Glazialzyklen wurde das topische thermokline Nitrat δ^{15}N vor allem durch Prozesse im südlichen Ozean bestimmt und durch das Subantarctic Mode Water in die Tropen transportiert. Im Laufe des Plio-Pleistozän-Übergangs konnte das Einsetzen von FB-δ^{15}N-Zyklen mit der Periodizität von 41'000 Jahre beobachtet werden, welche der bekannten orbitalen Variation der Schiefe der Erdachse folgen. Die tiefen FB-δ^{15}N-Werte in Zeiten hoher Primärproduktion interpretieren wir als Perioden mit unvollständigem Nitratverbrauch im äquatorialen Atlantik. Dies belegt, dass die Nährstoffversorgung im Vergleich zu heute stark erhöht war. Die CB-δ^{15}N-Daten aus dem Nordatlantik widerspiegeln den prognostizierten δ^{15}N-Export in den Gebieten mit unvollständigem Nitratverbrauch innerhalb des subpolaren Wirbel. Es zeigte sich, dass CB-δ^{15}N eine geeignete Methode darstellt, um die Position des subpolaren Wirbel und somit des Zustand der Nordatlantischen Oszillation während des Holozäns zu rekonstruieren.

Contents

List of Abbreviations

[NO_3^-] Nitrate Concentration.
Gsacc *Globigerinoides sacculifer*.
Ndut *Neogloboquadrina dutertrei*.

AABW Antarctic Bottom Water.
AMOC Atlantic Overturning Circulation.
AZ Antarctic Zone.

CB-δ^{15}N coral-bound δ^{15}N.

DB-δ^{15}N diatom-bound δ^{15}N.

EEA Eastern Equatorial Atlantic.
EEP Eastern Equatorial Pacific.
ENSO El Niño Southern Oscillation.

FB-δ^{15}N foraminifera-bound δ^{15}N.

GNAIW Glacial North Atlantic Intermediate Water.

ITCZ Inter Tropical Convergence Zone.

LGM Last Glacial Maximum.

MAR Mass Accumulation Rate.
MIS Marine Isotope Stage.
Myr BP Million years Before Present.

NADW North Atlantic Deep Water.
NAO North Atlantic Oscillation.
NHG Northern Hemisphere Glaciation.

ODP Ocean Drilling Program.
OM organic matter.

POM particulate organic matter.
PON particulate organic Nitrogen.

SAMW Subantarctic Mode Water.
SAZ Subantarctic Zone.
SO Southern Ocean.
SPG Subpolar Gyre.
SPNA Subpolar North Atlantic.
SST Sea Surface Temperatures.

WOA13 World Ocean Atlas 2013.

List of Figures

List of Tables

1 Introduction

Lukas E. Oesch[1]

[1]Geological Institute, Department of Earth Sciences, ETH Zürich, Zürich, Switzerland

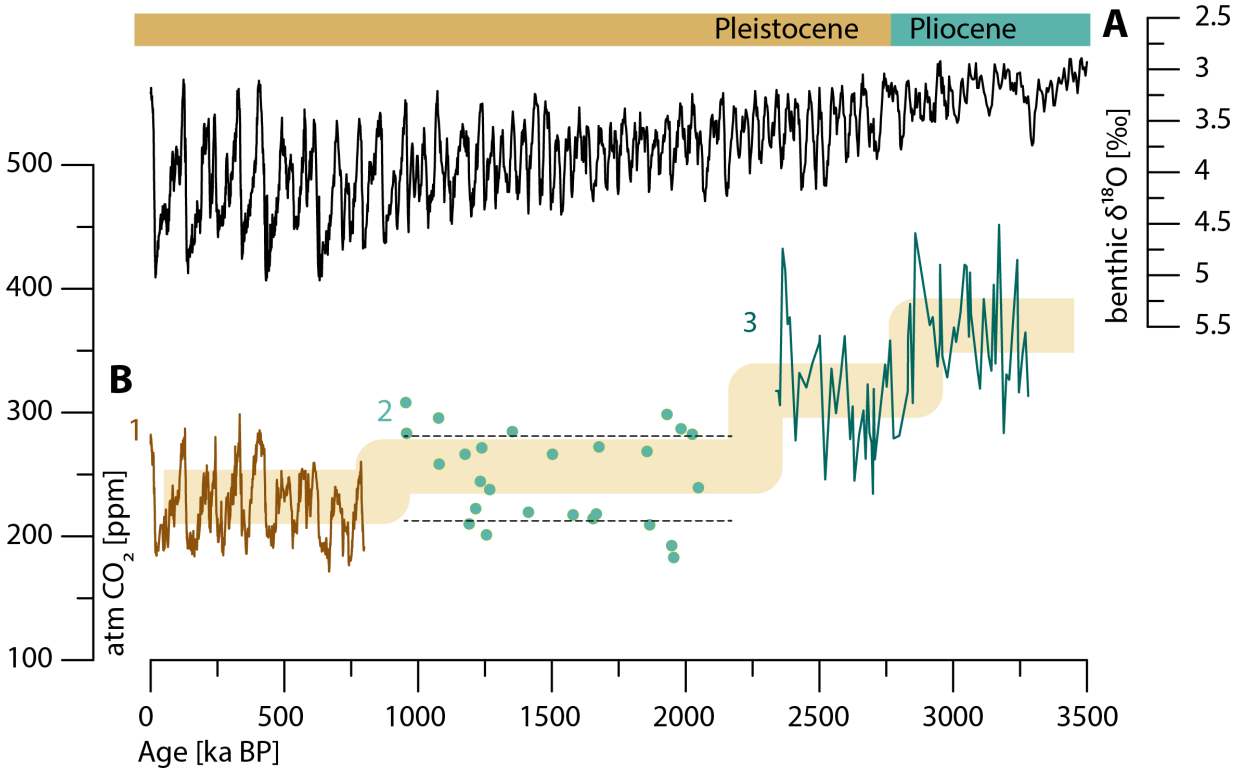

Figure 1.1 – ***Glacial cycles and atmospheric CO_2 during the last 3.5 Myr- A:*** *Benthic $\delta^{18}O$ stack (Lisiecki and Raymo, 2005) as a proxy for global ice volume and temperature features glacial-interglacial cycles with increasing amplitude towards present -* ***B:*** *Atmospheric CO_2 [ppm] from 1. air trapped in polar ice, EPICA Dome C ice core (Jouzel et al., 2007), 2. Boron isotopes measured on planktonic foraminifera from ODP662 with estimated glacial-interglacial boundaries (dashed) (Hönisch et al., 2009), and 3. Boron isotopes measured on planktonic foraminifera from ODP662 and ODP999 (Martínez-Botí et al., 2015). Ice core CO_2 is a direct measurement in air-trapped in bubbles, whereas boron isotopes serve as a proxy to estimate atmospheric CO_2.*

1.1 Atmospheric CO_2 and glacial cycles

The climate during Earth's recent history was dominated by cyclic climate changes that alternated between warm interglacials and cold glacials with gradually increasing amplitudes towards present (Fig. 1.1A) (Lisiecki and Raymo, 2005). For half a century, the scientific community seeked to understand the detailed mechanisms leading to those cyclic climate changes. A pervasive global change like a glacial-interglacial cycle with simultaneous effect on different latitudes asks for a global forcing mechanism. The apparent coherence of the ice age cycles with changes in solar insolation due to variations in Earth's orbit was recognized early in the scientific process (Hays et al., 1976). Around the Plio-Pleistocene transition at 2.7 Million years Before Present (Myr BP), the 41 kyr cycle of Earth's obliquity started pacing glacial cycles. During the Mid-Pleistocene transition, this period changed to 100 kyr following the eccentricity of Earth's orbit. Yet orbital parameters failed to fully explain the nature of ice-ages alone, mainly due to the variations in insolation being very small (max. $\pm 2-5 W/m^2$) (Berger and Loutre, 1991). Nevertheless, the temporal coherence of the ice ages and the orbital parameters are significant. Therefore, it is thought that the small changes in insolation trigger feedback mechanisms within the biogeochemical system, which lead to altered radiative forcing through variable green house gas concentrations (Imbrie, 1982).

Ongoing research within the last decades developed several methods to reconstruct past atmospheric CO_2

concentrations (Fig. 1.1B). We observe a step-wise decrease of atmospheric CO_2 leading from the warm Pliocene (Fig. 1.1B3) to the 41 kyr-world of the early to mid Pleistocene (Fig. 1.1B2) and the 100 kyr cycles of the last 800 kyr (Fig. 1.1B1). Air bubbles trapped in Antarctic ice cores revealed the most recent and detailed history (up to 800 kyr) of CO_2 concentrations. During this period the atmospheric partial pressure of CO_2 correlates closely to the global mean temperature (Petit et al., 1999; Jouzel et al., 2007; Lüthi et al., 2008). The observed difference of $\approx$ 100ppm between glacial and interglacial atmospheric CO_2 suits well to explain a significant part of the observed temperature change (Siegenthaler and Wenk, 1984), although the enhancing feedback mechanisms are not yet understood. The excess CO_2 that is observed to suddenly appear at the glacial terminations and to continuously vanish during the glacials is thought to be outgassed and reabsorbed by the deep ocean. Broecker (1982) showed that the deep ocean is the only carbon reservoir that is large enough and equilibrates with the atmosphere on an appropriate timescale[1]. Although CO_2 is water soluble, the processes involved in the absorption and release of carbon from and to the deep ocean, proved to be more complex than simple solution and diffusion. In vast parts of the ocean, the CO_2 saturated surface layer is separated from the deep ocean by a strong thermocline, which prevents vertical diffusion or convection of dissolved CO_2. The big reservoir of the deep ocean is therefore capped and atmospheric CO_2 is not able to diffuse directly. An auspicious explanation for the rapid carbon exchange is to pump the carbon into the deep ocean by biological production, the so called biological pump (Sarmiento and Toggweiler, 1984; Knox and McElroy, 1984; Siegenthaler and Wenk, 1984). Changes in the amount of carbon sequestered by the biological pump are thought to alter the atmospheric CO_2 concentration in the range and time needed for a glacial-interglacial change (Sigman et al., 2010).

1.1.1 The biological pump

In the sunlit surface layer of the ocean, phytoplankton produces organic matter using photosynthesis. This binds dissolved inorganic carbon from the surface layer to particulate organic matter and reduces the concentration of CO_2 in the surface layer. The organic matter subsequently sinks into the deep ocean, where it is remineralized to DIC again. This way, deep water is continuously enriched in dissolved CO_2 and remineralized nutrients. In the upwelling regions at the ocean margins, the equatorial divergence zone and in the Southern Ocean (SO) upwelling zones, the CO_2 charged deep water is physically brought to the surface. If it were not for the biological production, the higher CO_2 concentration of the exposed deep water would equilibrate with the atmosphere and excess CO_2 would be emitted. Since the upwelled deepwater has a high nutrient concentration, biological production is induced and consumes the excess CO_2. The organic matter that is produced subsequently sinks into the ocean interior and is remineralized back into dissolved CO_2 and nutrients. In polar regions with incomplete nutrient consumption (due to iron and/or light limitation), the biological production is not able to consume all the nutrients before the water descends again into the oceans interior (Studer et al., 2015; Martínez-Garcia et al., 2014). In this situation, the excess CO_2 brought to the surface exceeds the respired carbon, which leads to a net emission of CO_2 to the atmosphere.

The level of nutrient consumption in the surface is therefore essentially important for the efficiency of the biological pump. Counterintuitively, the amount of organic matter exported to the subsurface does not determine the extent of carbon sequestration alone. As described above the ratio between the CO_2 used for biological production and the respired CO_2 coming from the deep ocean defines whether CO_2 is net emitted or sequestered. If the nutrient supply is higher than the amount of nutrients needed by the production until the water descends again into the deep ocean, the nutrient consumption is not complete. In this case, the biological production did not bind as much carbon as the nutrient supply would allow for and the opportunity to sequester carbon is missed.

[1] deep ocean carbon $\approx$ 37000 PgC (Ciais et al., 2013)

Equation 1.1 describes the relationship between biological productivity (P), nutrient consumption (C) and the supply of the main nutrients (S). The supply is determined by the physical supply of water to the locus of production and its nutrient concentration. The productivity describes the amount of organic matter being produced, which is proportional to the amount of nutrients consumed. Therefore, the nutrient consumption is the ratio between the actual consumed and the supplied nutrients.

$$C = \frac{P}{S} \tag{1.1}$$

In situations with $C = 1$, the consumption is complete and the water is depleted in nutrients. Whereas at locations with $C < 1$ the supply of the major nutrients exceeds the capability of the biological system and the nutrients are only partially consumed. Whether the biological pump efficiently sequesters carbon out of the surface layer into the deep ocean, depends not only on the level of nutrient consumption in the surface layer. The possibility for the unused nutrients to reenter the deep ocean is essential as well. As described further down (Sec. 1.1.2) in vast part of the ocean the surface water is warmer and thus lighter than the deep water. In those regions, unused nutrients are not able to reenter the subsurface right away. They are transported on the surface towards the polar regions and eventually all consumed. Only in the polar regions where the density gradient is weak, an opportunity for deep water formation is given.

Therefore the ratio of unused (preformed) nutrients relative to regenerated (biologically derived) nutrients leaving the ocean's surface describes the efficiency of the biological pump (Sigman and Boyle, 2000).

1.1.2 Atlantic oceanography

The Atlantic oceanography influences the global climate on many levels. It dominates the global meridional circulation (de Boer et al., 2008; Rhein et al., 2013) and its water circulation impacts the energy distribution within the climate system, the global biogeochemical cycles by nutrient distribution, and the composition of the atmosphere from glacial-interglacial- down to decadal timescales (Rhein et al., 2011; Schuster and Watson, 2007; Hurrell et al., 2010; Elmore and Wright, 2011; Kohfeld et al., 2005)

Water density in the Atlantic

The deep circulation is mainly influenced by density differences. The density in turn is controlled by the salinity and the temperature (Winton, 1997; Wang et al., 2002; Sigman et al., 2004). According to the Thermodynamic Equation of Seawater (TEOS-10)(IOC et al., 2010) the density of warm water is dominantly controlled by temperature. When the temperature of the water approaches the freezing point, the temperature control on the density decreases and the influence of salinity dominates the density (Fig. 1.2). Applied to the Atlantic Ocean, this explains one of the main difference between low- and high latitude water masses. The majority of the Atlantic basin (low-to midlatitudes) is characterized by a strong thermocline that divides the uppermost surface water from the deep ocean. Surface warming leads to a stable stratification of the ocean with warm, light water on the top and cold dense water in the abyss (Fig. 1.2A). In the polar regions of both hemispheres, the density gradient between deep water and surface is vanishing or even inverted. An instable watercolumn with heavier water on top of lighter water allows for vertical convection and deep water formation (Fig. 1.2B). Hereby, the polar and subpolar ocean basins connect the deep water with the surface layer and the atmosphere and thus play a crucial role for the biological pump.

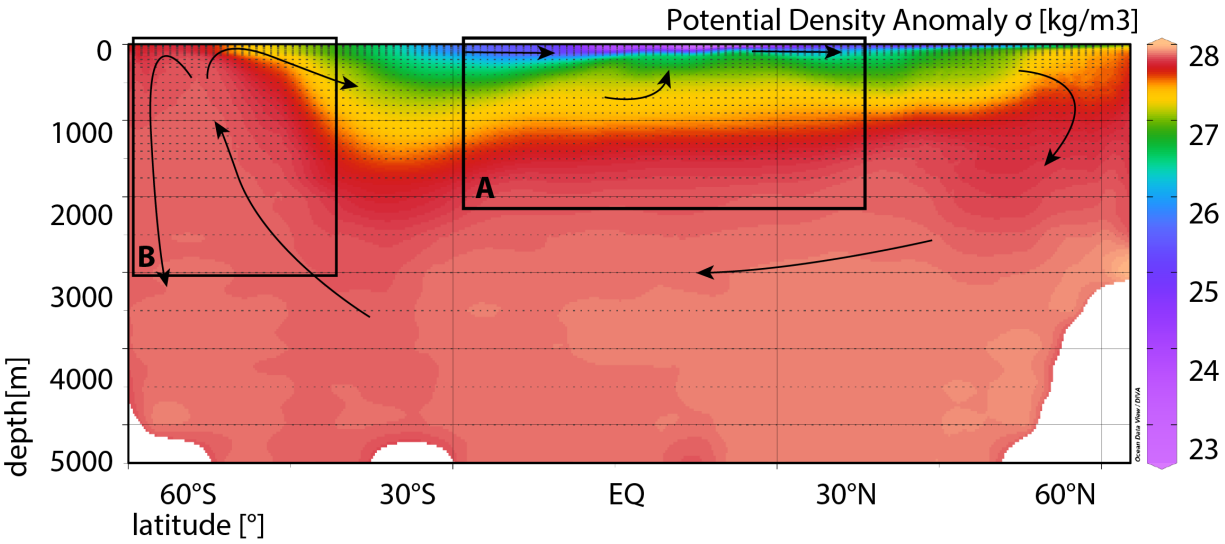

Figure 1.2 – ***Potential density on a cross section through the Atlantic Ocean*** *- Different latitudes feature different density gradients. -* ***A:*** *In the low latitudes a strong thermocline, induced by surface warming, leads to a permanent steady stratification. The only vertical movement possible is wind forced upwelling at the equator or in coastal regions. -* ***B:*** *In the SO, the temperature looses its control on density (Sigman et al., 2004). The salinity gradient with saltier water over fresher drives the deep water formation. Density data from World Ocean Atlas 2013 (WOA13) (Locarnini et al., 2013)*

Water circulation

In the North Atlantic, warm surface water from the Subtropics and the Caribbean propagates northwards into the high latitude North Atlantic. The lower temperatures and the loss of freshwater to the ice shields, lead to increasing salinity, which enhances the density of the water until it sinks. This cold dense water, termed North Atlantic Deep Water (NADW), is propagating southward at 1500-4000m depths. (Fig. 1.3). In the SO it converges with the Antarctic Circum Polar Current and is distributed to the Indian Ocean and into the Pacific, where it ascends again to the surface. In the SO , water from the Antarctic Circum Polar Current ascends and is exposed to the surface of the Antarctic Zone (AZ). At the Antarctic sea ice margin this cold and salty water is further enriched with salinity, descends to the deep ocean and forms the Antarctic Bottom Water (AABW). In the northern part of the SO , in the Subantarctic Zone (SAZ) the Ekman forcing of the southern westerlies pushes the surface water equator-wards. While entering the mid latitudes, it warms up before it enters the subsurface as Subantarctic Mode Water (SAMW). Since it is still saltier than the Atlantic surface water but warmer than NADW, its intermediate density leads to an intermediate depth of SAMW (500-1500m). At the equator, trade wind induced equatorial divergence leads to equatorial upwelling of SAMW, which is then incorporated into the gulf stream.

Tropical Convergence and Equatorial upwelling

Earth's latitudinal climate variability is mainly driven by the difference of the received energy between the tropics and the polar regions. The energy contrast drives atmospheric and marine circulation, which distributes the excess energy form the low latitudes towards the high latitudes. The intense warming of the ground air in the tropics induces convection and surface low pressure systems near the Equator around the globe. The surface winds pulled towards those equatorial low pressure systems are called northern and southern trade winds. They converge at the zone of strongest convection, the so called Inter Tropical

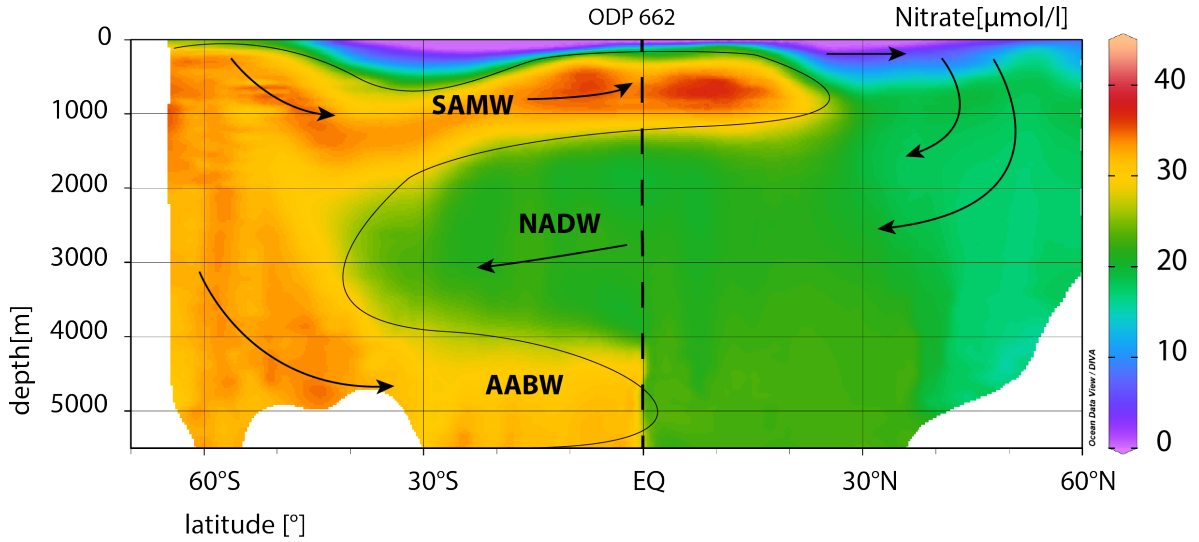

Figure 1.3 – ***Depth profile of nitrate concentration in the Atlantic Ocean*** *[micro**mol/l**] - From the abyssal ocean to the surface the equatorial Atlantic Ocean consists of Antarctic Bottom Water (AABW), North Atlantic Deep Water (NADW), Sub Antarctic Mode Water (SAMW), and above the thermocline the surface water - Nitrate data from WOA13 (Locarnini et al., 2013)*

Convergence Zone (ITCZ) (Waliser and Gautier, 1993). Due to the seasonal changing insolation, the location of the ITCZ is shifting in the course of a year from a northern most position during boreal summer to its southern most position during austral summer (Fig. 1.4A). Since the position of the continents strongly influences the latitude of the main convection, the Atlantic ITCZ is always located north of the Equator exerting strong impacts on the surface water currents (Philander et al., 1996). The tropical Atlantic surface water currents are characterized by the equatorial divergence. The southeast trade winds that cross the Equator induce Ekmann transport. Due to the coriolis effect, the surface water south of the Equator is deflected to the left (southwards) and the surface water north of the Equator to the right. This results in upwelling of cold, nutrient rich subsurface water along the equator, the so called equatorial upwelling (Denny, 2008; Ruddiman, 2008; Garrison, 2009)

This constant supply of nutrients to the surface affects the biological production in the equatorial upwelling region. Although modern equatorial Atlantic is characterized by no residual nutrients in the surface water (Fig. 1.5A), a substantial primary production is observed (Fig. 1.5B). Equatorial upwelling accesses nutrient rich subsurface SAMW (Fig. 1.3). In the high nutrient environment, the primary production works efficient and is able to assimilate all the nutrients close to the locus of upwelling.

1.2 The marine nitrogen cycle

Biological available nitrogen (mainly nitrate, nitrite, and ammonia) is one of most important nutrients for biological production in the ocean along with carbon and phosphorous (Gruber and Galloway, 2008). It has been empirically proven that marine biological production uses nutrients in a unique, remaining stoichiometric ratio (C:N:P = 106:16:1) (Redfield, 1934). Since carbon is omnipresent in the ocean, it never limits primary production and is therefore only of marginal interest regarding nutrient cycles and productivity. Of the two remaining nutrients, nitrogen features two stable isotopes (^{14}N and ^{15}N) in contrast to phosphorous, which is only stable in one isotope (^{31}P). This allows for isotopic analysis and closer studies of the nitrogen cycling processes (Sec. 1.2.2). Due to the mostly parallel cycling of biological available

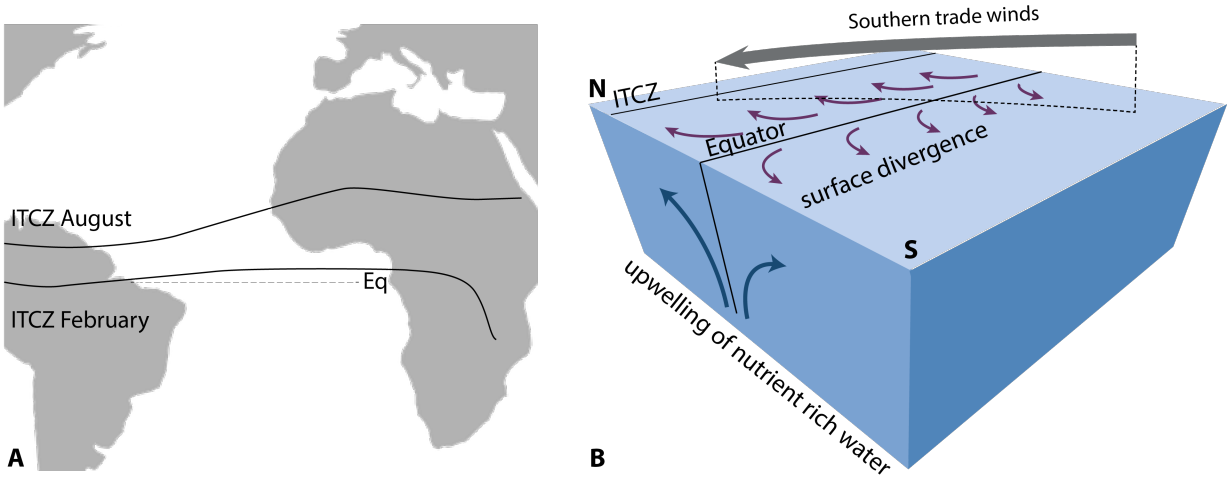

Figure 1.4 – ***Equatorial upwelling in the context of the ITCZ - A:*** *Map of the Intertropical Convergence Zone (ITCZ) in the Atlantic for austral- (February) and borealsummer (August). Data from the international Research Institute for Climate Prediction.* ***- B:*** *Schematic visualization of the trade wind induced equatorial divergence, modified after Garrison (2009).*

nitrogen and phosphorous, combining them to a common term is a fair assumption to do. In this thesis I therefore focus on nitrogen, implying that cycling and consuming processes of phosphorous proceed similar. Although within the last decades the marine Nitrogen cycle (N-cycle) (Fig. 1.6) has been studied intensively, (Altabet and Francois, 1994; Sigman et al., 1999; Ganeshram et al., 2000; Deutsch et al., 2001; Capone et al., 2005; Gruber, 2008; Montoya, 2009) its processes, fluxes and inventories are not completely understood. This is mainly due to their high level of complexity. Nitrogen occurs in a big variety of organic and inorganic forms in different oxidation states that feature diverse reaction chains and transformation processes (Capone et al., 2008). Here I present a very brief overview on the most important marine N cycling processes that are relevant within the framework of this thesis.

1.2.1 Sinks and sources of biological available nitrogen

The main source for biological available nitrogen in the ocean is bacterial reduction of inert atmospheric nitrogen N_2 into ammonia, a process called N fixation (Sigman and Casciotti, 2001; Galbraith et al., 2008; Knapp et al., 2008). In a nutrient depleted surface environment, diazotrophic organisms like *Trichodesmium* are more competitive than organisms that rely on bio-available nitrogen whereas in a nutrient rich environment, diazotrophs do not feature a significant advantage (Knapp et al., 2012). The atmospheric N_2 is fixed by the activation of the responsible enzyme, nitrogenase, which is able to split the triple bond between the two N atoms. The activation of this enzyme requires a substantial amount of iron. It has been observed that *Trichodesmium* prospers mainly in regions with high iron input and stable stratified upper ocean waters (Capone, 1997; Deutsch et al., 2001). This fits into the general picture we have from oceanographic studies regarding Atlantic thermocline nitrate δ^{15}N, that N fixation is mainly happening in warm stratified surface water of suptropical gyres (Capone et al., 2005; Meckler et al., 2007, 2011; Straub et al., 2013b; Subramaniam et al., 2013; Marconi et al., 2015).

The sink term of nitrogen out of the marine system is embodied by bacterial conversion of organic nitrogen into N_2. Denitrification is the main process that removes biological available nitrogen from the marine system . In hypoxic environments, denitrifiers can reduce nitrate into N_2O and N_2 (Hulth et al., 2005). 80% of denitrification is happening on the continental shelfs and slopes where the high sedimentation rate

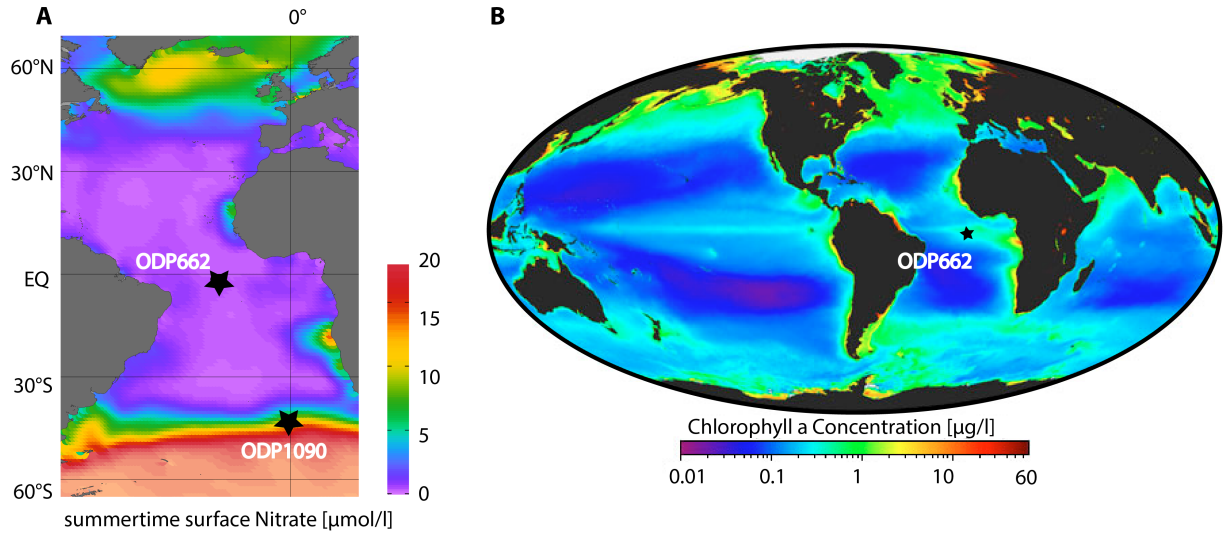

Figure 1.5 – ***Seasurface nitrate concentration and productivity in the equatorial Atlantic - A:*** *Summertime seasurface nitrate concentration [µmol/l], data from WOA13 (Locarnini et al., 2013)* ***- B:*** *Summertime seasurface chlorophyll concentration [mg/m^3] data from Sea-viewing Wide Field-of-view Sensor (SeaWiFS) (https://seawifs.gsfc.nasa.gov)*

is promoting anoxic conditions within the porewaters (Hulth et al., 2005; Granger et al., 2008). Within ocean anoxic zones, denitrification occurs in the watercolumn as well. In the modern ocean this process happens in eastern suptropical Pacific and the poorly ventilated marginal seas like the Red Sea and Arabian Sea (Altabet et al., 1999a; Sigman and Casciotti, 2001).

1.2.2 Stable nitrogen isotopes as a tracer for N cycling

The analysis of the isotopic ratio of organic matter can reveal detailed information about the temporal and geographical extent of different parts within the N cycle. The ratio between ^{14}N and ^{15}N is stated as δ^{15}N (Eq. 1.2). It is the ratio of the heavier to the lighter isotope in the sample, normalized against this ratio in air. For convenience reasons it its multiplied by 1000 and stated in permil [‰].

$$\delta^{15}N\,[‰] = \left(\frac{\left(^{15}N/^{14}N\right)_{Sample}}{\left(^{15}N/^{14}N\right)_{air}} - 1 \right) 1000 \tag{1.2}$$

Thermocline nitrate δ^{15}N in the ocean is influenced by both the input and output terms as well as through internal cycling (Tab. 1.1, Fig. 1.6). N fixation introduces biological available nitrogen with δ^{15}N of 1-4‰. The isotope effect of denitrification is strongly positive (20‰) (Galbraith et al., 2008). In contrast to watercolumn denitrification, where there is a continuous supply of new nitrate, in sedimentary denitrification the available nitrate is completely converted within the enclosed pores. Therefore no net fractionation is occurring. The third process, and for this thesis the most important one that influences marine nitrate δ^{15}N is preferential assimilation of ^{14}nitrate compared to ^{15}nitrate in regions with only partial nitrate consumption (Miyake and Wada, 1971; Altabet and Francois, 1994). It is energetically favorable for primary producers to assimilate ^{14}nitrate. This leads to the production of low δ^{15}N organic matter and an enrichment of the δ^{15}N of the residual nitrate in the water. The Rayleigh fractionation model (Sigman and Casciotti, 2001) describes the isotopic fractionation in a situation with a limited pool of the reactant as it occurs in the ocean during seasonal upwelling (Chapters 3 and 4). The Steady State

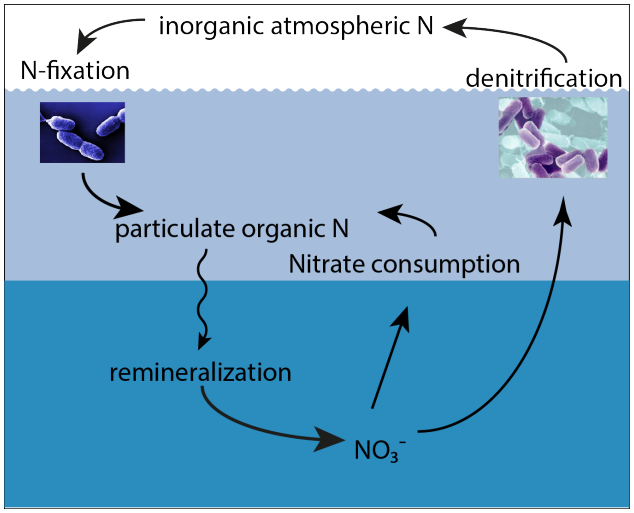

Figure 1.6 – ***Marine nitrogen cycle*** *modified after Sigman and Casciotti (2001)*

Table 1.1 – ***Nitrogen isotope fractionation in the ocean*** *modified after Sigman and Casciotti (2001)*

	kinetic effect ε
watercolumn denitrification	20‰
sedimentary denitrification	0‰
nitrate assimilation	5‰
N fixation	1-4‰

fractionation model (Sigman and Casciotti, 2001) takes into account a continuous supply of the reactant. They both have in common that the δ^{15}N of the organic matter produced is lower, the smaller the level of nutrient consumption. Once productivity reaches complete consumption, the δ^{15}N of the integrated product equals the δ^{15}N of nutrient supply. Therefore the δ^{15}N of the produced organic matter works as an archive for the level of nutrient consumption in the euphotic zone.

1.2.3 Fossil-bound δ^{15}N

Stable nitrogen isotopes track different processes in the nitrogen cycle and can work as an archive. However sedimentary bulk δ^{15}N is associated with diagenetic (Altabet and Francois, 1994; Altabet et al., 1999b) or detrital (Schubert and Calvert, 2001) artifacts, which makes interpretation difficult and often unreliable. Organic nitrogen incorporated into the shells of marine organisms pose a promising archive for undisturbed δ^{15}N. During the last decade foraminifera-bound δ^{15}N (FB-δ^{15}N) analysis became a well established tool for tracking nitrogen cycling and nutrient dynamics (Steph et al., 2009; Ren et al., 2009; Ren, 2010; Ren et al., 2012; Straub et al., 2013a; Martínez-Garcia et al., 2014). An elaborate overview on the analytic work and the laboratory protocol is found in Chapter 2 of this thesis.

Foraminifera are single celled protists with a heterotroph metabolism. They are divided into the bottom living benthic foraminifera, which are not subject of this thesis and the surface and intermediate water dwelling planktonic foraminifera. The habitat associated with planktonic foraminifera are mainly surface and subsurface waters in the open ocean and less frequent in shelf areas and shallow seas (Schiebel and Hemleben, 2001). We focus on the two most commonly abundant planktonic foraminifera in the sediment investigated (low latitude Atlantic):

Globigerinoides sacculifer

Globigerinoides sacculifer (*Gsacc*) is one of the most abundant tropical species and therefore intensely investigated. It lives in the photic zone and bears dinoflagellate symbionts. They tolerate temperatures from 14-31°C and salinity in the range of 25‰ to 47‰ (Hemleben et al., 1989). *Gsacc* is very variable in the morphology of its chambers. The most common two types *G. sacculifer sacculifer* and *G. saculifer trilobus* (with and without the typical kummerform sac) occur in the warm tropical water during Pliocene, Pleistocene and Holocene. It is unclear if the two types represent separate species, subspecies or morphotypes reacting to ecological variations (Saito et al., 1981). We tested the FB-δ^{15}N of the two variations and did not observe any significant differences between them (Chapter 2). In the framework of this thesis the two variations are combined and commonly referred to as *Gsacc*.

Neogloboquadrina dutertrei

The non-spinose species *Neogloboquadrina dutertrei* (*Ndut*) has a wide variation of morphotypes living along a diverse set of climatic settings from mid latitudes to the equator. Within this thesis the most commonly used morphotype was the trochospire *Neogloboquadrina eggeri* with typically 5 big chambers and 7 to 12 small ones (Saito et al., 1981). It can tolerate salinity from 25 to 46‰ and temperatures between 13 and 33° C, although its ability to grow is restricted to temperatures warmer than 15°C. Its food source consists of phytoplankton, mostly unicellular chrysophytes (Hemleben et al., 1989). *Ndut* is not associated with dinoflagelate symbionts although photosynthesizing organisms have been observed within the cellular matrix of *Ndut* (Gastrich, 1988). However, it is unlikely that those organisms work as symbionts. It has been sugested that they are stacked for digestion and *Ndut* thus feature the possibility of food storage (Hemleben et al., 1989). Since *Ndut* is lacking autotroph symbionts its depth habitat is not restricted to the photic zone. Nevertheless it spends most of its live time within the uppermost 50-70m. During its reproductive cycle it descends down to 400-800m (Haynes, 1981), which has to be considered regarding isotopic analysis of their organic matter. In the sediment, different test sizes represent individuals in different stages of the reproduction cycle, they thus lived at different depths. It is unclear if they reflect the isotopic composition according to their changing depth habitat. Most likely they do not feed during gametophasis (Hemleben et al., 1989) and therefore descending into deeper layers would not affect the isotopic composition of the organic matter but rather the composition of the calcite test since they feature high calcification rates during this time. We tested the FB-δ^{15}N of different size fractions and did not observe any significant differences between them (Chapter 2).

The impact of symbioses on δ^{15}N

Previous work on foraminifera bound nitrogen (Ren et al., 2012) revealed FB-$\delta^{15}N_{Gsacc}$ to be 1-1.5‰ lower than FB-$\delta^{15}N_{Ndut}$. This offset is thought to be caused by the different feeding system of symbiotic species like *Gsacc* and non-symbiotic species like *Ndut*. The endosymbionts excrete low δ^{15}N ammonia which is subsequently assimilated by the host cell again. This works like a short cut in the metabolism hiding partially one eutrophic step. It results in foraminifera organic N with low δ^{15}N very close to its food source. FB-$\delta^{15}N_{Gsacc}$ therefore reflects the δ^{15}N of supplied nitrate. In contrast, modern measurements of the non symbiotic thermocline dwelling species *Ndut* reveal a δ^{15}N elevation of around 1‰ in respect to their food source.

1.2.4 Coral- Bound δ^{15}N (CB-δ^{15}N)

In the last few years a new attempt to reconstruct nitrogen dynamics have evolved. Instead of using planktonic dwelling foraminifera, stationary deep-sea corals were taken into account archiving organic nitrogen (Wang et al., 2014). Corals are primary associated with the well known colorful surface water corals found in tropical and subtropical reefs around the globe. Nevertheless recent studies on biodiversity revealed that the number of deep sea coral species exceeds the surface corals (Cairns, 2007). Deep sea corals were rediscovered in the 1960 with advances in submarine sampling technologies (Stetson et al., 1962). In the North Atlantic the most abundant species are hard skeleton building, scleractinian corals *Lophelia Pertusa* and *Desmophyllum Dianthus* (Hovland, 2008; Roberts et al., 2009). The main difference between the tropical surface- and the deep-sea corals is their lack of endosymbionts. In the dark deep ocean, corals do not feature photosynthesizing symbionts. Although their food source is not entirely clear, it is thought that they mostly feed on particulate organic matter raining down as export production. Similar to the foraminifera, they incorporate organic matter within their inorganic calcareous structures where the isotopic composition of the export production is archived. Compared to FB-δ^{15}N, coral-bound δ^{15}N (CB-δ^{15}N) features the advantage of higher growth rate and thus potentially better temporal resolution and they present more material which simplifies the analytical work. The disadvantage is the restriction to study areas and the rather complicated sampling. In contrast to foraminifera, deep-sea corals do not occur anywhere in the ocean but are restricted to closely defined habitats. Further, since foraminifera are widely used in different field of geology, biology and oceanography, access to a diverse set of samples from all over the globe is easily granted.

1.3 Earth's orbital parameters

The long term forcing of orbital parameters on Earth's climate are well studied (Milankovitch, 1920; Hays et al., 1976; Imbrie, 1982). Their prominent and widely disperse impacts on the global climate are observed in different times on various latitudes (Lisiecki and Raymo, 2005; Cleaveland and Herbert, 2007; Jouzel et al., 2007; Abe-Ouchi et al., 2013; Straub et al., 2013a; Lawrence et al., 2013). Apart from the obvious spinning around the axis and around the sun, Earth's orbit features three main movements, which influence the climate each in a different way. The ellipsoid orbit around the sun changes its eccentricity from near circular (ε=0.005) to clearly elliptical (ε=0.06) in two cycles at 100 kyr and 413 kyr. The eccentricity is the only orbital forcing that influences the net radiation received from the sun.

The second orbital forcing is a group of different movements that manifests in a wobbling of the Earth's tilted axis (Fig. 1.7A). The axial precession is a turning of the direction of Earth's axis in space with a cycle of 25 kyr, whereas the precession of the ellipse is a rotation of the elliptical orbit around the sun as a whole with a periodicity of 22 kyr. The combination consists of a strong precessional cycle at 23 kyr and a weaker at 19 kyr. The effect of precession is more complicated. In a perfectly circular orbit the precessional movement would only have the effect of shifting the seasons on the orbit but would not alter Earth's radiation budget. However, as discussed above, since the orbit is elliptical not every position on the orbit is equally distant to the sun. Due to the wobbling of the axis, the equinoxes and solstices are moving on the orbital plane among positions with variable insolation. Precession therefore magnifies or suppresses the insolation effects caused by the elliptic orbit. Precessional variations cause climatic changes that are out of phase between the two hemispheres. A situation with perihelion position at the northern solstice would cause northern summer insolation to be increased. This implies that the southern summer solstice would be at the aphelion causing summer insolation on the southern hemisphere to be weak.

The obliquity of the axis (Fig. 1.7B) is the third orbital movement. The angle between Earth's axis and a

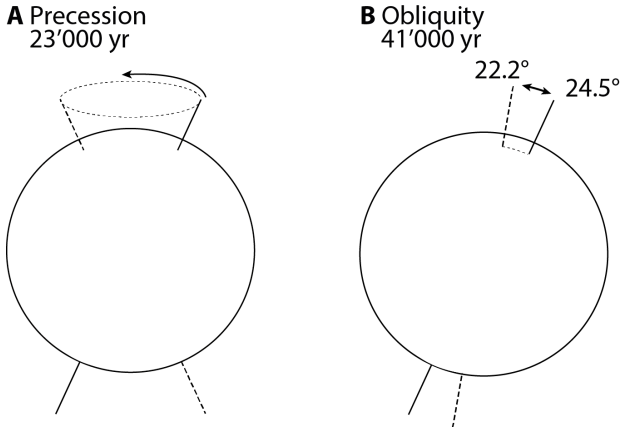

Figure 1.7 – ***Schematic view of the Earth's orbit*** *- **A:** Precession of Earths's axis. Wobbling motion causes the seasons to change with respect to the orbit around the sun. It causes climatic changes that are out of phase between the two hemispheres. - **B:** Orbital obliquity is a tilt motion of Earth's axis. A changing angle between the axis and the ecliptic causes stronger seasonal differences. It causes insolation to change in phase between the two hemispheres.*

line normal to the ecliptic plane is varying on 41 kyr cycles from the most tilted position (24.5°) to the least tilted position (22.2°). It causes insolation to change in phase between the two hemispheres. If obliquity increases, the axis is more tilted towards the sun in summer and away from the sun in winter. This leads to increased summer insolation and decreased winter insolation in both hemispheres (Ruddiman, 2008).

In paleoceanographic studies, the effects of changes in Earth's orbital cycles can be detected in the measured signals and attributed to a geographical origin. A spectral analysis of the mean insolation for the last 1 Myr during northern hemisphere summer (Fig. 1.8) reveals the orbital forcing on different latitudes. Low latitudes are predominantly influenced by precession, whereas high latitudes are influenced during summer by precession and obliquity and during winter by obliquity only.

1.3.1 Precessional forcing on equatorial upwelling and African Monsoon

In the low latitude Atlantic (Fig. 1.5), the most relevant study region within the framework of this thesis (Chapter 3 and Chapter 4), the predominant authochtonous forcings are precessional cycles in monsoon intensity (de Menocal et al., 1993) and equatorial upwelling (Molfino and McIntyre, 1990). Monsoon circulations are driven by by temperature and thus pressure gradients between the North African continent and the open equatorial Atlantic ocean (Ruddiman, 2008). Although the total insolation changes due to precessional forcing cancel each other out in the course of the year, the impact of winter and summer changes are different. In the modern situation with perihelion during southern hemisphere summer (Fig. 1.9A), northern summer insolation is close to its minimum and the ITCZ is on a southern position. The pressure gradient between open ocean and the African continent is weak, leading to a feeble landfall of summer monsoon winds. Accordingly, the SE trades along the Equator intensified and enhance equatorial upwelling (Molfino and McIntyre, 1990). During times with perihelion in northern hemisphere summer (Fig. 1.9B) and stroger northern insolation, a greater part of the SE trade winds along the Equator are deflected. This leads to an alleviation of the zonal tradewinds, which in turn weakens the equatorial upwelling (Ruddiman, 2008). The northern position of the ITCZ causes stronger landfall of warm moist summer monsoon. Accordingly, winter insolation minima lead to an intensified high pressure system over the continent and enhanced winter monsoon winds.

The latitude of the ITCZ governs the pressure gradient and thus the intensity of the monsoon and equatorial

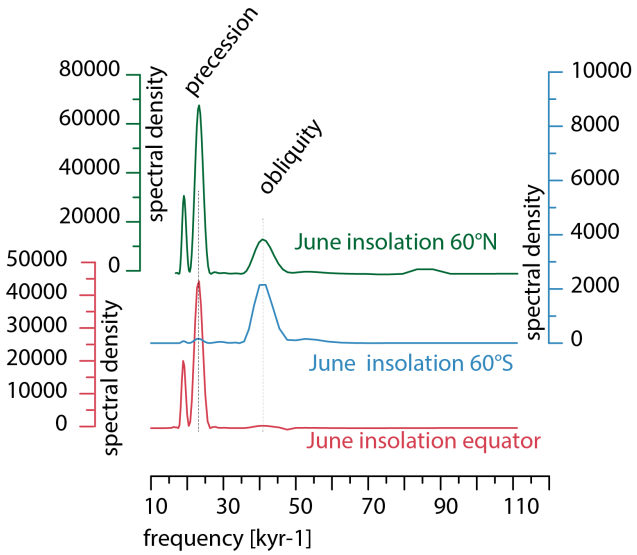

Figure 1.8 – ***Orbital forcing on different latitudes*** *- Spectral analysis of mean insolation at different latitudes over time. Spectral densities for daily mean June insolation on the Equator (red), on 60°S (blue) and on 60°N(green) over the last mio years. Precessional forcing affects low latitude insolation and high latitude summer insolation whereas obliquity affects mid to high latitude summer and winter insolation. Insolation data from Laskar et al. (2004), spectral analysis preformed with the ARAND software package by Howell (2001).*

upwelling (Schneider et al., 2014). Its position is variable relative to the insolation received by each hemisphere, causing a shift of the ITCZ towards the warmer hemisphere (Chiang and Friedman, 2012). This shifting of the ITCZ in the past is observed around the globe and is not restricted to precessional forcing but applies as well to North Atlantic stadial/interstadial cycles (Deplazes et al., 2013).

However, although the available nitrate at Site 662 is expected to originate the equatorial upwelling and the shifting of the ITCZ during the last glacial cycles are known, we do not observe nitrate dynamics to follow precessional forcing during the last 160 kyr (Chapter 3). From 2.7 to 2.4 Myr BP we observe a clear cycling in obliquity frequency (Chapter 4). As discussed further down this is interpreted as a lacking connection of upwelling circulation and nutrient dynamics in Chapter 3 and as a high latitude influence on low latitude biogechemistry in Chapter 4. Orbital forcing thus works as a geographic tracer for the origin of a climatic signal.

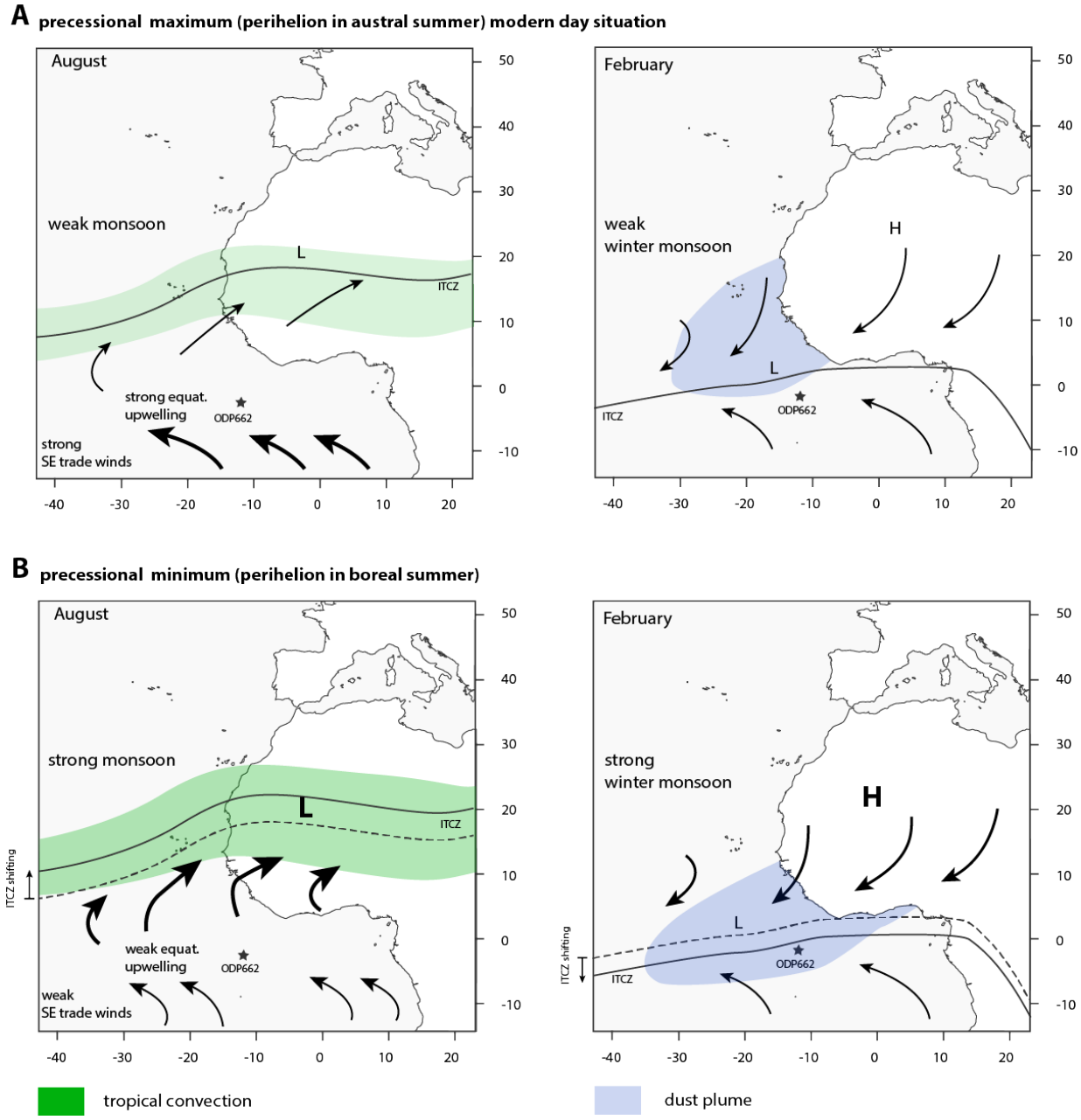

Figure 1.9 – ***Precessional forcing on African monsoon - A:*** *Modern situation (perihelion during southern hemisphere summer). During phases with weaker northern summer insolation, African summer monsoon weakens, which leads to intensified SE trade winds along the Equator and enhanced equatorial upwelling. Wintertime cooling of the African landmass drives a downwards flow of cool dry air out of the continent.* ***- B:*** *Situation during precession minimum (perihelion during northern hemisphere summer). Stronger northern summer insolation over the African continent lead to intensified Monsoon. Therefore a greater part of the SE trade winds along the Equator are deflected, which leads to a decreased equatorial upwelling. Accordingly, winter insolation minima lead to an intensified high pressure system over the continent and enhanced winter monsoon winds. Modified after Ruddiman and Janecek (1989); de Menocal et al. (1993); Ruddiman (2008)*

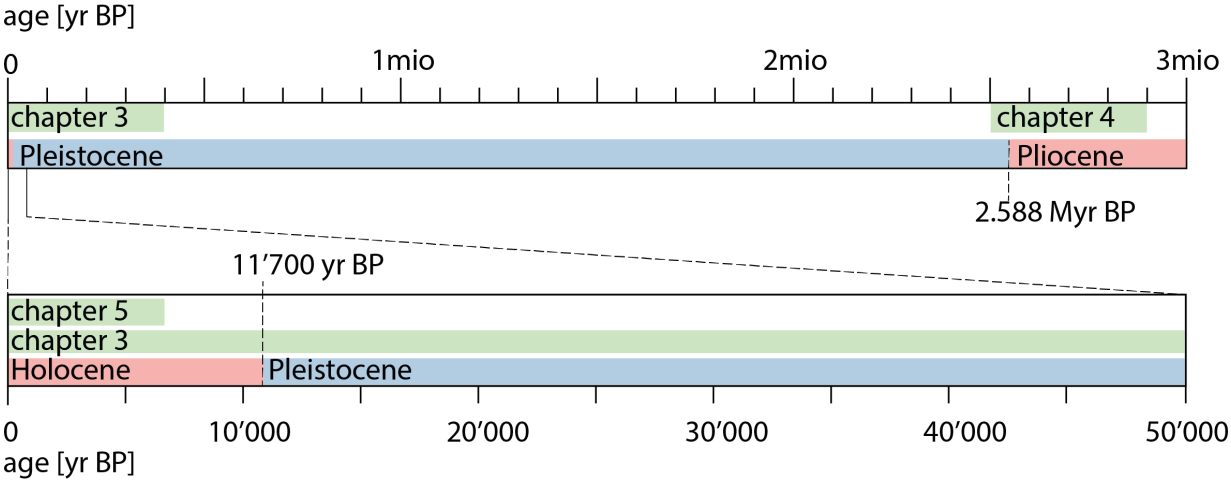

Figure 1.10 – ***Geological timeframe of the thesis***

1.4 Objectives of the thesis

With respect to the current anthropogenic CO_2 emissions and its implications on the global climate it is vital to understand the nature of climate transitions like glacial/interglacial cycles. Studying nutrient cycling in the oceans and its link to the carbon cycle helps to improve the understanding of feedback effects and dynamic processes in a rapidly changing biogeochemical system. We have evidence of changes in the level of nutrient consumption of the North Atlantic (Straub et al., 2013b) and the SO (Martínez-Garcia et al., 2014; Studer et al., 2015) within glacial-interglacial timescales. The impacts of changing nutrient dynamics on the biological pump in the high latitudes are thought to play a crucial role governing the atmospheric CO_2 concentration. On the other hand it is known that processes in the high latitude polar regions are able to affect as well the worlds most productive regions in the low latitudes by the flow of SAMW (Sarmiento et al., 2004; Rickaby and Elderfield, 2005). However, the implications of changing polar nutrient dynamics on low latitude biogeochemistry are still unclear.

The main purpose of this thesis was to take a look at nutrient cycling in the Atlantic high productive regions and to assess the high latitude influence on low latitude biogeochemistry.

The goals of this thesis were:

1. Improving the understanding of the impact of the water leaving the SO on the low latitude Atlantic with respect to the changing nutrient dynamics in the Antarctic- and Subantarctic zone. For this reason we measured the first record of SAMW FB-δ^{15}N back to the penultimate glacial maximum (Chapter 3) on 1 kyr temporal resolution. The insights on low latitude nutrient dynamics gained during this project were applied to measure the first record of SAMW FB-δ^{15}N during the Plio- and Pleistocene climate transition (Chapter 4) with 2 kyr resolution.

2. Ground truthing work on CB-δ^{15}N and assess its potential as a proxy for changes in the position of the North Atlantic Subpolar Gyre (SPG) during the Holocene. We measured the CB-δ^{15}N on Holocene deep-sea corals from a transect through the SPG (Chapter 5). To determine whether deep sea corals reflect sea surface nutrient consumption on a regional scale the CB-δ^{15}N was compared with modern δ^{15}N export estimated from modern sea surface nitrate concentrations.

The δ^{15}N data measured within the framework of this thesis is covering different ranges of the geological time in adjusted temporal resolution for describing processes occurring on various timescales.

1.5 Chapter summaries

1.5.1 Foraminifera-bound δ^{15}N isotope analysis (Chapter 2)

FB-δ^{15}N poses a powerful tool to assess the marine nitrogen cycle. Here I present the analysing techniques used in this thesis, originally published by Ren et al. (2009) and based on the bacterial denitrification method of Sigman et al. (2001) summarized in an updated laboratory protocol. Tests on nitrogen content of planktonic foraminifera from the equatorial Atlantic and North Atlantic deep sea corals confirm significant differences in N-content between different species and time. Further, I present preliminary tests on species- and size dependence of foraminifera-bound δ^{15}N.

1.5.2 Nitrogen isotope changes in the equatorial Atlantic as a response to Southern Ocean nitrate consumption (Chapter 3)

We measured FB-δ^{15}N on two species of foraminifera at Ocean Drilling Program (ODP) Site 662 in the Eastern Equatorial Atlantic (EEA) back to the penultimate glacial maximum 160,000 years ago. The main features of the combined record are δ^{15}N maxima at each of the two major deglaciations extending into the early interglacials, as well as a maximum centered on 82,000 years ago, near the Marine Isotope Stage (MIS) 5b/5a transition, which would have been most easily caused by a rise in the preformed nitrate δ^{15}N of SAMW. Here, we propose a mechanism for low latitude δ^{15}N elevation during shifts in SO nitrate consumption. This mechanism suggests that the low latitude surface ocean is affected by polar and subpolar biogeochemical change through the flow of intermediate waters.

1.5.3 Incomplete Nitrate consumption in the equatorial Atlantic (Chapter 4)

During the Plio-Pleistocene transition (2.9 - 2.4 Myr BP), Earth's climate and ocean circulation underwent substantial changes. The focus is here on the equatorial Atlantic Ocean and its response to the intensification of northern hemisphere glaciation at 2.7 Myr BP. At ODP Site 662 in the Eastern Equatorial Atlantic, foraminifera-bound δ^{15}N was measured on two species of planktonic foraminifera through the Plio-Pleistocene transition. The main feature is an onset of obliquity paced 41 kyr cycles at 2.7 Myr BP, with minima in δ^{15}N coinciding with maxima in benthic δ^{18}O. Glacial periods with lower sea surface temperatures, higher productivity, and lower FB-δ^{15}N alternated with interglacial phases, characterized by warm sea surface water, low production and higher δ^{15}N. These simple correlations of δ^{15}N with climate parameters are not observed over the last 160 kyr of the late Pleistocene at this site. Moreover, the background FB-δ^{15}N between 2.4 and 2.9 Myr BP is 0.5‰ lower than over the last 160 kyr. We propose that the cyclic changes in FB-δ^{15}N starting at $\approx$ 2.65 Ma are due to obliquity paced contractions of the Atlantic warm pool, resulting in higher nitrate concentration in the waters upwelled in the equatorial Atlantic (Lawrence et al., 2013). Unlike in the late Pleistocene, the nitrate concentration in the water below the warm pool (which is ultimately sourced from Subantarctic Mode Water) was adequately high that nitrate consumption was incomplete along the equator during the obliquity-paced Plio-Pleistocene cold intervals, causing the observed decline in FB-δ^{15}N during those intervals. The lower mean FB-δ^{15}N over the entire investigated Plio-Pleistocene period suggests that SAMW nitrate δ^{15}N was lower during this period, consistent with Sub Antarctic nitrate consumption being weak during the Pliocene and early Pleistocene due to a lack of dust-derived iron input at that time (Martínez-Garcia et al., 2011; Lawrence et al., 2013).

1.5.4 Coral-bound nitrogen isotopes as an archive for Holocene North Atlantic nutrient utilization (Chapter 5)

The Subpolar North Atlantic is a key region within the global climate system. The arctic climate in turn is strongly affected by the North Atlantic Oscillation, which influences the position of the Subpolar Gyre in the North Atlantic. The perennially incomplete surface nitrate consumption, which marks the area of the Subpolar Gyre, is likely to result in low δ^{15}N of organic matter exported into the deep ocean. Here we analyze coral-bound δ^{15}N of (CB-δ^{15}N) on organic matter incorporated into the skeletons of scleractinian deep sea corals for its potential as a proxy for the δ^{15}N export production and thus the position of the Subpolar Gyre over time. We predict the δ^{15}N export by the means of Rayleigh dynamics and compare to measured CB-δ^{15}N. We found good coherence, with higher CB-δ^{15}N in regions with more complete nitrate consumption and vice versa. An absolute offset between CB-δ^{15}N and δ^{15}N export of 6-8‰ was observed, which matches the reported offset of previous studies. To reconstruct the position of the Subpolar Gyre and the strength of the North Atlantic Oscillation over the late Holocene, we measured CB-δ^{15}N on deep sea corals with ^{14}C ages between 0 and 2000 yr BP. We observed CB-δ^{15}N potentially consistent with a more negative North Atlantic Oscillation at 500 to 600 yr BP, which corresponds to a negative North Atlantic Oscillation during this time as reconstructed by Greenland limnological studies. Our data show the potential of CB-δ^{15}N.

2

Foraminifera-bound nitrogen isotope analysis

Lukas E. Oesch[1]

[1]Geological Institute, Department of Earth Sciences, ETH Zurich, Zurich, Switzerland

Abstract

Foraminifera-bound nitrogen isotope analysis poses a powerful tool to assess the marine nitrogen cycle. Here I present the analysing techniques used in this thesis, originally published by Ren et al. (2009) and based on the bacterial denitrification method of Sigman et al. (2001) summarized in an updated laboratory protocol. Tests on nitrogen content of planktonic foraminifera from the equatorial Atlantic and North Atlantic deep sea corals confirm significant differences in N-content between different species and time. Further, I present preliminary tests on species- and size dependence of foraminifera-bound δ^{15}N.

2.1 Introduction

The sedimentation of the calcareous tests of planktonic foraminifera on the seafloor represents a well known geological archive of sea surface and euphotic zone processes. Measuring the isotopic composition of organic N incorporated into their tests offers insights to in- and outputs to the marine N cycle as well as internal N cycling processes. Here we describe the analytical procedure of FB-δ^{15}N first established by Ren et al. (2009) using the denitrifier method (Sigman et al., 2001). The small nitrogen content (Sec. 2.4) of the foraminifera test poses the main challenge of the method. It demands high analytical precision while analyzing sample quantities as low as 5nmol of nitrogen. Nevertheless we reach an overall precision of replicated measurements of $0.2‰$ with a starting sample volume of 10-15mg uncleaned foraminifera.

2.2 Sample preparation

We wet sieved 10cm^3 sediment to dissever the foraminifera ($> 63\mu$m) from the bulk material. If the sediment is previously freeze dried, the clay particles disaggregate more easily. This allows for much faster wet-sieving. However, some of the foraminifera tests may break during the freezing process. Therefore freeze-drying is only recommended for samples with high abundance of the desired species. The wet sieved tests are dried overnight at 40°C and further divided into different size fractions by dry sieving (fine fraction: 63µm - 125µm, medium fraction: 125µm - 350µm, coarse fraction: >350µm). For each sample 400-500 single species specimens (10-15mg) were manually picked from the medium and coarse fraction with a dissecting microscope. The foraminifera were gently crushed to open the chambers allowing for complete cleaning on the inner surface as well. The cleaning was preformed following the protocol of Ren et al. (2012). Clay and other coarse sedimentary particles were removed by adding 10ml 2% neutralized polyphosphate solution and sonification for 1min. When dealing with thin walled, fragile species like *Neogloboquadrina pachyderma* or foraminifera from the fine fraction, sonification should be minimized to avoid complete destruction of the vulnerable tests. The samples prepared within the framework of this thesis originate from the tropical surface ocean and were pricked from the coarse and medium fractions. Vulnerable tests were thus not a problem. The cleaning solution was poured off and the sample washed three times with milli-Q water. 10ml of bicarbonate buffered dithionite-citric acid was added as a reductive reagent to remove metal coatings. To assure complete reduction, the samples were kept in a water bath at 80°C for 1h. The cleaning solution was poured off and the samples were rinsed again three times with milli-Q water. To remove all the contaminant organics on the inner and outer surface of the calcite test fragments, an oxidizing cleaning was preformed. For that reason the sample was transfered into a glass vial with a single droplet of milli-Q water. 3ml of basic potassium persulfate reagent was added and the sample was autoclaved for 1h. To prevent contamination of the cleaned sample from here on, the remaining analytical work was performed in a clean environment. All the glassware and aluminum foil used hereafter is previously combusted at 500°C for 5h. The sample handling is carried out in a laminar flow hood equipped with an ammonium filter. The clean samples were rinsed five times with milli-Q water and dried over night in an evacuated clean oven (40°C). Due to minor dissolution and loss of contaminants on the tests, we lose between 10% and 15% of the sample mass during the cleaning, leaving us with a sample volume of 8-12mg per sample.

2.2.1 Preliminary testing

Empirically, the appropriate size fractions to pick and whether or not one can combine different fractions, depends on the life cycle of the foraminifera and the location and time period from which the sediment is from. If no further information is available, previous testing is required. In our studies (Chapter 3 and

Chapter 4) not all of the samples contained enough specimens for replicated measurements in the same size fraction, such that we tested for differences between the coarse fraction (>350µm) and the medium fraction (125-350µm). The results indicated no consistent offset between the two size fractions of the tested samples from the Pleistocene equatorial Atlantic (Fig. 2.1). We concluded that combining the size fractions of both the species does not alter the data. Additionally, we tested for FB-δ^{15}N differences between the two abundant varieties of *Globigerinoides sacculifer (Gsacc)* (*Globigerinoides trilobus sacculifer* and *Globigerinoides trilobus trilobus*). 300 to 400 specimens of each were single picked and measured. Since no significant differences were revealed (Fig. 2.1), we concluded to combine them (hereafter *Gsacc*). Measurements were preformed at the Sigman Lab by Anja Studer and Lukas Oesch.

2.3 Oxidation of foraminifera-bound nitrogen into nitrate

3-5mg of cleaned foraminifera were weighed into clean glass vials. The transfer of the cleaned shell fragments in to the vial was done using previously combusted aluminum foil. To release the organic N into solution, the cleaned foraminifera tests were dissolved by adding 4N ACS grade HCl (usually 10µl/mg). By adding 1ml of an oxidant reagent (1g potassium persulfate, 1g ACS grade NaOH, 100ml milli-Q water), we oxidized the organic N to nitrate. To avoid further contamination by external organics, we recrystallized the potassium persulfate five times and distilled the milli-Q water in a low temperature setting (Savillex DST-1000). To ensure complete oxidation, samples were autoclaved for 1h. When sodium hydroxide is added and therefore the pH is raised, the dissolved carbonate will precipitate again. After autoclaving, big chunks of carbonate precipitates cover the ground of the vial and have to be removed. Previous studies revealed an interference of the calcium ions and the phosphate buffer used in the bacterial media (Ren, 2010). To remove the calcium carbonate, we centrifuge the samples (10min at 4000rpm) and pipette the supernatant solution into a new combusted vial. Prior to the determination of the N content and the bacterial conversion (Sec. 2.2 & 2.5), the pH of the sample has to be adjusted to a level of compatibility for the bacteria (pH:6-8). Small amounts of ACS grade 6N HCl are used to lower the pH, which is measured by pipetting small droplets onto pH stripes.

2.4 Determination of N content

To avoid linearity effects during the mass spectrometer measurement, sample volumes are adjusted to yield a final sample size of 5nmol (or 10nmol) of N. Therefore the N content of the sample is measured after oxidation. The sample nitrate is reduced to nitric oxide in a vanadium(III) reactor (Braman and Hendrix, 1989). To detect the nitric oxide we use a Teledyne chemiluminescence nitrogen oxides analyzer model 200E. The pH-adjusted sample is injected into a vanadium(III) reactor at 90°C where the nitrate is reduced to NO. With an Argon carrier gas stream the NO is transported through a cooled NaOH trap to remove acidic contaminants and most of the water. It is further transported into the analyzer where the NO is detected by the means of chemiluminescence reaction with ozone. The sample concentration is calculated by regression from a series of potassium nitrate standards of known concentration that are injected into the vanadium reactor in parallel with the samples. In addition, the nitrogen content of the foraminifera samples (given in $\mu molN/g_{calcite}$) is back-calculated after isotopic measurement with the N_2O peak area given by the mass spectrometer.

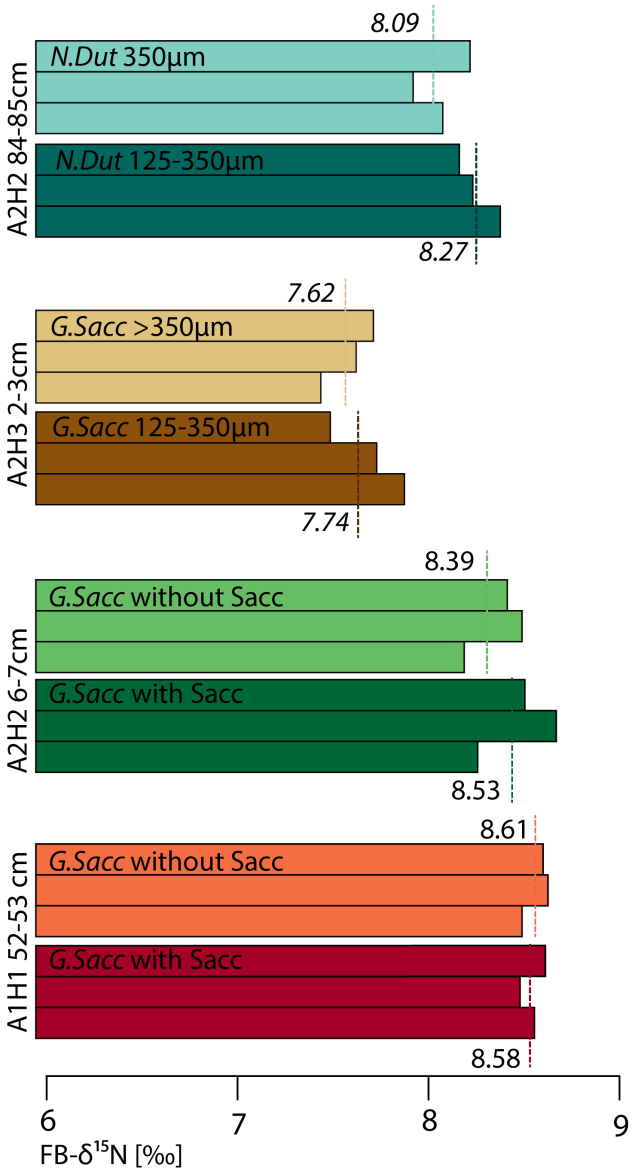

Figure 2.1 – ***Preliminary testing of FB-δ^{15}N differences according to foraminifera properties.*** *Two abundant varieties of Gsacc, Globigerinoides trilobus sacculifer and Globigerinoides trilobus trilobus (with- and without additional sacc-chamber) were tested and resulted in a difference lower than the analytical precision. The foraminifera were picked from two samples from equatorial Atlantic Site 662 from two different depths (A1H1 52-53cm: mcd=52cm, age=7.8 kyr BP and A2H2 6-7cm: mcd= 4.76m, age=82 kyr BP). Gsacc with additional chamber and Gsacc without additional chamber were measured three times each (full procedural replicate). We also tested small to medium size fraction ($125-350\mu m$) compared to the coarse fraction ($> 350\mu m$) on the two species Gsacc and Ndut. No significant differences were revealed. The foraminifera were picked from sediment from equatorial Atlantic Site ODP662 from two different depths along the core (A2H2 84-85cm: mcd=5.54cm, age=102.8 kyr BP and A2H3 2-3cm: mcd= 6.22, age=121 kyr BP). The two different size fractions of both species were measured three times each (full procedural replicate).*

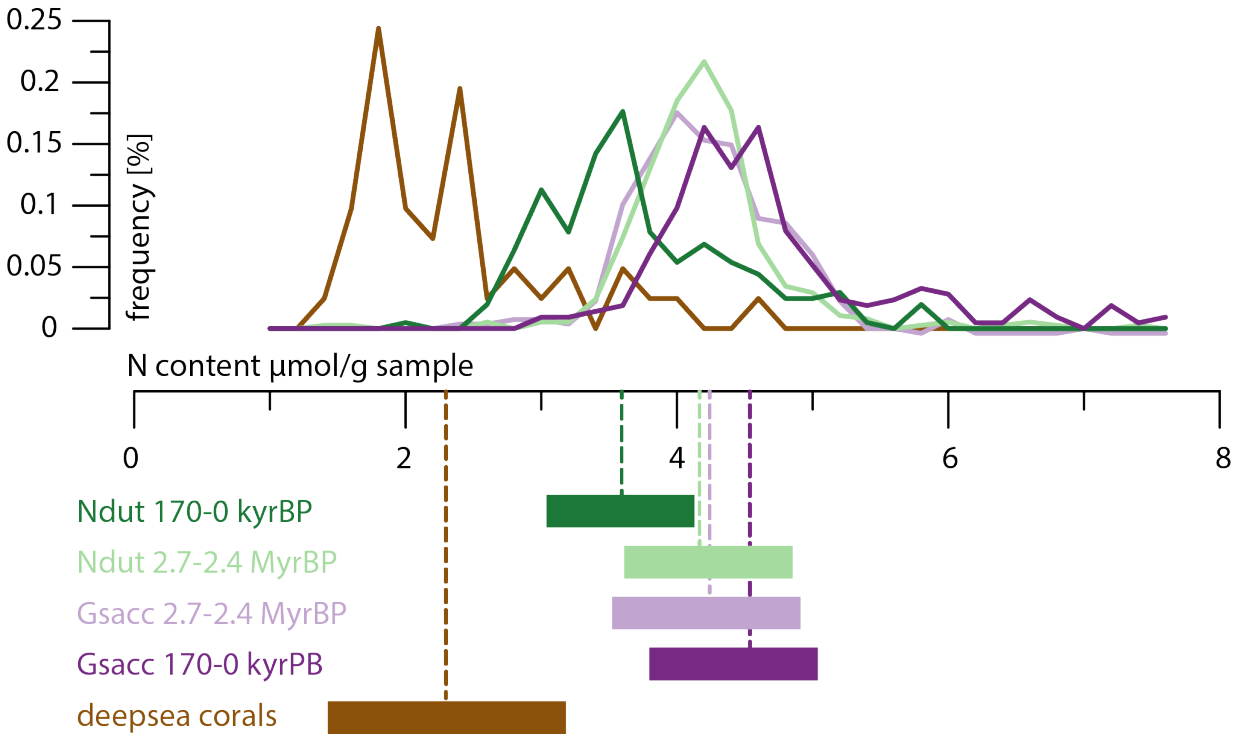

Figure 2.2 – ***Nitrogen content of low latitude planktonic foraminifera and North Atlantic deep sea corals.*** *Normalized frequency of N content on different of different samples and its 80% quantiles (bars at the bottom). N content of Gsacc during the last glaciation is slightly elevated (3.8-5$\mu mol/g$) compared to specimens from the early Pleistocene (3.6-5$\mu mol/g$). The N content of the thermocline dwelling species Ndut decreased throughout the Pleistocene from 3.8-5 $\mu mol/g$ during early Pleistocene to 3-4$\mu mol/g$ during the last glaciation. Additionally measured deep sea corals from the North Atlantic feature a significantly lower N content but a higher intra-species variability (1.2-3 $\mu mol/g$)*

2.4.1 N content of different samples

The N content of foraminifera varies among species, depth, and age and ranges from 3 to 5µmol/g (Fig. 2.2). *Gsacc* of the last glacial cycle yield a N content of 3.5 to 5µmol/g whereas *Neogloboquadrina dutertrei (Ndut)* yield a lower N content of 3 to 4µmol/g. The samples from the Plio-Pleistocene boundary have an average N content of 3.5-5µmol/g for both species. Previous studies revealed a difference in N content according to the sample latitude (Straub, 2012). Since the foraminifera samples used in this thesis are all from the same latitude, we cannot address meridional changes. During the last glacial cycle, the N content of *Gsacc* appears to be higher in the Caribbean (4-5.5µmol/g) than in the eastern equatorial Atlantic. Straub (2012) observed an increase in N content of surface dwelling symbiotic species *G.ruber* during the Pleistocene. We measured an increase in the N content of the symbiotic surface dwelling species *Gsacc* on the same time scale. The subsurface dwelling non-symbiotic species *Ndut* on the other hand, features a decrease in N content during Pleistocene. Within one set of samples of the same age range and the same species, we expect the N content to be within the same range. This is used for contamination detection and as a quality control for the final data. We excluded data points from samples with N contents higher than 5µmol/g as they were likely contaminated during sample handling. The N content of deep sea corals behaves differently. The variation between different deep sea corals is bigger than within foraminifera, but generally they contain less nitrogen (between

Table 2.1 – ***Chemical standards used for FB-$\delta^{15}N$ analysis***

standard	δ^{15}N	purpose	
oxidation standard 5.4	5.4‰	estimation of blank δ^{15}N (blank estm.)	in-house standard
oxidation standard 3.6	3.6‰	blank estm.	in-house standard
USGS40	-4.52‰	blank estm.	international standard
USGS41	47.75‰	blank estm.	internat. standard
IAEA-N3	4.7‰	absolute reference	internat. standard
N_2O	0-1‰[1]	control MAT stability, drift correction	

Table 2.2 – ***Typical procedure vial set-up***

Oxidation	NO_x-Box	Denitrification	Massspectrometry
60 samples	60 samples	60 samples	60 samples
		10 denitrification-replicates	10 denitrification-replicates
10 blanks	10 blanks	3 combined blanks	3 combined blanks
25 oxidation standards		25 oxidation standards	25 oxidation standards
		22 IAEA standards	22 IAEA standards
			10 N_2O standards
95 vials	70vials	120vials	130vials

1 and 3µmol/g), such that the sample size has to be increased accordingly to yield 5nmol (or 10nmol) of N.

2.5 Bacterial denitrification and mass spectrometry

The dissolved nitrate in the sample solution is subsequently reduced into nitrous oxide by bacterial conversion according to Sigman et al. (2001). The denitrifier *P. chlororaphis* lacks the enzyme to reduce N_2O to N_2. Previously combusted 20ml bacterial vials are filled with 1.5ml concentrated bacteria solution and sealed with milli-Q washed rubber septa. To ensure the evacuation of ambient N_2O and complete consumption of residual nitrate in the bacteria media, vials are then sparged with N_2 for 4h. Usually 5 or 10 nmol of sample N (depending on the sample mass available) is injected into the concentrated bacteria solution. The vials are kept in the dark over night to assure complete conversion. If not measured the other day, the samples are stored in the freezer (-40°C) until the day of the mass spectrometer measurement. As an international absolute reference and to obtain a measurement of stability of the denitrification, we prepare 22 vials of IAEA-N3 nitrate standards ($\delta^{15}N$ = 4.7‰) that are injected into additional bacteria vials from the same stock in comparable concentration.
The isotopic ratio is determined with a GC-MS setting according to Weigand et al. (2016) with chemical traps for the residual CO_2, nafion traps for the water and a well elaborated setting of cryotraps and GC-columns to measure the δ^{15}N of N_2O in high precision (0.06‰). Together with the samples and the IAEA standards, 10 N_2O standards are measured as machine standards to correct for possible drift and to have control on the stability of the mass spectrometer performance. For the N_2O standards a previously combusted bacteria vial with 1ml of degassed water is sparged for 10min with N_2. N_2O from a 1000ppm N_2O in He tank is injected through the septum and measured along with the samples.

[1] The isotopic composition of the N_2O standards differs between individual gas tanks slightly

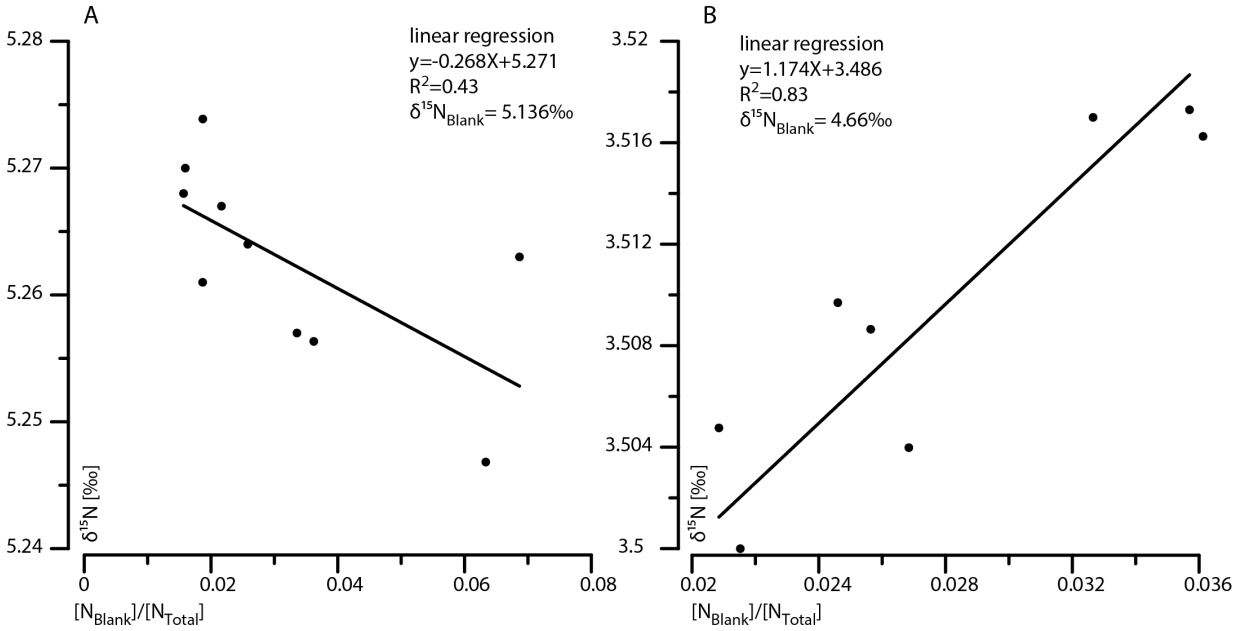

Figure 2.3 – ***Blank*** δ^{15}***N estimation through regression.*** *Two different oxidation standards are used with known N concentration and* δ^{15}*N.-* ***A****: In-house oxidation standard with* δ^{15}*N=5.4‰ measured at* $\frac{[N_{Blank}]}{[N_{Total}]}$: $0.02 - 0.07$ *resulting in* $\delta^{15}N_{Blank}$*=5.136‰ -* ***B****:In-house oxidation standard with* δ^{15}*N=3.6‰ measured at* $\frac{[N_{Blank}]}{[N_{Total}]}$: $0.02 - 0.04$ *resulting in* $\delta^{15}N_{Blank}$*=4.66‰. To determine the final* $\delta^{15}N_{Blank}$ *the direct measurement on the mass spectrometer is taken into consideration as well.*

2.6 Blank $\delta^{15}N$ estimation and correction

$$\delta^{15}N_{MS} = \frac{[N_{Blank}]}{[N_{Total}]}\delta^{15}N_{Blank} + \frac{[N_{Sample}]}{[N_{Total}]}\delta^{15}N_{Sample} \tag{2.1}$$

The measured isotopic ratio ($\delta^{15}N_{MS}$) has to be corrected for the contribution of blank nitrogen originating from residual organic N in the milli-Q water and the potassium persulfate reagent. $\delta^{15}N_{MS}$ is defined as described by Eq. 2.1. Typical blank concentrations are in the range of 0.15-0.25µM. Given the assumption that within the same batch of samples the isotopic ratio of the blank ($\delta^{15}N_{Blank}$) is equal for all of the samples, we can estimate the $\delta^{15}N_{Blank}$ including an array of oxidation standards and blank vials in the whole procedure. If we measure a standard with known δ^{15}N and known N concentration, we can calculate $\delta^{15}N_{Blank}$. From the oxidation step onwards (Sec. 2.3) we include 20 to 30 oxidation standards and 10 blank vials. We use two in-house standards and two international USGS standards (USGS40: δ^{15}N = -4.52‰ and USGS41: δ^{15}N = 47.75‰). The in-house standards used here are a mixture of ACA(amino acids) and glycine with δ^{15}N = 3.6‰ and 5.4‰, respectively. The concentrations of the oxidation standards were chosen to yield a ratio of blank nitrogen to total nitrogen (2-4%) comparable to the samples ($\frac{[N_{Blank}]}{[N_{Total}]}$). As blank vials we used the same clean combusted glass vials as used for the samples and treated them similarly to the samples. Their N concentration is measured on the same chemiluminescence nitrogen oxides analyzer (sec. 2.4). The measured N_{Blank} concentration was typically in the range of 0.15-0.25µM and yield a mass less than 5nmolN for all blank vials combined. For denitrification we combined 3 blank vials and injected them into one bacteria vial. The N content of this blank bacteria vial (0.5-0.75 nmol) is substantially lower than the N content of the sample vials (5nmol or 10nmol) to which the mass spectrometer is tuned. Additionally we can not exclude disturbances during the denitrification step due to the bigger volume of the blank liquids (3ml per 1ml bacteria solution). Therefore the measured

$\delta^{15}N_{Blank}$ is to treat with caution.
In addition, we can also calculate the $\delta^{15}N_{Blank}$ by using the oxidation standards. According to Eq.2.1 in a given situation where the ratio of blank nitrogen to total nitrogen equals 1 ($\frac{[N_{Blank}]}{[N_{Total}]} = 1$) the measured $\delta^{15}N_{MS}$ equals $\delta^{15}N_{Blank}$. On the other hand in a given situation with almost no blank nitrogen, the ratio blank nitrogen to total nitrogen would be close to zero and $\delta^{15}N_{MS}$ would equal $\delta^{15}N_{sample}$.
In a first step we plot the measured data of the oxidation standards against their ratio of blank nitrogen to total nitrogen (Fig. 2.3). In a second step we calculate a linear regression forced through the actual isotopic value of the used oxidation standard at X=0. In the resulting linear equation we set X=1 and result in a estimation of the isotopic ration of N_{Blank}.

2.7 Interpretation of FB-δ^{15}N

Planktonic foraminifera are heterotrophic protists who feed on particulate organic matter (POM) originating from primary production in the surface layer. The $\delta^{15}N$ of zooplankton in known to be 3‰ lower than that of their foodsource. The excretion of low $\delta^{15}N$ - ammonia in turn lowers the $\delta^{15}N$ of the suspended ammonia and therefore lowers the $\delta^{15}N$ of the food source of the foraminifera (Montoya et al., 2002). Regarding foraminifera species who feature dinoflagellate symbionts, the excreted low $\delta^{15}N$ ammonia is partly reassimilated by the symbionts. This effectively hides an eutrophic step and lowers the FB-$\delta^{15}N$ of symbiont bearing foraminifera compared to non symbiotic species (Ren et al., 2009). The FB-$\delta^{15}N$ of foraminiferas from the euphotic zone do not reflect a potential stratification or a consumption gradient within the ocean's upper layer since their food source consists only from POM formed in the surface layer by primary producers and not from the surrounding dissolved inorganic N in the water. For the organic N of tropical planktonic foraminifera we can conclude that the FB-$\delta^{15}N$ reflects the integrated $\delta^{15}N$ of the new N supply to the euphotic zone (Checkley and Miller, 1989), wheras non symbiontic species feature an offset of around 1‰ higher FB-$\delta^{15}N$. The temporal and spatial resolution of the data discussed in chapter 3 and 4 are strongly limited by the abundance of foraminifera and their preservation in the sediment. Using two different species therefore enables to combine those data and increase the resolution. Although the used foraminifera *Gsacc* and *Ndut* are not dwelling in the same depth, it is safe to assume that they reflect a common $\delta^{15}N$ signal. Since foraminifera do not feed directly on nitrate but on organic matter produced in the surface layer we do not expect any variations in FB-$\delta^{15}N$ between *Ndut* and *Gsacc* (Ren et al., 2009, 2012).

2.8 Analytical protocol

2.8.1 Sample cleaning

1. Put the uncleaned, crushed foraminifera tests into a 15ml centrifuge tube and add ≈10ml of pH adjusted (pH>8) 2% sodium-polyphosphate solution.
2. Sonificate for 1min. Skip this step if dealing with fragile tests.
3. Pour off the cleaning solution and fill the tube with milli-Q water. Let the sample settle and pour off the water. Repeat the rinsing 3 times.
4. Prepare the reductive reagent:
   Dithionic-citric acid: 500ml milli-Q water, 31gr sodium citrate ($Na_3C_6H_5O_7*2H_2O$), 10g sodium bicarbonate ($NaHCO_3$), 25g sodium dithionite ($Na_2S_2O_4$), adjust the pH with NaOH to pH=8.
5. Add 10ml of dithionite-citric acid to the sample.
6. Put the sample in a water bath at 80°C for 1h.
7. Pour off the cleaning solution and rinse the sample 3 times with milli-Q water as described above.
8. Transfer the sample into a clean 12ml glass vial using single dropplets of milli-Q water
9. Prepare the oxidative cleaning reagent:
   Persulfate-reagent: 2.5g potassium persulfate ($K_2S_2O_8$), 2.5g NaOH, 100ml milli-Q water
10. Add 5ml of persulfate reagent to the sample. Assure yourself that no test fragments stick to the glass vial wall.
11. Add the lid and put the sample into the autoclave (121°C for 65min)
12. Work in a clean environment from here on (e.g., laminar flow bench equipped with ammonium filter)
13. To pour off the cleaning solution, let the sample settle and remove the supernatant water with a previously combusted glass pipette and rinse the sample with milli-Q water. Repeat the last rinsing at least 5 times.
14. Dry the samples in a clean, evacuated oven over night.

2.8.2 FB-δ^{15}N-analysis protocol

1. Calculate the target sample mass according to the expected N content of the foraminifera (fig. 2.2) and target an N concentration of the vial of 10 to 15µM.
2. weigh-in the target mass (3-5mg) of cleaned sample into clean, previously combusted vials
3. Prepare a series of oxidation standards with concentrations bracketing the target sample concentration (e.g. 8µM, 12µM, 15µM, and 20µM)
4. Add 10µl/g_{sample} 4N HCl ACS grade to the sample, all the oxidation standards, and the blanks to dissolve the sample.

5. Prepare the oxidative reagent:
   Persulfate-reagent: 1g clean, recrystallized potassium persulfate ($K_2S_2O_8$), 1g clean ACS grade NaOH, 100ml milli-Q water(low temperature distilled)

6. Add 1ml of the persulfate reagent to each sample ($\approx$ 60 vials/run), 10 blank vials and all of the oxidation standards.

7. Put all the vials into the autoclave (121°C for 65min)

8. Centrifuge the samples for 10min at 4000rpm. Pipette the sample solution into a new clean vial to remove the calcite precipitates. To avoid the introduction of new contaminants, reuse the cap from the old vial.

9. Adjust the pH (6-8) of all the samples, oxidation standards and blank vials by adding 6N HCl ACS grade.

10. Inject 100µl of the sample solution to the vanadium(III) reactor in parallel with in-house standards of known N concentrations (1, 2.5, 10, 20µM) to determine the N concentration of the sample.

11. Harvest the *P. chlororaphis* bacteria after 5-6 days of growth, and resuspend them in a nitrate free medium.

12. Inject 1.5ml of the resuspended bacteria solution to clean, previously combusted 20ml headspace vials (max. 120vials). Cap the vials with milli-Q washed rubber caps and seal them.

13. Flush the bacteria vials with N_2 for 4 hours to ensure complete conversion of any residual N in the bacteria solution.

14. Calculate the injection volume according to the N content measurements with respect to the target amount N of 5 or 10 nmol.

15. Inject the sample nitrate solution and the oxidation standards to the bacteria solution. Combine always 3 blank vials and inject them as well.

16. Put the vials in the dark and let them sit over night.

17. After full bacterial conversion, add 10N NaOH solution to each vial to bind CO_2 and lyse the bacteria. Shake the vials, and add 2 drops of antifoam to each vial.

18. Measure the δ^{15}N of the N_2O in the vials with the mass spectrometer.

19. Reference the δ^{15}N values relative to the IAEA-N3 standard and correct the FB-δ^{15}N measurements for the contribution of the blank nitrogen.

3

Nitrogen isotope changes in the equatorial Atlantic as a response to Southern Ocean nitrate consumption

Lukas E. Oesch[1], Anja S. Studer[2], Daniel M. Sigman[3], Gerald H. Haug[1,2]

[1]Geological Institute, Department of Earth Sciences, ETH Zurich, Zurich, Switzerland
[2]Max Planck Institute for Chemistry, Climate Geochemistry Department, Mainz, Germany
[3]Department of Geosciences, Princeton University, Princeton NJ, USA

Abstract

At ODP Site 662 in the eastern equatorial Atlantic, foraminifera-bound δ^{15}N was measured on two species of foraminifera back to the penultimate glacial maximum 160,000 years ago. The main features of the combined record are δ^{15}N maxima at each of the two major deglaciations extending into the early interglacials, as well as a maximum centered on 80,000 years ago, near the marine isotope stage 5/4 transition which would be most easily caused by a rise in the preformed nitrate δ^{15}N of Subantarctic Mode Water. Here we propose a mechanism for low latitude δ^{15}N elevation during shifts in Southern Ocean nutrient consumption. It demonstrates that the low latitude surface ocean is affected by polar and subpolar biogeochemical change through the flow of intermediate waters.

3.1 Introduction

The deep ocean is the biggest carbon reservoir that interacts with the atmosphere on millennial timescales (Broecker, 1982). Previous work suggests that the deep ocean- atmosphere interaction is responsible for a significant part of the 100ppm change in atmospheric CO_2 concentration accompanying glacial interglacial changes (Lüthi et al., 2008). It is widely accepted that the Southern Ocean (SO) plays a key role connecting the deep ocean with the atmosphere (Knox and McElroy, 1984; Sarmiento and Toggweiler, 1984; Siegenthaler and Wenk, 1984). In the modern SO, CO_2 charged deep water is upwelled in the Antarctic Zone (AZ). Subsequent primary production is unable to assimilate as much carbon as the upwelling of carbon loaded nutrient rich deep-water releases, leaving most of the nutrients unused. This inefficient biological pump represents the biggest leak of CO_2 from the ocean to the atmosphere (Sigman et al., 2010). Sealing this leak by changing the efficiency of the SO biological pump is thought to alter the global carbon budget in the range needed for interglacial-glacial changes in atmospheric CO_2 concentrations (François et al., 1997; Martin and Fitzwater, 1988). Several high latitude studies have previously found evidence for a higher level of nitrate consumption during glacial times (François et al., 1997; Robinson and Sigman, 2008; Studer et al., 2015). In the AZ of the SO, diatom-bound δ^{15}N (DB-δ^{15}N) from the Pacific indicate more complete nitrate uptake during the last two ice ages as a result of strong upper ocean stratification (Studer et al., 2015). In the Subantarctic Zone (SAZ), the same pattern of greater ice age nitrate consumption is attributed to result from increased iron fertilization during glacial periods (Martin, 1990; Martínez-Garcia et al., 2014).

The less efficiently the biological pump operates in the high latitude SO, the higher is the concentration of residual nutrients transported northwards through Ekman pumping. These nutrient rich waters are then subducted near the Subantarctic front and become entrained into Subantarctic Mode Water (SAMW), supplying nutrients to upwelling zones in the low latitudes of the Pacific Ocean, along the western coast of South America (Toggweiler et al., 1991), and to the low latitudes of the Atlantic Ocean (Sarmiento et al., 2004). Here, we seek to analyze SAMW nitrate dynamics in the past, using nitrogen isotopes in order to track past changes in biochemical processes occurring in the SO surface waters and to identify the potential capability of the SO to significantly influence the ocean's most productive low latitude regions.

Stable nitrogen isotopes of organic matter encased in foraminifera tests pose a promising tool for acquiring insights into the marine nitrogen cycle. In contrast to bulk sedimentary δ^{15}N (where $\delta^{15}N = (({}^{15}N/{}^{14}N)_{sample}/({}^{15}N/{}^{14}N)_{air})1000$), foraminifera-bound δ^{15}N (FB-δ^{15}N) is not associated with diagenetic (Altabet et al., 1999b) or detrital (Schubert and Calvert, 2001) artifacts. Thus FB-δ^{15}N records pristine conditions. Foraminifera record the δ^{15}N of nitrate supplied to the euphotic zone because they feed on phytoplankton that have assimilated the nitrate. When the foraminifera sink through the water column and accumulate in sediments on the ocean floor, the foraminifera-bound organic matter is hermetically sealed within the calcite wall and bears the δ^{15}N of the consumed nitrate. Previous studies revealed δ^{15}N of shell bound organic matter from planktonic foraminifera *Globigerinoides sacculifer* (*Gsacc*) to be very close to the δ^{15}N of thermocline nitrate (Ren et al., 2009).

Changes in thermocline nitrate δ^{15}N can be caused by the main marine source of bio-available N (N fixation), the main sink (denitrification), and by preferential assimilation of ^{14}nitrate by primary producers in regions with partial nitrate consumption (Altabet and Francois, 1994). Locations where planktonic foraminifera record the nitrate δ^{15}N of SAMW are restricted to the low latitude Atlantic (Fig. 3.1) and the eastern equatorial Pacific where SAMW outcrops at the surface. However, unlike the equatorial Atlantic, the eastern equatorial Pacific is characterized by incomplete nitrate consumption where autochtonous N isotope fractionation (Altabet and Francois, 1994) could alter the source signal of SAMW nitrate δ^{15}N. In addition, extensive denitrification zones in the eastern tropical North Pacific (Liu et al., 2005) and the eastern tropical South Pacific (Robinson et al., 2007) also influence and overprint the nitrogen isotope sig-

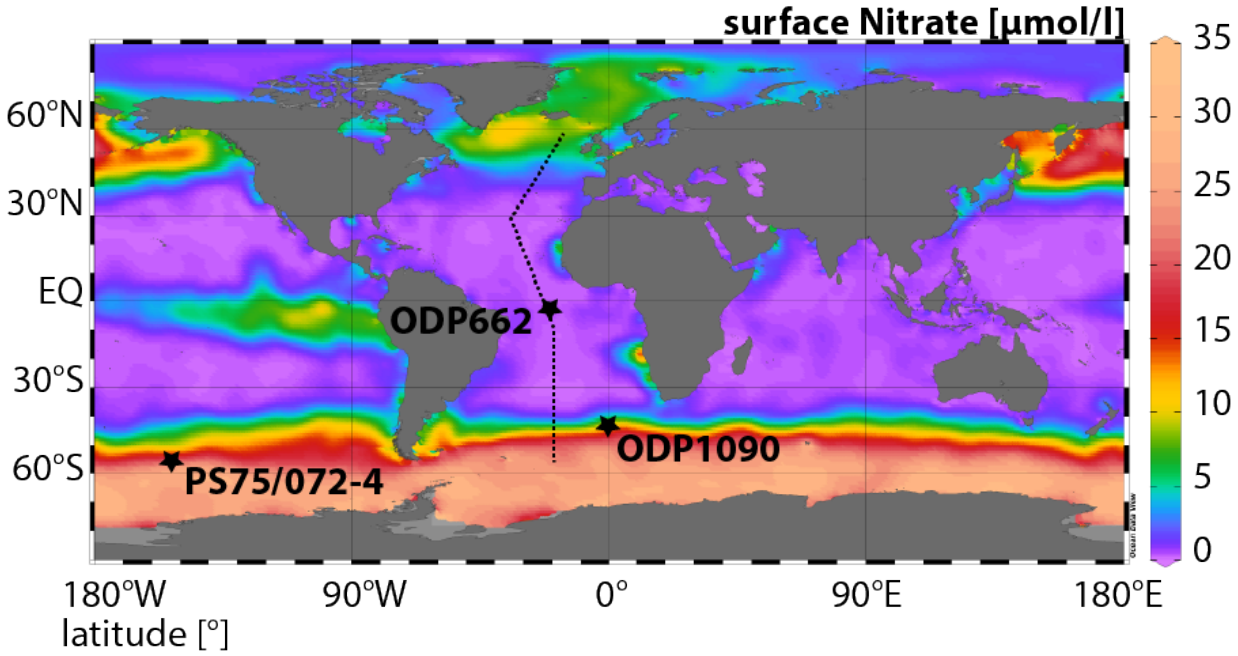

Figure 3.1 – ***Core locations in the context of surface nitrate concentrations*** *- Map of annual mean surface nitrate concentration, location of meridional cross-section used in Fig. 3.2 (dashed). In contrast to the eastern equatorial Pacific, the equatorial Atlantic is characterized by no residual surface nitrate, which we interpret as complete nitrate consumption. Locations of cores that are discussed in the main text are shown (black stars). Nitrate data from World Ocean Atlas 2013 (WOA13) (Locarnini et al., 2013).*

nal from SAMW, rendering the equatorial Pacific unsuitable to reconstruct changes in SAMW nutrient dynamics through time. As described below, in well-ventilated high production regions of the Atlantic equatorial upwelling N fixation and denitrification are not expected to occur. In such systems, where phytoplankton completely consume all of the available nitrate, no net fractionation due to partial assimilation occurs and the δ^{15}N of the export production should equal δ^{15}N of the supplied nitrate. Thus the Eastern Equatorial Atlantic (EEA) represents an ideal location to assess changes in the nitrate δ^{15}N of SAMW in the past.

Changes in EEA nitrate δ^{15}N over time could be caused by variations in whole-ocean nitrate δ^{15}N due to changes in relative fluxes of N fixation and denitrification. Alternatively, fractionation processes occurring in the source region of the upwelled waters could modify the nitrate δ^{15}N signal that is transported to the EEA by ocean currents. Placing constraints on either of these scenarios would be useful to understanding biogeochemical cycling in the past. The former scenario would provide an assessment of the nitrogen cycle of the whole ocean and its impacts on global marine biological production. The latter scenario would enable an assessment of nitrate consumption changes in the SO and a characterization of the strength and extent of the biogeochemical connection between high- and low latitudes.

Here, we present two EEA foraminifera-bound N isotope records from two different species over the last two glacial cycles (≈160 kyrs). Our records provide new insights into how nitrogen cycling in subducted SAMW reacted to changes in the level of nutrient consumption in the SO and how equatorial biogeochemistry was remotely controlled by polar and subpolar changes in nutrient consumption and productivity over the past two glacial cycles.

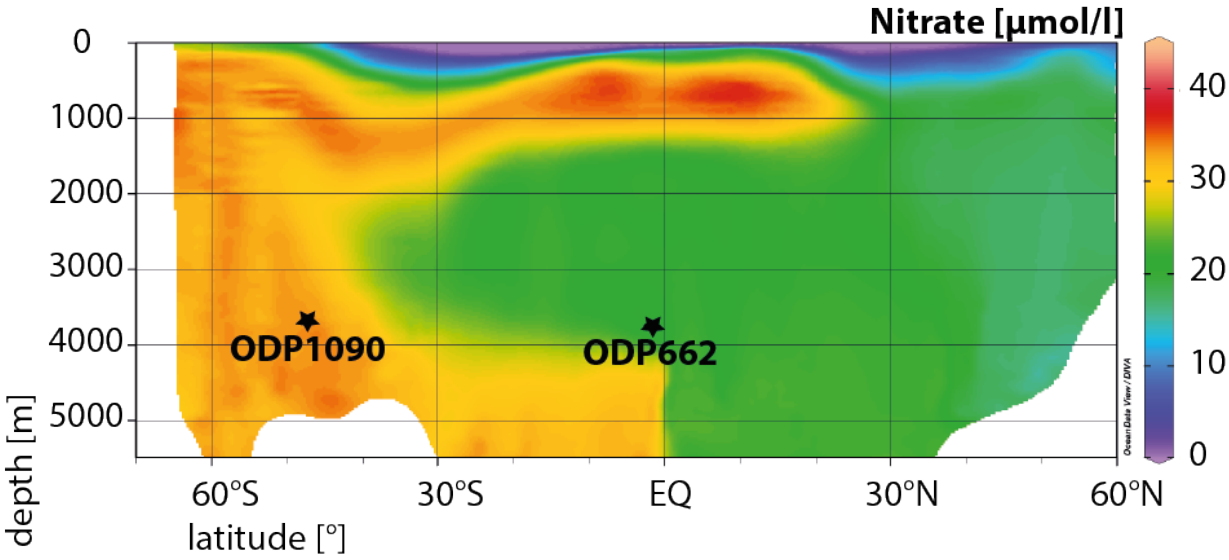

Figure 3.2 – ***Depth cross-section of Atlantic nitrate concentrations*** *- Meridional cross-section (average of 300km width) of nitrate concentrations through the Atlantic Ocean. Locations of cores that are discussed in the main text are shown (black stars). High nitrate bearing subsurface waters leaves the SO at intermediate depths propagating north to the low and mid latitude Atlantic. Nitrate data from WOA13 (Locarnini et al., 2013).*

3.2 Samples and Methods

3.2.1 Study site ODP 662

We performed foraminifera-bound N isotope measurements on samples from Ocean Drilling Program (ODP) Site 662 from the EEA (1°23.41 S, 11°44.35 W, 3831.8 mbsl, Fig. 3.1). The site is located in the western end of the Guinea Basin south of the South Equatorial Current in the main equatorial divergence zone (Ruddiman et al., 1988). Surface water in the EEA is completely depleted in nitrate (Fig. 3.1) due to complete consumption close to the surface. During Northern Hemisphere summer, the southern trade winds lead to divergence and upwelling of cool, nutrient rich waters originating in the SO (Fig. 3.2). Primary production as measured by chlorophyll concentration is highest from June to October (Pérez et al., 2005). Given its location at the equatorial divergence which upwells SAMW, ODP Site 662 is ideally suited to measure preformed nitrate δ^{15}N of SAMW. While carbonate dissolution is a potential concern for any study that utilizes foraminifera, we are fairly confident that this concern is not an issue at Site 662. The modern ocean floor at this site does not reach calcite under saturation. Additionally, previous work in the EEA has shown that the lysocline has been below 3800m water depth during the entire Pleistocene (Bickert and Wefer, 1996). Thus, within our period of study, we expect well-preserved foraminifera. Alkenone Sea Surface Temperatures (SST) and alkenone Mass Accumulation Rate (MAR) data from ODP Site 662 were previously published by Herbert et al. (2010) and Lawrence et al. (2013); planktonic stable oxygen and stable carbon isotope data were published by Karlin et al. (1989).

3.2.2 Materials and age model

The uppermost 8.3m of ODP Site 662 hole A were sampled every 5 to 10 cm, yielding a total of 152 samples. At a depth of 3m, the gap between section 1 and 2 was filled with four samples from hole B, sampled with 6cm spacing. The composite depth scale was transferred from the shipboard party report

from ODP Leg 108 (Ruddiman et al., 1988). The sedimentation rates at Site 662 vary from from 2 to 10 cm/kyr with an average of 5.7cm/kyr. The age model was previously published by Herbert et al. (2010) and is based on the alignment of foraminiferal benthic δ^{18}O to the global benthic oxygen isotope stack (Lisiecki and Raymo, 2005).

3.2.3 FB-δ^{15}N analysis

We analyzed non-spinose thermocline dweller *Neogloboquadrina dutertrei* (*Ndut*) and the symbiotic euphotic zone dweller *Globigerinoides trilobus sacculifer* and *Globigerinoides quadrilobatus sacculifer* herein combined as *Gsacc*. The sediment samples were sieved at 250µm and 10-15 mg (400-500 individuals) of two foraminifera species were manually picked from the coarse fraction (>250µm). The foraminifera were gently crushed to open the chambers and cleaned following the protocol for persulfate cleaning of Ren et al. (2015). FB-δ^{15}N was analyzed using the denitrifier method according to Sigman et al. (2001) (updated by Weigand et al. (2016)). In short, 3-5mg of clean sample foraminifera shell was dissolved with HCl (10µl/mg ACS grade, 4N) to release the organic matter nitrogen into solution. Subsequently the sample nitrogen was oxidized to nitrate by adding an alkaline potassium persulfate reagent. The nitrogen content of the sample was measured by chemiluminescence (Braman and Hendrix, 1989). Planktonic foraminifera of the tropical Atlantic contain between 3.5 and 4.5 µmolN/g calcite. For bacterial conversion of nitrate into nitrous oxide, the natural abundant denitrifier *P. chlororaphis* was used, which lacks the enzyme to convert N_2O into N_2. The N isotopic ratio of the N_2O was measured with a Thermo MAT253 mass spectrometer (analytical precision < 0.03‰) following the protocol of Weigand et al. (2016). Measured δ^{15}N values were referenced to the international nitrate isotope standard (IAEA-NO3, δ^{15}N = 4.7‰). FB-δ^{15}N data were corrected for the contribution of the blank nitrogen (on the order of 2 - 3.5%) through parallel analysis of amino-acid standards of known isotopic composition and concentration. Typical $\delta^{15}N_{Blank}$ ranges between 2‰ and 8‰. Roughly 50% of the samples were analyzed in full procedural replication, resulting in an overall standard deviation of 0.2‰ (Fig. 3.3).

3.2.4 Calculation of FB-δ^{15}N - thermocline

Previous work on foraminifera bound nitrogen (Ren et al., 2009) revealed FB-$\delta^{15}N_{Gsacc}$ to be 1-1.5‰ lower than FB-$\delta^{15}N_{Ndut}$. This offset between symbiotic species *Gsacc* and non-symbiotic species *Ndut* is most likely caused by the uptake of low δ^{15}N ammonia excreted by the symbionts of *Gsacc* and the subsequent internal N cycle to the host, which would lower the δ^{15}N of the foraminifera organic N. FB-$\delta^{15}N_{Gsacc}$ is thought to be very close to the δ^{15}N of its food source and thus reflects the δ^{15}N of supplied nitrate. In contrast, modern measurements of the non symbiotic thermocline dwelling species *Ndut* reveals a δ^{15}N elevation of around 1‰ with respect to the nitrate consumed in their ecosystem. Throughout the measured record FB-$\delta^{15}N_{Gsacc}$ (Fig. 3.3A) shows a stable background of 7‰ and FB-$\delta^{15}N_{Ndut}$ of 8‰, which indicates a δ^{15}N of nitrate to be elevated by 2‰ from the modern ocean mean of 5‰. The very high correlation between the two species facilitates the calculation of a combined thermocline δ^{15}N record (FB-$\delta^{15}N_{TC}$) (Fig. 3.3B). To analytically remove the trophic difference between FB-$\delta^{15}N_{Gsacc}$ and FB-$\delta^{15}N_{Ndut}$ we calculated the offset between FB-$\delta^{15}N_{Gsacc}$ and FB-$\delta^{15}N_{Ndut}$ at sample depths with replicated measurements for both the species only (Fig. 3.3C). The resulting mean offset (0.98‰) was subtracted from the FB-$\delta^{15}N_{Ndut}$ values, adjusting them to FB-$\delta^{15}N_{Gsacc}$. The offset is fairly constant between the two records, supporting this approach.

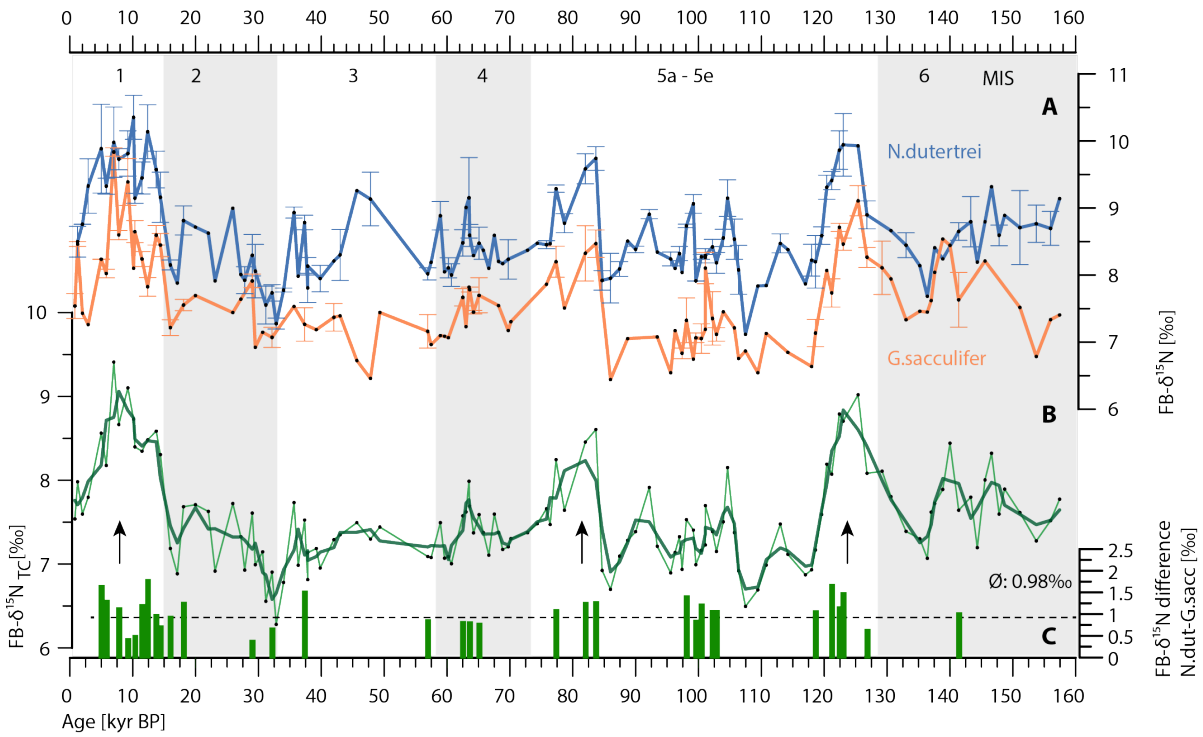

Figure 3.3 – ***Measured and compiled FB-δ^{15}N data from equatorial Atlantic Site ODP662*** *- **A:** FB-δ^{15}N [‰] measured on the thermocline dwelling species Ndut (blue) and on the euphotic zone- dwelling species G.Sacculifer (orange). Error bars indicate standard deviation on full procedural replicates. Average standard deviation Ndut: 0.21‰, Gsacc=0.17‰ -* ***B:*** *FB-$\delta^{15}N_{TC}$ [‰]. As a consequence of the good correlation, a combined thermocline-FB-δ^{15}N was calculated and a three-point center running average was superimposed (dark green) -* ***C:*** *Difference in FB-δ^{15}N between Gsacc and Ndut (green bars) at samples with replicate measurements for both species and average difference (dashed line). In the background (grey shaded) marine isotope stages according to (Lisiecki and Raymo, 2005)*

3.3 Results

Throughout the last 160 kyr, average FB-$\delta^{15}N_{TC}$ is relatively stable at (7.2 - 7.5‰) interrupted by three short termed (8 - 10 kyr) maxima that represent an increase of 2‰ from the baseline. The first occurs at the penultimate deglaciation centered at Marine Isotope Stage (MIS) 5e, the second at 84 kyr at the MIS 5b/5a transition and the last one at termination 1 extending into the early Holocene. Before 130 kyr FB-δ^{15}N is stable at a higher level of around 7.5‰. At 132 kyr it increases to 9‰ before it drops to 7‰ at 120 kyr. Between 70 kyr and 20 kyr δ^{15}N has a slightly higher variability and reaches its minimum of 6.4‰ at 34 kyr to rise again to 9.5‰ into the early Holocene. The stable average background of FB-$\delta^{15}N_{Gsacc}$ indicates a δ^{15}N of the nitrate supply around 7-7.5‰, which is elevated relative to the modern ocean mean of 5‰.

3.4 Interpretation and Discussion

The modern EEA is characterized by seasonal upwelling with a deep thermocline and weak upwelling from January to April and a shallow thermocline with strong upwelling between May and October (Christian and Murtugudde, 2003). We interpret FB-δ^{15}N from ODP662 to reflect the nitrate δ^{15}N of the source water controlled by processes occurring at higher latitudes where the water originates. Within

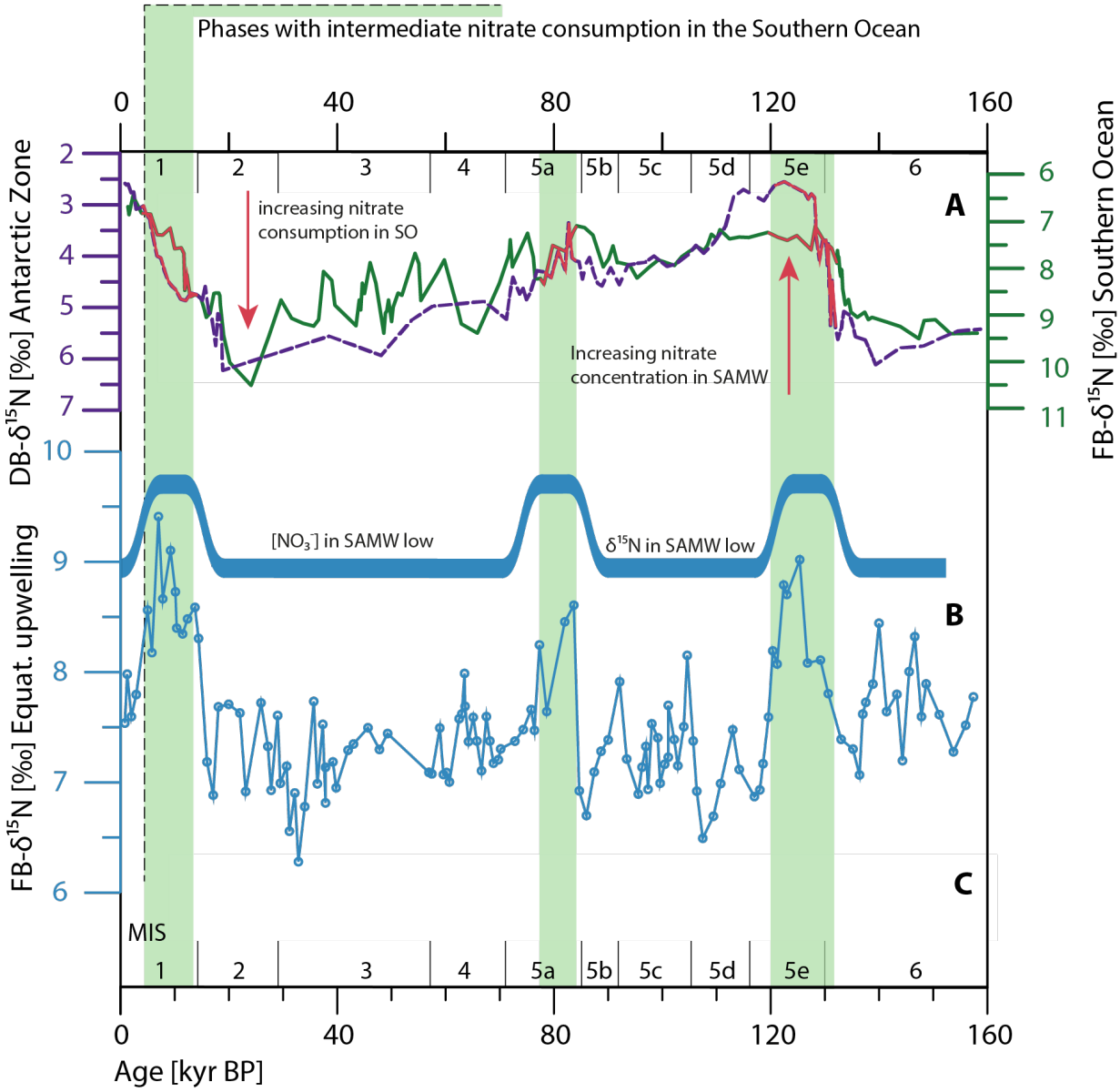

Figure 3.4 – ***Low latitude nitrate δ^{15}N as a result of SO nitrate consumption levels - A:*** *DB-δ^{15}N [‰] from core PS75/072-4 from the Antarctic zone (dashed) (Studer et al., 2015) and FB-δ^{15}N [‰] from Subantarctic Zone ODP 1090 (solid) (Martínez-Garcia et al., 2014)-* ***B:*** *FB-$\delta^{15}N_{TC}$ [‰] from ODP662 (this study) with schematic outline of nitrate δ^{15}N in SAMW -* ***C:*** *expected origin of equatorial upwelling water at Site ODP662 (Straub et al., 2013a). During phases with intermediate consumption in the SO, nitrate δ^{15}N of Atlantic equatorial upwelling Site 662 is elevated.*

the well ventilated high nutrient waters of the EEA we do not expect any local N isotope fractionation processes to occur through biological N fixation or bacterial denitrification. N fixation is unlikely to represent a large fraction of the N supply in a region with active nitrate supply by upwelling, whereas denitrification only happens in ocean suboxic zones (Brandes et al., 1998; Knapp et al., 2012; Marconi et al., 2015; Meckler et al., 2011; Straub et al., 2013a). Neither do we expect the nitrate δ^{15}N at Site 662 to be influenced by fractionation associated with partial nitrate assimilation (Altabet and Francois, 1994). Unlike in the equatorial Pacific, where nitrate δ^{15}N increases as nitrate concentrations decline off the axis of upwelling, upwelled nutrients in the modern tropical Atlantic are completely consumed close to the locus of upwelling, leaving only scarce residual nitrate left at the surface (Fig. 3.1). Therefore, the three FB-δ^{15}N maxima at Site 662 cannot be explained as a result of more complete nitrate consumption. In order to explain the FB-δ^{15}N peaks, we propose a scenario that suggests temporal changes in the δ^{15}N of the nitrate that is upwelled in the EEA.

3.4.1 Origin of equatorial upwelling water

Both the North Atlantic and the SO ventilate the modern Atlantic Ocean. Most of its volume is comprised of cold North Atlantic Deep Water (NADW) with high salinity flowing southwards, underlain by even colder and more dense Antarctic Bottom Water (AABW) originating in the southern hemisphere's polar zone. SAMW, which is formed near the Subantarctic front, is significantly warmer than AABW and NADW and also less saline. The resulting lower density causes SAMW to overlay NADW. SAMW propagates northwards reaching intermediate depths in the EEA and is the main supplier of waters to equatorial upwelling zones in the EEA (Sarmiento et al., 2004). Like underlying Antarctic Intermediate Water (AAIW), it is characterized by low salinity and a high concentration of preformed nutrients. During the last two glacials (MIS 4-2 and MIS 6) the Atlantic Overturning Circulation (AMOC) underwent substantial changes when NADW shoaled and the density gradient between southern- and northern waters was strengthened. Thus during these glacials, the upper part of the water column (<2000m depth) was nearly entirely ventilated by Northern water whereas the deeper part was filled with AABW (Curry and Oppo, 2005). At the equator, it is unclear if this shallower Glacial North Atlantic Intermediate Water (GNAIW) suppressed SAMW from reaching low latitude intermediate depths or just diluted its impact (Marchitto and Broecker, 2006; Lynch-Stieglitz et al., 2007; Meckler et al., 2013). An observed reduction in N fixation in the Caribbean subtropical Atlantic during MIS 4-2 was interpreted to result from a change in the upwelled water at the equator from SAMW characterized by high excess P to GNAIW with low excess P (Straub et al., 2013a). Based on these previous data, it may be that the origin of the nitrate upwelled in the EEA changed from southern sourced during MIS 5 and 1 to northern sourced during MIS 4-2 in the course of our record. However, our records do not show substantial changes in nitrate δ^{15}N from MIS 5d-5b compared to MIS 4-2. This allows for two possible interpretations. Either the nitrate δ^{15}N of GNAIW is similar to that of modern SAMW in a way that a water source change is not reflected in the FB-δ^{15}N data or GNAIW did not reach ODP Site 662 during peak glaciation. Thus, a possible impact of GNAIW to equatorial upwelling Site 662 during MIS 4-2 cannot be excluded. Nevertheless, if a change in northern vs southern source water did occur at Site 662 during MIS 4-2, it cannot explain the three FB-δ^{15}N elevations, as they occur during times when there is no evidence for northern GNAIW formation.

3.4.2 High latitude influence on low latitude nitrate δ^{15}N

The δ^{15}N of nitrate leaving the SO propagates northwards within SAMW. The rather weak density gradient between SAMW and underlying NADW allows for considerable mixing. Whether or not low latitude

thermocline nitrate δ^{15}N is elevated not only depends on the δ^{15}N of nitrate leaving the SO, but also on the impact of the subsequent mixing of SAMW with underlying deep water.

For the last glacial cycle previously published FB-δ^{15}N from the SAZ (Martínez-Garcia et al., 2014) and DB-δ^{15}Nfrom the AZ (Studer et al., 2015) show the same pattern of a high degree of nutrient consumption during MIS 6 and MIS 4-2 and a low degree of nutrient consumption during MIS 5e-5a and the Holocene (Fig. 3.4A). In the SAZ, nitrate consumption is more complete during ice ages as a result of enhanced iron fertilization and greater productivity (Martínez-Garcia et al., 2014) whereas in the AZ, ice age nitrate consumption was increased due to reduced nutrient supply to the euphotic zone as a result of glacial stratification of the Antarctic water column (Studer et al., 2015).

The interglacial periods in the SAZ and AZ, on the other hand, were characterized by low degrees of nitrate consumption (Fig. 3.4A) as a result of vigorous upwelling in the AZ and a decline in export production in the SAZ (Martínez-Garcia et al., 2014; Studer et al., 2015). During the time intervals in between those two extremes, SO nitrate consumption reached intermediate values, namely during the last two glacial terminations as well as during the MIS 5b/5a transition. These periods appear to coincide with the three observed maxima in FB-δ^{15}N at ODP662 (Fig. 3.4B).

We propose a conceptual model, which is able to explain the short termed low latitude FB-δ^{15}N maxima in the context of SO nitrate consumption (Fig. 3.5). Assuming the Nitrate Concentration ([NO_3^-]) of the deep ocean water and the degree of mixing with SAMW to be constant in time, [NO_3^-] of SAMW leaving the SO determines the impact of the mixing with deep water on low latitude nitrate δ^{15}N. The mixing fluxes more efficiently dilute the SAMW nitrate δ^{15}N nitrate the greater the [NO_3^-] gradient between SAMW and underlying deep water. Furthermore, both [NO_3^-] of SAMW and its nitrate δ^{15}N depend on the level of nitrate consumption in the SO, i.e., the degree to which nitrate has been assimilated by phytoplankton growth. Rayleigh fractionation dynamics predict that as the degree of nitrate consumption progresses and thus nitrate concentrations decline, the δ^{15}N of the residual nitrate increases. This adds up to the nitrate with the highest elevated isotopic signal being the lowest concentrated and thus the most vulnerable to dilution and vice verse.

In particular, this implies that in a situation with high SO nitrate consumption (Fig. 3.5A), the δ^{15}N of the residual nitrate is strongly elevated but the water is almost depleted in nitrate. While propagating northwards, the mixing flux with the underlying deepwater is able to dilute this elevated δ^{15}N nitrate completely. This leads to an entire alleviation of the SO nitrate consumption signal once it arrives at low latitudes. On the other hand, in a situation with a low degree of nitrate consumption in the SO (Fig. 3.5C) [NO_3^-] remains high and thus resistant against dilution. However, in this situation nitrate δ^{15}N is not elevated and does not differ from deep ocean δ^{15}N in the first place. During periods with intermediate nitrate consumption in the SO (Fig. 3.5B), at times when the consumption regime switches from almost complete to incomplete consumption, the nitrate δ^{15}N is elevated due to partial nitrate assimilation. However, in contrast to the glacial situation, the residual water is not completely depleted in [NO_3^-]. During those time intervals of intermediate degrees of nitrate consumption in the SO the N isotopic signal reaches lower latitudes, because its elevated [NO_3^-] reduces the impact of mixing and dilution with deep water.

3.4.3 Variability in equatorial upwelling

Alkenone mass accumulation rates (Fig. 3.6A) (Lawrence et al., 2013) from Site 662 suggest pulses in productivity that are paced by Earth's precessional cycle (21 kyr). Coinciding with the elevated FB-δ^{15}N (Fig. 3.6B) reported in this study, SST was warmer (Herbert et al., 2010) and productivity in the EEA was lower. In addition, Molfino and McIntyre (1990) performed coccolithophoric assemblage studies at a nearby site, which show minimal occurrence of warm water species *F. Profunda* during negative precession phases. This interpreted as a periodic deepening of the nutricline due to low equatorial upwelling.

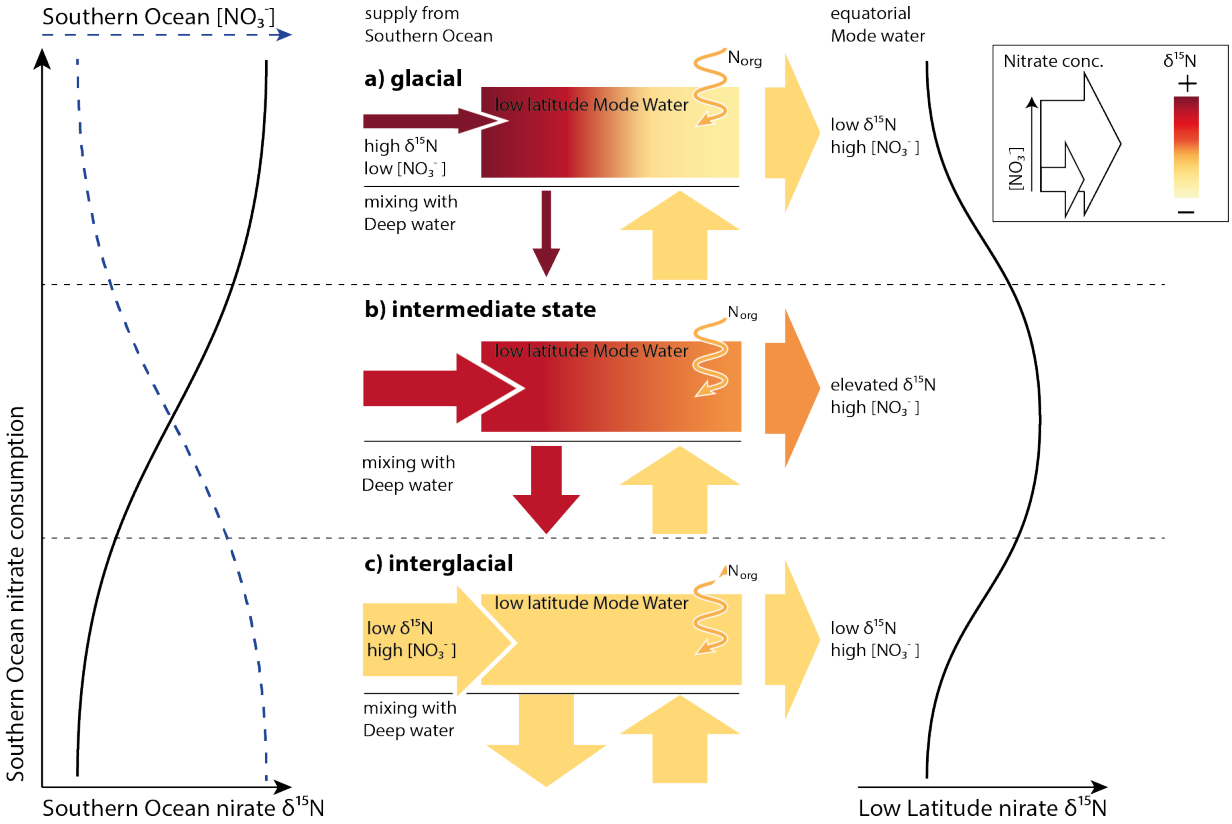

Figure 3.5 – ***Conceptual model of isotopic mixing as process sensitive to nitrate concentration in SAMW*** *- **A:** during glacials, SO nitrate consumption level is high causing a strong isotopic fractionation of nitrate. Remaining water that feeds SAMW exhibits low nitrate concentration [NO_3^-] and high nitrate $\delta^{15}N$. Underlying deep-water features high [NO_3^-]and a nitrate $\delta^{15}N$ of ocean mean (5‰). Because mixing is more effective the greater the [NO_3^-] gradient, it causes nitrate $\delta^{15}N$ and [NO_3^-] of SAMW to adjust to deep water while flowing northwards. This results in low nitrate $\delta^{15}N$, high [NO_3^-] equatorial Mode Water - **C:** During interglacials, SO nitrate consumption level is low. Thus SAMW leaving the SO features high [NO_3^-] and a nitrate $\delta^{15}N$ close to ocean mean. Mixing during northwards propagation has little to no effect, leading to equatorial Mode Water with high [NO_3^-] and a nitrate $\delta^{15}N$ close to 5‰ - **B:** In a suggested state with intermediate consumption the source water bears higher [NO_3^-] than during glacials but its nitrate $\delta^{15}N$ is elevated due to partial nitrate assimilation. Thus the efficiency of mixing is tempered and the elevated nitrate $\delta^{15}N$ will reach the low latitudes.*

Thus, FB-δ^{15}N partly correlates with equatorial upwelling strength, with low equatorial upwelling intervals coinciding with elevated FB-δ^{15}N. However, although the temporal coherence is compelling, we argue against a connection of equatorial upwelling strength and FB-δ^{15}N. Weak upwelling is not likely to cause a FB-δ^{15}N elevation. According to Rayleigh fractionation dynamics, only an increase in nitrate consumption would lead to an elevation in FB-δ^{15}N. However, nitrate consumption in the modern EEA is already complete, such that the FB-δ^{15}N elevations during precessional minima cannot be caused by an even more complete consumption. Furthermore, our FB-δ^{15}N record does not show a regular pacing of Earth's precessional cycle as observed in other equatorial upwelling data (Mc Intyre and Ruddiman, 1989; Nürnberg et al., 2000; Herbert et al., 2010; Straub et al., 2013a) but singular events of apparent correlation. The three observed maxima in FB-δ^{15}N (MIS 5e, MIS 5b/5a, and MIS 1) each take place during minima in precession parameter and thus low equatorial upwelling.

We explain the distinct temporal coherence of FB-δ^{15}N maxima and equatorial upwelling strength with solar insolation as a mutual cause for equatorial upwelling dynamics and SO productivity changes. As

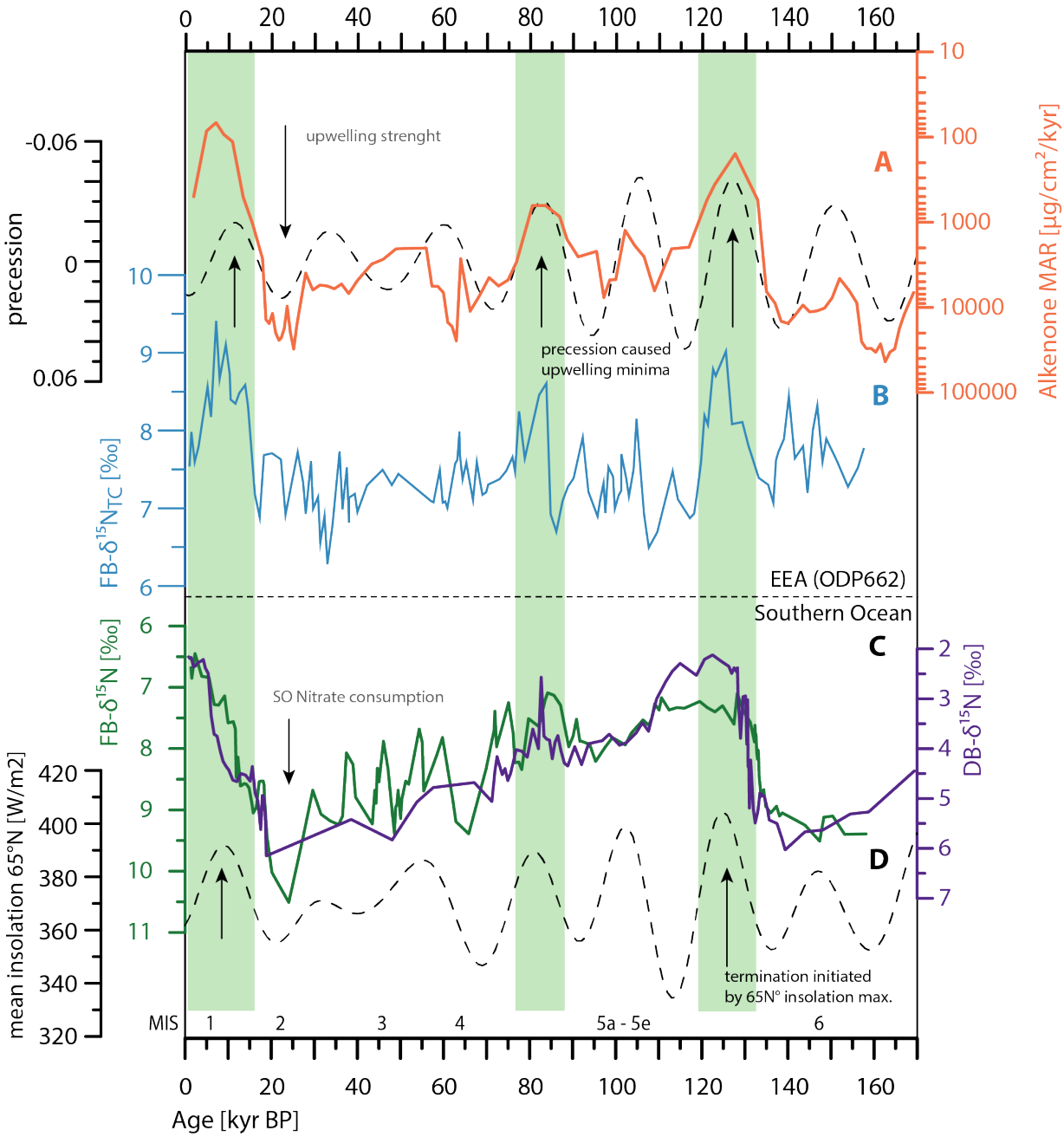

Figure 3.6 – ***Equatorial upwelling proxies compared to Southern Ocean climate - A:*** *ODP662 (Lawrence et al., 2013) as a proxy for primary production overlain by precession parameter (dashed) modeled after (Laskar et al., 2004)* ***- B:*** *FB-δ^{15}N [‰] from ODP662 (this study) calculated combination from two different species* ***- C:*** *SO consumption proxies DB-δ^{15}N [‰] from Antarctic core P275/072-4 (purple) (Studer et al., 2015) and FB-δ^{15}N [‰] from Subantarctic core ODP1090 (green)(Martínez-Garcia et al., 2014) - D: Modeled annual mean insolation at 65°N (Laskar et al., 2004).*

described above, SO productivity changes are likely to cause a nitrate δ^{15}N elevation in SAMW. The required intermediate consumption levels occur during times when the global climate system switches from colder to warmer states or back, which is triggered by changes in Northern Hemisphere summer insolation (Imbrie, 1982). This insolation (Fig. 3.6D) is affected by the net influence of the combined orbital variations of Earth's precession, obliquity, and eccentricity.

At the same time, equatorial upwelling is known to be controlled by insolation changes driven by Earth's precessional cycle (Fig. 3.6A) (Mc Intyre and Ruddiman, 1989; Molfino and McIntyre, 1990). In times with perihelion during Northern Hemisphere summer (minimal precession parameter, Fig. 3.6A,B), equatorial divergence is weak due to a more northwards position of the Inter Tropical Convergence Zone (ITCZ) and thus a strong African monsoon. However, in times with perihelion position during Northern Hemisphere summer, 65°N insolation is at the maximum as well (Fig. 3.6D), potentially triggering a deglaciation (Broecker, 1984; Imbrie et al., 1993; Raymo, 1997). As discussed above, the level of nitrate consumption in the SO is observed to change from complete nitrate consumption during glaciation to incomplete during interglacials (Fig. 3.6C). The intermediate level of nitrate consumption, which leads to an elevation of nitrate δ^{15}N in the EEA, takes place during the transition from glacial to interglacial climate. Intensified Northern Hemisphere insolation thus appears to trigger upwelling strength and intermediate consumption levels in the SO independently. This is supported by the observation that not each precession minima coincides with a FB-δ^{15}N maxima, but the switches in nitrate consumption leading to a FB-δ^{15}N maxima coincide with precession minima.

3.5 Conclusion

We measured FB-δ^{15}N on the two foraminifera species *Gsacc* and *Ndut* from sediments from the EEA Site ODP662 back to the penultimate glacial maximum (160 kyr BP-0) and calculated a combined thermocline FB-δ^{15}N record.

- We found a stable background FB-δ^{15}N of 7-7.3‰ interrupted by three (5-8 kyr) maxima at each of the terminations and one close to the 5b/5a transition (82 kyr BP).
- The FB-δ^{15}N cannot be explained by temporal changes in N fixation or denitrification. Neither can more complete nitrate consumption explain the positive excursions in FB-δ^{15}N, since nitrate consumption is already complete in modern EEA (Locarnini et al., 2013).
- We interpret FB-δ^{15}N of ODP Site 662 to reflect changes in the δ^{15}N of preformed nitrate of upwelled SAMW, originating in the SO.
- We present a mechanism for how changes in SO nitrate consumption may lead to short term excursions in low latitude thermocline nitrate δ^{15}N. During times of intermediate levels of nutrient consumption in the SO, the residual nitrate concentration is adequately high and its δ^{15}N elevated such that it is not diluted with low nitrate δ^{15}N deep water while propagating northwards to the equator.
- We explain the apparent correlation of FB-δ^{15}N with the strength of equatorial upwelling during our study period with solar insolation as mutual cause. Both low latitude trade winds, which in turn influence upwelling strength, and glacial terminations are known to follow insolation changes on Milancovic-scale (Mc Intyre and Ruddiman, 1989; Sigman et al., 2010).

Our data suggest that nitrogen cycling in the EEA is strongly linked to the SO. Since SAMW does not only supply EEA but also fills much of shallow subsurface of the global low latitude ocean, it delivers the ocean's most productive regions around the globe with nutrients. With regard to the reconstructed changes in SO nutrient consumption and productivity (Lawrence et al., 2013; Martínez-Garcia et al., 2014; Studer et al., 2015) during the Pleistocene, teleconnections to equatorial upwelling systems in the Atlantic, the eastern equatorial Pacific, and coastal upwelling systems on South America and Africa should emerge.

4

Incomplete Nitrate consumption in the early Pleistocene equatorial Atlantic

Lukas E. Oesch[1], Anja S. Studer[2], Daniel M. Sigman[3], Gerald H. Haug[1,2]

[1]Geological Institute, Department of Earth Sciences, ETH Zurich, Zurich, Switzerland
[2]Max Planck Institute for Chemistry, Climate Geochemistry Department, Mainz, Germany
[3]Department of Geosciences, Princeton University, Princeton NJ, USA

Abstract

During the Plio-Pleistocene transition (2.9 - 2.4 Million years Before Present (Myr BP)), Earth's climate and ocean circulation underwent substantial changes. The focus is here on the equatorial Atlantic Ocean and its response to the intensification of northern hemisphere glaciation at 2.7 Myr BP. At ODP Site 662 in the Eastern Equatorial Atlantic, foraminifera-bound δ^{15}N was measured on two species of planktonic foraminifera through the Plio-Pleistocene transition. The main feature is an onset of obliquity paced 41 kyr cycles at 2.7 Myr BP, with minima in δ^{15}N coinciding with maxima in benthic δ^{18}O. Glacial periods with lower sea surface temperatures, higher productivity, and lower foraminifera-bound δ^{15}N (FB-δ^{15}N) alternated with interglacial phases, characterized by warm sea surface water, low production and higher δ^{15}N. These simple correlations of δ^{15}N with climate parameters are not observed over the last 160 kyr of the late Pleistocene at this site. Moreover, the background FB-δ^{15}N between 2.4 and 2.9 Myr BP is 0.5‰ lower than over the last 160 kyr. We propose that the cyclic changes in FB-δ^{15}N starting at $\approx$ 2.65 Ma are due to obliquity paced contractions of the Atlantic warm pool, resulting in higher nitrate concentration in the waters upwelled in the equatorial Atlantic (Lawrence et al., 2013). Unlike in the late Pleistocene, the nitrate concentration in the water below the warm pool (which is ultimately sourced from Subantarctic Mode Water) was adequately high that nitrate consumption was incomplete along the equator during the obliquity-paced Plio-Pleistocene cold intervals, causing the observed decline in FB-δ^{15}N during those intervals. The lower mean FB-δ^{15}N over the entire investigated Plio-Pleistocene period suggests that SAMW nitrate δ^{15}N was lower during this period, consistent with Sub Antarctic nitrate consumption being weak during the Pliocene and early Pleistocene due to a lack of dust-derived iron input at that time (Martínez-Garcia et al., 2011; Lawrence et al., 2013).

4.1 Introduction

The warm climate of the Pliocene is of interest to scientists as an analogue for anthropogenic warming (Kürschner et al., 1996; Haywood et al., 2000). It was a sustained period comparable to what Earth will face within the next centuries (Rogelj and Knutti, 2016), with a global mean temperature of 3-4°C warmer than today (Dowsett et al., 2009) and atmospheric CO_2 levels around 400 to 450ppm (Raymo et al., 1996; Seki et al., 2010; Bartoli et al., 2011; Martínez-Botí et al., 2015). At 2.7 Myr BP, intensified northern hemisphere glaciation and the emergence of obliquity paced glacial cycles changed the climate drastically. Understanding the transition, its cause and effects would improve our understanding of global climate system feedbacks and the biogeochemical processes involved. Although the detailed mechanisms leading to the intensified glaciation are not understood yet, it is known that simultaneous tectonic activity including the closure of the Panama seaway (Keigwin, 1982), and the Indonesian through-flow (Cane and Molnar, 2001) and increased Himalayan uplift (Raymo et al., 1988) were occurring simultaneously with prominent oceanographic changes such as shoaling of the thermocline (Philander and Fedorov, 2003) and increased North Pacific stratification (Haug et al., 1999). As a consequence, altered heat transport and decreased atmospheric CO_2 (100-150ppm CO_2, Seki et al. (2010)) led to a shift into Pleistocene climate characterized by intensified glacial interglacial cycles.

The reduction in atmospheric CO_2 over the Plio-Pleistocene transition may have been due to enhanced sequestration in the deep ocean, due to changes in polar ocean regions(Knox and McElroy, 1984; Sarmiento and Toggweiler, 1984; Siegenthaler and Wenk, 1984). The efficiency of the biological pump to sequester CO_2 into the deep ocean is set by the ratio of preformed nutrients to remineralized nutrients in the ocean interior (Sigman et al., 2010). Remineralized nutrients derive from the production of organic matter by phytoplankton in the euphotic zone. The production of organic matter by photosynthesis binds inorganic carbon. The transport into the deep ocean as export production and subsequent remineralization into inorganic compounds pumps this carbon effectively into the ocean interior. Preformed nutrients, on the other hand, originate from dissolved nutrients in the ocean's surface that have not been taken up by biology but instead transported into the ocean interior along with subducting watermasses. This incomplete assimilation of upwelled nutrients leads to a net emission of sequestered deep ocean carbon (Sigman et al., 2010). In the modern ocean, southern sourced Antarctic Bottom Water (AABW) features a high ratio of preformed:remineralized nutrients and thus represents a carbon leak to the atmosphere. Northern sourced North Atlantic Deep Water (NADW), on the other hand, represents a more efficient biological pump due to its low amount of preformed nutrients.

4.1.1 General situation

The late Pliocene and early Pleistocene is characterized by a generally warmer climate with lower meridional temperature gradients. In the course of the intensification of Northern Hemisphere Glaciation (NHG), a sudden decline in high latitude productivity has been documented in the North Pacific (Haug et al., 1999), the Southern Ocean (SO) (Sigman et al., 2004), as well as in the North Atlantic (Lawrence et al., 2013). At the same time, obliquity paced glacial cycles emerged (Lisiecki and Raymo, 2005) and sudden pulses of very high glacial productivity are seen as high C_{37} alkenone Mass Accumulation Rate (MAR) from the Eastern Equatorial Atlantic (EEA) up to 41°N (Lawrence et al., 2013). Since productivity changes appear within the whole Atlantic basin simultaneously, a common mechanism able to explain all the processes is needed.

Lawrence et al. (2013) proposed a conceptual model that explains both the high latitude productivity declines as well as the productivity pulses in the low latitudes. According to their theory, global cooling led to a bihemispheric equatorward shift in the westerly winds, moving the zone of maximum upwelling

equatorward. Focusing on the SO, this would reduce upwelling in the Antarctic Zone (AZ) allowing stratification to strengthen and causing the reduction in productivity. At the same time, upwelling in Subantarctic Zone (SAZ) would increase and shift the subduction of Subantarctic Mode Water (SAMW) northward. Altogether, this shoaled the isopycnals of the Atlantic thermocline and raised the nutrient content of the waters. During the early Pleistocene glacials, a threshold was reached where those nutrient rich mid-depth waters outcropped in the equatorial Atlantic surface ocean, leading to the observed productivity pulses discussed above. However, up to now there has been no validation for the cause of the increased production at low latitudes, i.e. whether nutrient supply increased, local upwelling strengthened or the degree of nutrient consumption increased.

By tracking both nutrient conditions and productivity, we can discern among these possibilities. Along with phosphate, nitrate is a major nutrient for primary productivity. Stable nitrogen isotopes track processes in the nitrogen cycle through fractionation and can work as an archive for nitrogen cycling. However, sedimentary δ^{15}N is vulnerable to diagenetic processes and may be affected by allochthonous N input, which makes interpretation difficult and often unreliable. Organic nitrogen incorporated into the calcareous shells of planktonic foraminifera poses a promising archive for pristine δ^{15}N (Ren et al., 2009). During the last decade FB-δ^{15}N analysis has been developed for tracking nitrogen cycling and nutrient dynamics (Ren, 2010; Straub et al., 2013a; Martínez-Garcia et al., 2014). By analyzing FB-δ^{15}N in equatorial Atlantic sediments across the Plio-Pleistocene transition we can reconstruct the nutrient dynamics, approximate the nutrient concentration of SAMW and test the conceptual model of Lawrence et al. (2013) that suggests a shoaling of the nutricline. Combined with the existing productivity data, FB-δ^{15}N may allow us for reconstructing the nutrient supply to the low latitude Atlantic and clarify whether the increased productivity after 2.7 Myr BP was caused by an increased nutrient supply. Here we report new FB-δ^{15}N data from an equatorial Atlantic divergence site measured on two foraminifera species from 2.9 to 2.4 Myr BP with the goal to achieve insights into early Pleistocene low latitude productivity and nutrient consumption and of SO originated SAMW nutrient concentration across the Plio-Pleistocene climate transition.

4.2 Samples and Methods

Ocean Drilling Program (ODP) Site 662 is located in the Guinea Basin in the EEA (1°23.41'S, 11°44.35'W) in the focus of equatorial divergence. The EEA is strongly influenced by seasonal cycles that affect productivity and Sea Surface Temperatures (SST). During northern hemisphere summer, trade wind convergence lead to increased open water divergence and create upwelling of cool nutrient rich waters (Mc Intyre and Ruddiman, 1989). Peaking productivity is usually observed from June to October along with low SST (Pérez et al., 2005). In the modern ocean, subsurface temperature at 50m depth reaches up to 28°C during January to April and decreases during upwelling season to 16°C (Peterson and Stramma, 1991). We expect calcareous microfossils to be well preserved throughout the whole core section. The modern ocean floor does not reach calcite under saturation at Site 662. Studies in the EEA have shown that the lysocline is not expected to have risen above 3800m water depth during entire Pleistocene (Bickert and Wefer, 1996). UK_{37} SST and Alkenone C_{37} MAR data were previously published by (Herbert et al., 2010; Lawrence et al., 2013) and stable oxygen isotope data were published by (Lisiecki and Raymo, 2005).

4.2.1 Materials and age model

The sediment cores at Site 662 were raised during ODP Leg 108 in March 1986 from a depth of 3821.3 m. Three cores A17, A18 and B9 were sampled at composite depths 148 to 161 mbsf at every 5 to 10 cm,

yielding a total of 194 samples. Over this interval, the sedimentation rate is ≈ 4.5cm/kyr, resulting in an average temporal resolution of one sample every 1.2 kyr per sample. The composite depth correlation was made according to the shipboard report from ODP Leg 108 and is based on magnetic susceptibility. The stratigraphy is published by (Herbert et al., 2010; Lawrence et al., 2013) and is based on the correlation of benthic δ^{18}O to the global δ^{18}O-stack (Lisiecki and Raymo, 2005). The operational drilling protocol and shipboard treatments of the sediment are published in the scientific shipboard report of Leg 108 (Ruddiman et al., 1988).

Throughout the interval studied, calcareous micro-fossil abundance was very high. The main planktonic foraminiferal species were (1) *Globigerinoides sacculifer sacculifer* and *Globigerinoides sacculifer trilobus* (with and without a bigger sac-like chamber, herein combined as *Globigerinoides sacculifer* (*Gsacc*)) which are typical for the tropical surface ocean and (2) *Neogloboquadrina dutertrei* (*Ndut*) and (3) *Globorotalia menardii*, which both are typical for equatorial divergence zones (Mc Intyre and Ruddiman, 1989). Except for two short intervals, the non-spinose thermocline dweller *Ndut* was continuously abundant, suggesting an influence of equatorial divergence and upwelling throughout our study period (Kipp, 1976). The abundance of the symbiotic euphotic zone dwellers *Gsacc* was interrupted several times in the later half of the measurement interval. The main habitat of *Gsacc* is warm tropical sea surface water and is potentially impaired by colder temperatures (Mc Intyre and Ruddiman, 1989).

4.2.2 Methods

FB-δ^{15}N analysis

The analysis was preformed on two almost continuously abundant foraminifera species *Gsacc* and *Ndut*. They were picked from the coarse fraction (>250µm) of the previously wet sieved sediment. 4 to 10mg (400 to 1000 individuals) were crushed open and oxidatively cleaned according to the protocol of (Ren et al., 2015). Organic nitrogen within the wall of the foraminiferal tests was then converted to nitrous oxide using the persulfate-denitrifier method according to Sigman et al. (2001). Its N isotopic composition was then measured with a Thermo MAT253 mass spectrometer (analytical precision $< 0.03‰$) following the protocol of (Weigand et al., 2016). FB-δ^{15}N data were corrected for the contribution of the blank nitrogen (on the order of 1.5-3%) through parallel analysis of amino-acid standards of known isotopic composition and concentration. Typical $\delta^{15}N_{Blank}$ ranges between 2‰ and 8‰. Roughly 50% of the samples were analyzed in full procedural replication resulting in an overall standard deviation of 0.2‰ (Fig. 4.1A).

Calculation of thermocline - FB-δ^{15}N

From previous work on foraminifera-bound nitrogen (Ren et al., 2012) we know that FB-$\delta^{15}N_{Gsacc}$ is 1-1.5‰ lower than FB-$\delta^{15}N_{Ndut}$. This offset between symbiotic species *Gsacc* and non-symbiontic species *Ndut* is most likely caused by the uptake of excreted low δ^{15}N amonia by the symbionts and the subsequent internal N cycle to the host, which would lower the δ^{15}N of the foraminifera organic N. FB-$\delta^{15}N_{Gsacc}$ is thought to be very close to the δ^{15}N of its food source and thus reflects the δ^{15}N of supplied nitrate. In contrast, modern measurements of the non symbiotic thermocline dwelling species *Ndut* reveals a δ^{15}N elevation of around 1‰ in respect to the nitrate consumed in the euphotic zone. In our data, FB-$\delta^{15}N_{Gsacc}$ (Fig. 4.1A) varies from 5‰ to 7.5‰ and FB-$\delta^{15}N_{Ndut}$ from 6‰ to 8‰, which indicates a δ^{15}N of the nitrate supply of 5 to 7.5‰ and an offset between the two species of 0.5-1‰. The sample resolution of *Gsacc* is limited due to sporadic disappearance of the species. In the latter half study interval, there are

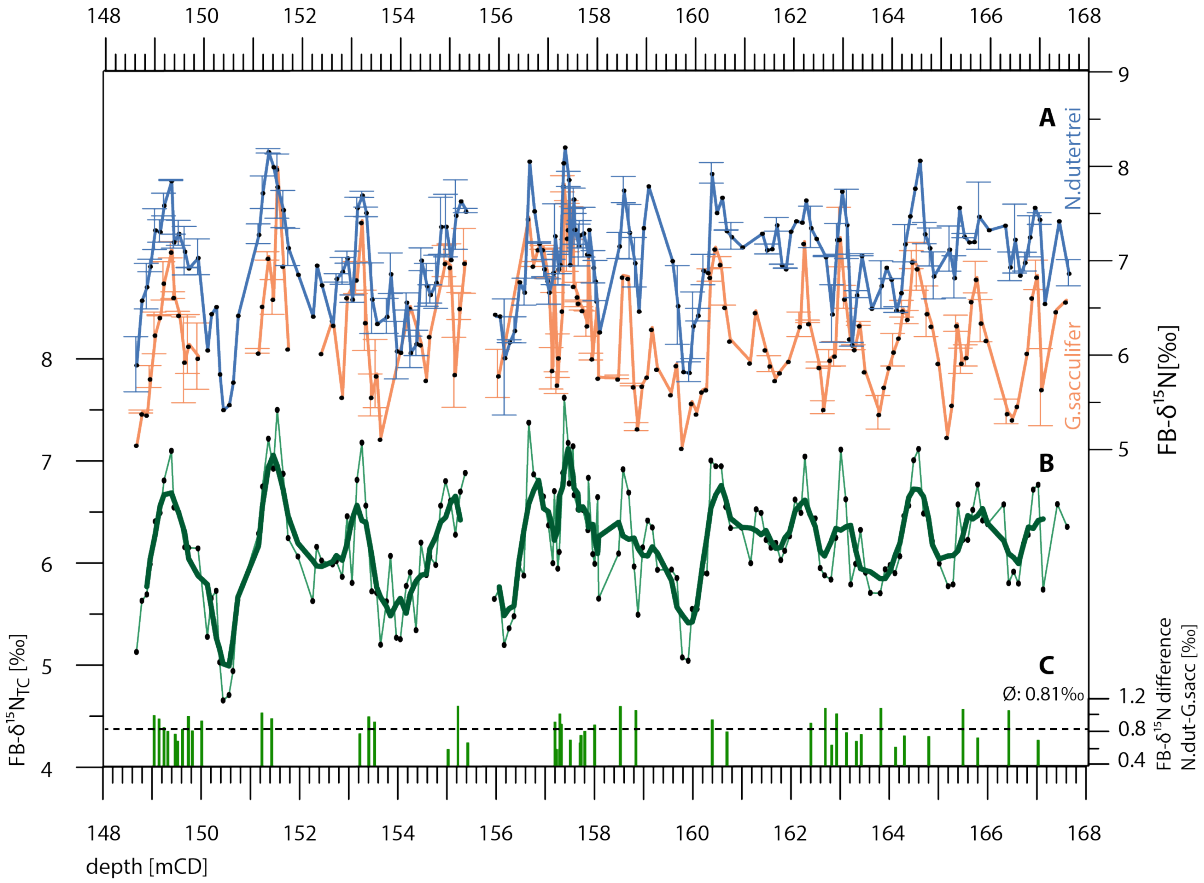

Figure 4.1 – ***FB-$\delta^{15}N$ from EEA Site ODP662 during Plio-Pleistocene transition.*** *- **A:** FB-$\delta^{15}N$ measured on the thermocline dwelling species N.dutertrei (blue) and on the euphotic zone dwelling species G.sacculifer (orange) - **B:** Thermocline-FB-$\delta^{15}N$ (thin line) and three point running mean (bold line). Average replicate standard deviation: Ndut: 0.16‰ Gsacc=0.15‰ - **C:** Difference FB-$\delta^{15}N_{Ndut}$ - FB-$\delta^{15}N_{Gsacc}$ at depths with replicate measurements for both species, average=0.81‰ (dashed) was used for the calculation of the FB-$\delta^{15}N_{TC}$.*

several gaps where the average sample resolution differs from the 10-20cm average and decreases to 60-123cm. We therefore decided to calculate combined data reflecting thermocline-δ^{15}N (FB-$\delta^{15}N_{TC}$, Fig. 4.1B). It is based on the average δ^{15}N difference of 0.81‰ between the two species at sample depths with replicated measurements for both species (Fig. 4.1C). This value was then subtracted from the *Ndut* data. (Fig. 4.1B). The combined FB-$\delta^{15}N_{TC}$ overlain by a three point running mean allows for identification of the most prominent features.

4.3 Results

The two measured species *Ndut* and *Gsacc* show a clear coherence with an absolute offset of *Ndut-Gsacc* = 0.81‰ (Fig. 4.1), in line with modern ocean observations (Ren et al., 2012). Between 2900 and 2700 kyr BP, FB-δ^{15}N varies between 5.8‰ and 7‰. FB-δ^{15}N shows a first prominent minimum (5‰) at 160 mCD / 2.7 Myr BP close to the Marine Isotope Stage (MIS) G6/G7 transition. At the same time an increase in amplitude is observable. The FB-δ^{15}N maxima slightly increase from 7‰ to 7.5‰ and FB-δ^{15}N minima decrease from ≈5.5‰ to 4.5‰, resulting in amplitude of 1-1.5‰ before 2.7 Myr and 3‰ after.

At Site ODP662 benthic δ^{18}O correlates very well with the global LR04 stack, showing small amplitude cycles before 2.65 Myr BP and sharply increasing amplitude at the MIS G6/G7 transition (Fig. 4.3A). UK_{37} SST data (Herbert et al., 2010) show 1-1.5°C colder mean temperatures during high productivity glacials and a weak general cooling trend. Additional, FB-δ^{15}N of ODP662 shows a clear negative correlation to alkenone MAR starting at 2.65 Myr BP. In net, Site 662 between 2.9 and 2.4 Myr BP is dominated by the intensification of climatic cycles between cool, high productive glacials featuring low FB-δ^{15}N and warmer interglacials with higher FB-δ^{15}N and low productivity.

The Pliocene-early Pleistocene FB-δ^{15}N data from ODP662 shows significant differences compared to late Pleistocene FB-δ^{15}N from the same core (Fig. 4.3A, Chapter 3). Pliocene FB-δ^{15}N is generally lower by 0.5-2‰ where the maxima during the early Pleistocene are about 0.3-0.5‰ lower than the baseline FB-δ^{15}N during late Pleistocene. The strong δ^{15}N cycles and clear correlation to δ^{18}O, MAR and SST are not observed during the last two glacial cycles.

4.3.1 Spectral analysis

In order to identify a cyclic patter in the FB-δ^{15}N data, we preformed a short-time Fourier transform after Welsh using the PAST software package(Hammer et al., 2001). The data were interpolated on an equal time interval (2k) scale and testet for auto correlation with a window of 70 kyr and a lag of 50%. We observe a dominant 41 kyr beat starting at 2.65 Myr BP, known from other late Pliocene records (Lisiecki and Raymo, 2007; Herbert et al., 2010).

4.4 Interpretation and Discussion

4.4.1 FB-δ^{15}N data

FB-δ^{15}N of euphotic zone dwelling species *Gsacc* is known to reflect the δ^{15}N of the nitrate supplied to the euphotic zone (Ren et al., 2012). In the modern EEA, nitrate is supplied by SAMW and is completely consumed close to the locus of upwelling (Locarnini et al., 2013). As such, there is no N isotopic fraction due to incomplete nitrate assimilation, and the δ^{15}N of export out of the euphotic zone equals that of the nitrate supply. However, the situation may have been different in the past. Based on our FB-δ^{15}N data, we will argue in the following section that nitrate consumption during glacials after 2.65 Myr BP in the EEA was incomplete. Alternative influences on thermocline δ^{15}N, such as bacterial dentirification in water column anoxic zones (Brandes et al., 1998) or biological nitrogen fixation (Knapp et al., 2012) are highly unlikely to contribute on a regional basis to the thermocline nitrate δ^{15}N at Site 662.

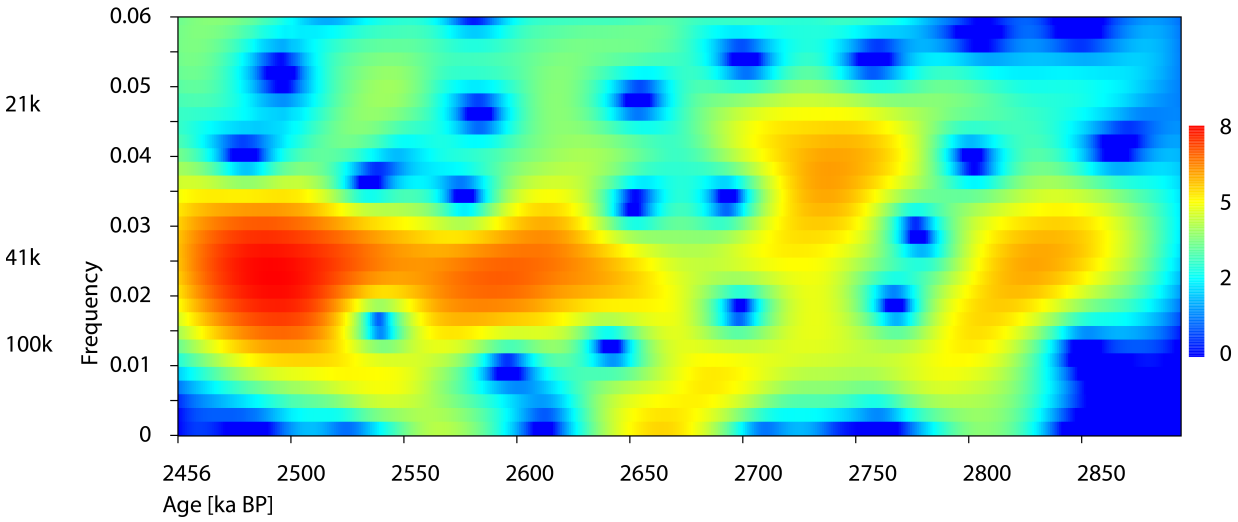

Figure 4.2 – ***Spectral analysis of FB-δ^{15}N from ODP662*** *using Short-time Fourier transform with indicated orbital frequencies. All data was interpolated to equal 2 kyr time intervals. We applied an auto covariance function, a window of 70 kyr and a lag of 50%. All calculations were done with PAST software (Hammer et al., 2001). We identify a clear 41 kyr periodicity between 2650 and 2450 kyr BP. This is interpreted as a pacing of Earths obliquity cycle.*

4.4.2 Incomplete nitrate consumption in early Pleistocene glacials

Given the temporal offset between nitrate supply to the surface and nitrate assimilation by phytoplankton, it is a reasonable starting point to use a Rayleigh model to describe the N isotope systematic associated with nitrate assimilation in the EEA. According to the Rayleigh model, the degree of nitrate utilization (or consumption) sets the δ^{15}N of the N exported out of the surface ocean relative to the nitrate supply. Applied to the early Pleistocene EEA, FB-δ^{15}N of Site 662 reflects the level of nitrate consumption. The coincidence of the early Pleistocene productivity pulses with the FB-δ^{15}N minima implies that nutrient supply was essentially high enough to result in incomplete nitrate consumption. This contrasts with the modern situation in the EEA, where nitrate consumption is essentially complete close to the locus of upwelling.

4.4.3 Iron limitation in equatorial Atlantic

At this point, one can ask why biological productivity was unable to consume the nutrients that were being supplied to the equatorial surface from the higher latitudes. Light limitation seems unlikely in the EEA, such that iron is the most likely limiting factor for phytoplankton growth. The primary source of iron to the low latitude Atlantic is eolian input from southern Sahara and Sahelian brought to the open ocean by winter trade winds (Ruddiman et al., 1988). Iron input at ODP662 was estimated by measuring the flux of terrigenous material (Ruddiman and Janecek, 1989). Surprisingly, iron input is highest when FB-δ^{15}N indicates that nitrate consumption is incomplete (Fig. 4.3A, 4.3D), suggesting that nitrate supply exceeded iron supply, on a stoichiometric basis.

If we compare the early and late Pleistocene (Fig. 4.3D), eolian input during early Pleistocene glacials was at the same level than during the Last Glacial Maximum (LGM). At the same time, productivity as seen in the alkenone MARs (Fig. 4.3E), was also comparable during those two time periods. However, the nitrate consumption during early Pleistocene glacials was incomplete (Fig. 4.3A). Two time periods

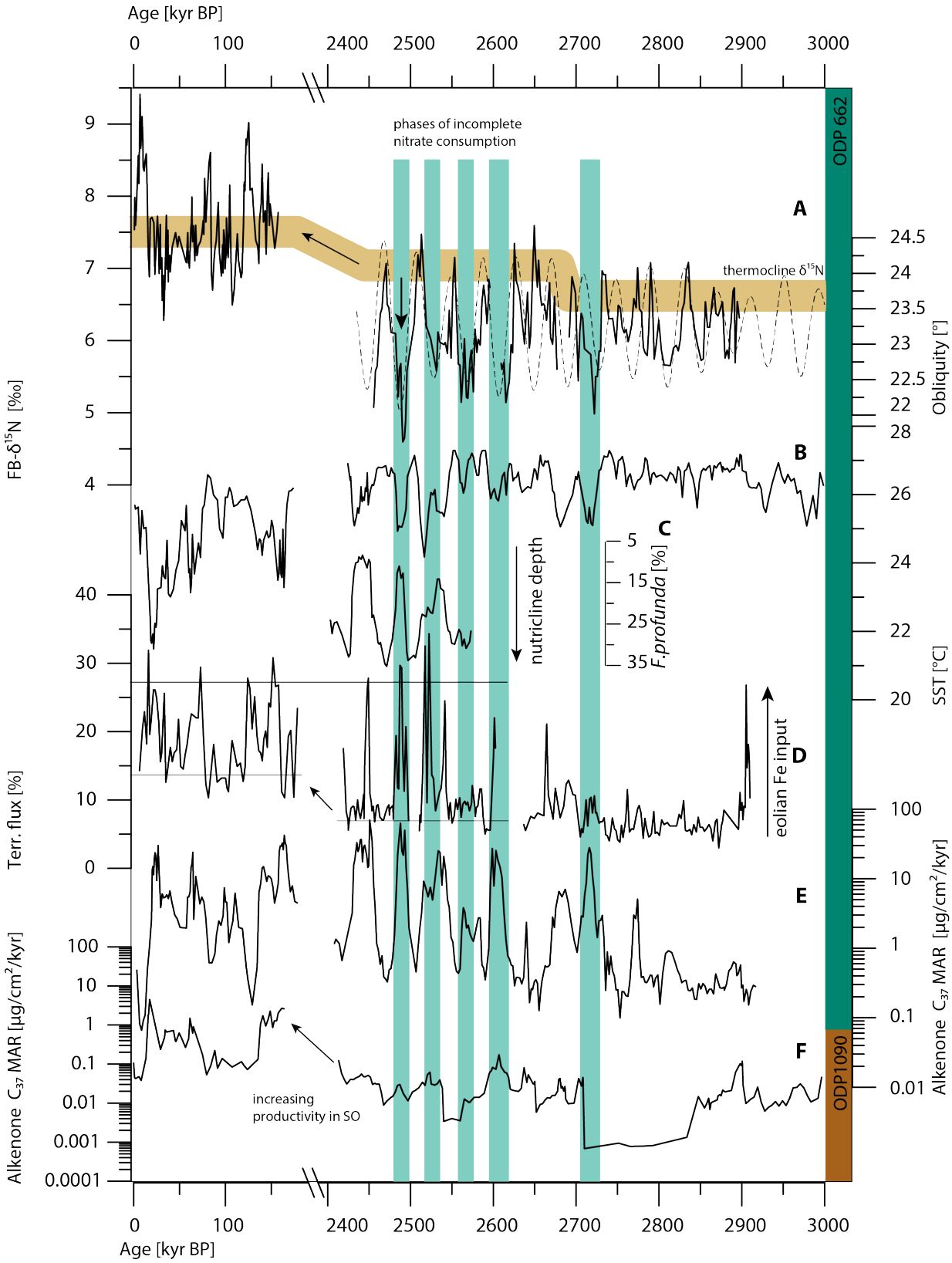

Figure 4.3 – ***Compiled data from ODP662***, ***A:*** *FB-$\delta^{15}N$-thermocline [‰] from ODP662 (solid)low $\delta^{15}N$ values between 2.7 Myr BP and 2.4 Myr BP are interpreted as phases with incomplete nitrate consumption pacing obliquity (dashed) (Laskar et al., 2004). During late Pleistocene thermocline $\delta^{15}N$ was 0.5‰ lower.* ***B:*** *SST UK_{37} [°C] from OPD662 (Herbert et al., 2010) feature a general cooling trend throughout the Pleistocene,* ***C:*** *F. profunda abundance [%] as a proxy for nutricline depth (Bolton et al., 2010),* ***D:*** *Terrigenous sediment [%] from ODP662 (2.9 - 2.4 Myr BP) (Ruddiman and Janecek, 1989) and from ODP663 (160 - 0 kyr BP) (de Menocal et al., 1993) as a proxy for eolian iron input,* ***E:*** *Alkenone MAR ODP662 [µg/cm^2/kyr] as a proxy for productivity (Lawrence et al., 2013),* ***F:*** *Alkenone MAR from Sub Antarctic Zone ODP1090 [µg/cm^2/kyr] as a proxy for Southern Ocean productivity (Lawrence et al., 2013) reflects nutrient content of SAMW.*

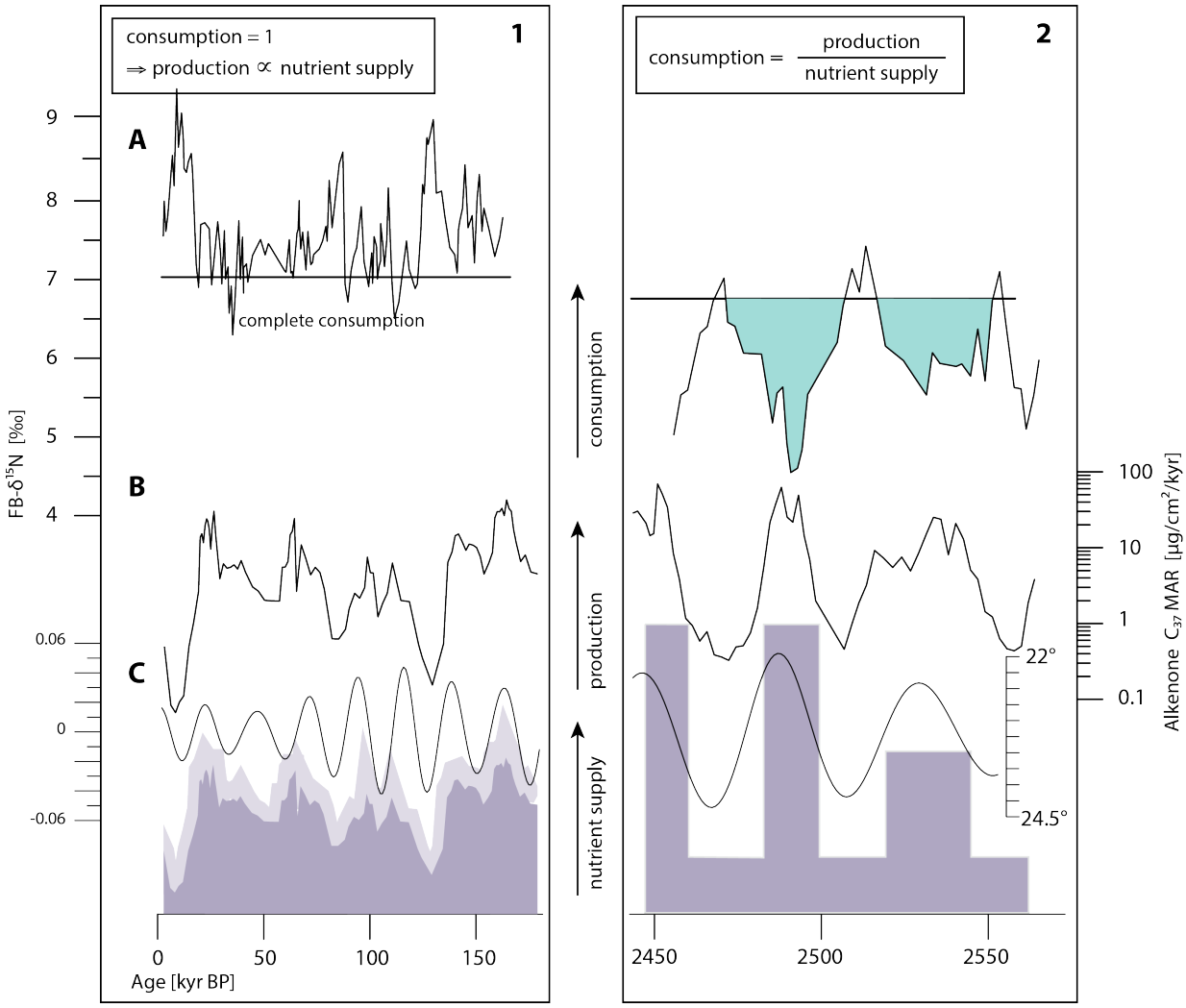

Figure 4.4 – ***Comparison of productivity and level of nitrate consumption between Late Pleistocene/Holocene (1) and Early Pleistocene (2) A:*** *FB-$\delta^{15}N$ data from ODP662 as a proxy for the level of nitrate consumption in the euphotic zone (this study),* ***B:*** *Alkenone MAR ODP662 [µg/cm^2/kyr] reflecting the productivity (Lawrence et al., 2013),* ***C:*** *Schematic representation of the nutrient supply to the euphotic zone of the equatorial upwelling Site 662 overlain by precession parameter (late Pleistocene) and Obliquity angle (early Pleistocene). High FB-$\delta^{15}N$ are interpreted as complete nitrate consumption during the last glacial cycle. The productivity therefore directly reflects the nutrient supply to the euphotic zone. During phases with high FB-$\delta^{15}N$, the complete nitrate consumption and low productivity indicates low nutrient supply. Along with pulses of high productivity, FB-$\delta^{15}N$ drops and indicates incomplete nitrate consumption. The nutrient supply to the euphotic zone has to be extensive enough to induce high productivity and still not be consumed completely. Orbital data from Laskar et al. (2004).*

with equal Fe input resulted in comparable productivity but nevertheless on two different levels of nitrate consumption. If we assume that the iron supply to the EEA during LGM was on the tipping point of being iron limited, a situation with equal iron input but higher nutrient concentration in SAMW, would have lead to iron scarcity and therefore incomplete nitrate consumption during early Pleistocene glacials. We tentatively conclude that the EEA primary production was iron limited during the early Pleistocene glacials.

4.4.4 Nutrient supply to the low latitude Atlantic

From FB-δ^{15}N and alkenone MAR we can infer changes in nutrient supply rate (Fig. 4.4). The minimum level of consumption during times with peaking productivity can only be explained by a substantial increase in nitrate supply compared to LGM. During the last two glacial cycles (Fig. 4.4), nitrate consumption at ODP662 was complete. The productivity therefore is proportional to the nutrient supply. During the early Pleistocene glacials (Fig. 4.4) when nutrient consumption was incomplete, productivity was at a comparable level to the LGM. This demonstrates that nitrate supply to the surface exceeded by far the demand of phytoplankton (Fig. 4.4C) and thus had to be strongly increased compared to LGM productivity peaks.

To increase nutrient supply to Site 662, either an increase in the concentration of nutrients in the source water or an increase in the upwelling strength is needed. A possible change in the strength of equatorial upwelling is unlikely as a source of the 41 kyr productivity peaks. The summer trade winds, which trigger equatorial divergence and hence upwelling, are likely modulated by meridional temperature gradients between the African continent and the EEA. Those gradients in turn are known to follow the precessional insolation changes rather than obliquity paced glacial cycles (Mc Intyre and Ruddiman, 1989; Molfino and McIntyre, 1990). The emergence of obliquity paced cycles suggests the high latitudes as the source region of the signal. This agrees with previous findings of intensified obliquity sensitivity of global climate between 4-2 Myr BP peaking at 2 Myr BP (Lisiecki and Raymo, 2007). This is supported by previous studies, which linked the low latitude productivity to the nutrient content in the high latitudes source water rather than changes in local wind stress (de Menocal et al., 1993; Lawrence et al., 2006; Dekens et al., 2007). We therefore conclude that the observed productivity and consumption patterns at Site 662 are not caused by changes in upwelling but rather by the nutrient concentration in SAMW.

Our data thus support the conceptual model of a contracting Atlantic warm pool by Lawrence et al. (2013): In the Pliocene, an increased density gradient between SAMW and the Atlantic surface water and an extended Atlantic warm pool lead to a deeper nutricline at the Atlantic equator compared to modern. Global cooling during the Pliocene caused increasing meridional temperature gradients and an equator wards shift of the locus of Ekman divergence in the high latitudes. The resulting contraction of the Atlantic warm pool shoaled the nutricline at the equator (Brierley et al., 2009).

Taking a closer look at the FB-δ^{15}N, reveals the first prominent minima at 2.72 Myr BP to be the first time the nutrient rich SAMW reached the low latitude surface. During the following two obliquity minima, the shoaling of the nutricline did not repeat until 2.62 Myr BP from whereon the regular 41 kyr cycles start. It thus seems likely that the pulses of high productivity and incomplete nitrate consumption are not the response to a singular unique climatic forcing but more a non linear response to a gradual initial change. During the glacials at 2.72 Myr BP and after 2.65 Myr BP, a threshold was passed and equatorial upwelling was able to access the nutrient rich SAMW.

4.4.5 Low latitude nitrate δ^{15}N controlled by Southern Ocean nitrate consumption

Over the investigated period in the late Pliocene and early Pleistocene, the observed FB-δ^{15}N was lower than during the last two glacial cycles (Fig. 4.4A and Chapter 3). As we discussed above, thermocline δ^{15}N at ODP662 during early Pleistocene is mainly controlled by incomplete nitrate consumption. According to the concept of a contracting warm water pool (Lawrence et al., 2013) and supported by FB-δ^{15}N SAMW did not reach the surface prior to 2.65 Myr BP and during early Pleistocene interglacials. The δ^{15}N maxima ($\approx$ 7-7.5‰) of each cycle thus can be interpreted to reflect the δ^{15}N of the nitrate within the Atlantic warm pool. During these maxima, thermocline nitrate at ODP662 is supposed to be completely consumed so that there would be no net fractionation due to partial assimilation. From 2.9 Myr BP to 2.65 Myr BP, the δ^{15}N of the Atlantic warm pool was $\approx$ 6.5-7‰ and during early Pleistocene around 0.5‰ higher. The background nitrate δ^{15}N in the late Pleistocene ($\approx$ 7.3 - 7.8‰) was higher again. The most likely explanation for this is the rising SO nitrate consumption during these time. With increasing level of nitrate consumption in the SO, the δ^{15}N of the residual nitrate in the water increases while nitrate concentration decreases. Alkenone MAR from ODP1090 (Fig.4.3F) (Lawrence et al., 2013) show very low productivity in the Atlantic sector of the Sub Antarctic Zone between 3 and 2.4 Myr BP with a slight increase at 2.7 Myr BP. Additionally, Martínez-Garcia et al. (2011) observed the eolian iron input to SAZ during late Pliocene and early Pleistocene to be much lower than during late Pleistocene glacials.These observations suggest that the SAZ production was strongly iron limited and thus the level of nutrient consumption low. This allows for interpreting the lower background nitrate δ^{15}N and the higher nutrient concentration of SAMW during early Pleistocene compared to LGM both to be caused by the most likely lower level of nitrate consumption in the SO during this time. Indeed, less complete nitrate consumption in the Plio-Pleistocene SAZ is required to increase the nitrate concentration of SAMW, so as to explain the incomplete nitrate consumption during the cold events when equatorial upwelling tapped this water.

4.5 Conclusion

We measured FB-δ^{15}N on two foraminifera species in the sediment of EEA Site 662 between 2.9 Myr BP and 2.4 Myr BP. Our data feature an onset of 41 kr cyclicity at 2.65 Myr BP with low FB-δ^{15}N during high productive glacials. We interpret the low FB-δ^{15}N as periods with incomplete nitrate consumption in the EEA. With regards to the very high productivity during the same periods, this suggests that the nutrient supply was strongly enhanced compared to modern values. Further, we elaborated that the biological production during the early Pleistocene glacials was most likely limited by iron although eolian input to Site 662 was peaking as well during those times. The most likely explanation is that the nitrate supply exceeded the iron demand of the phytoplankton due to the high nutrient content of the upwelled SAMW.

The FB-δ^{15}N maxima of each glacial cycle is interpreted to reflect the background δ^{15}N. The two slight increases at 2.7 Myr BP of 0.5‰ and between 2.4 Myr BP and 160 kyr BP of 0.3-0.5‰ are most likely results of increased nitrate consumption in the SO as proposed by Martínez-Garcia et al. (2011), causing the preformed nitrate δ^{15}N of SAMW to rise. To test this, further studies of FB-δ^{15}N in the SAZ during the Plio-Pleistocene transition are needed.

Our data are consistent with the conceptual model of a contracting Atlantic warm pool by Lawrence et al. (2013), when coupled with a strongly iron limited SO in the Plio-Pleistocene transition period (Martínez-Garcia et al., 2011). The orbitally paced pulses in productivity and δ^{15}N decline indicate that the shoaling of the nutricline was not a singular event but a non linear response to a gradual increasing forcing . The single period of low δ^{15}N at 2.72 Myr BP is interpreted as a precursor event when the equatorial upwelling accessed SAMWfor the first time.

5

Coral-bound nitrogen isotopes as an archive for Holocene North Atlantic Nutrient utilization

Lukas E. Oesch[1], Maria G. Prokopenko[2], Daniel M. Sigman[3], Xingchen T. Wang[3]
Anja S. Studer[4], Gerald H. Haug[1,4]

[1]Geological Institute, Department of Earth Sciences, ETH Zurich, Zurich, Switzerland
[2]Department of Geology, Pomona College, Claremont, CA, USA
[3]Department of Geosciences, Princeton University, Princeton NJ, USA
[4]Max Planck Institute for Chemistry, Mainz, Germany

Abstract

The Subpolar North Atlantic is a key region within the global climate system. The arctic climate in turn is strongly affected by the North Atlantic Oscillation, which influences the position of the Subpolar Gyre in the North Atlantic. The perennially incomplete surface nitrate consumption, which marks the area of the Subpolar Gyre, is likely to result in low δ^{15}N of organic matter exported into the deep ocean. Here we analyze coral-bound δ^{15}N of (CB-δ^{15}N) on organic matter incorporated into the skeletons of scleractinian deep sea corals for its potential as a proxy for the δ^{15}N export production and thus the position of the Subpolar Gyre over time. We predict the δ^{15}N export by the means of Rayleigh dynamics and compare to measured CB-δ^{15}N. We found good coherence, with higher CB-δ^{15}N in regions with more complete nitrate consumption and vice versa. An absolute offset between CB-δ^{15}N and δ^{15}N export of 6-8‰ was observed, which matches the reported offset of previous studies. To reconstruct the position of the Subpolar Gyre and the strength of the North Atlantic Oscillation over the late Holocene, we measured CB-δ^{15}N on deep sea corals with ^{14}C ages between 0 and 2000 yr BP. We observed CB-δ^{15}N potentially consistent with a more negative North Atlantic Oscillation at 500 to 600 yr BP, which corresponds to a negative North Atlantic Oscillation during this time as reconstructed by Greenland limnological studies. Our data show the potential of CB-δ^{15}N.

5.1 Introduction

The North Atlantic is a key region for the global carbon cycle. North Atlantic Deep Water (NADW) formation in the Subpolar North Atlantic (SPNA) works as a gateway for surface water into the deep ocean, affecting biogeochemical cycles and global atmospheric CO_2 concentration by ultimately providing a route for biological carbon sequestration (Sigman et al., 2010). Interactions between the deep ocean and the atmosphere mediated by the biological pump can significantly alter the atmospheric CO_2 concentration on millennial and orbital time scales (Knox and McElroy, 1984; Siegenthaler and Wenk, 1984; Sarmiento and Toggweiler, 1984). The efficiency of the global biological pump is set by the ratio of preformed to remineralized nutrients in the water entering the deep ocean. In this regard, the North Atlantic is particularly important, offering a gateway into the deep ocean for the surface waters of the low and middle latitudes in which nutrient consumption is complete. NADW, incorporating the signal of the efficient carbon uptake of the low latitudes, imprints a signature of low preformed to remineralized nutrients onto the deep ocean. An increase in the ratio of preformed versus regenerated nutrients within the NADW would lower the global efficiency of the biological pump and substantially increase the concentration of CO_2 in the atmosphere (Toggweiler, 1999; Marinov et al., 2008; Schmittner and Galbraith, 2008; Hain et al., 2010; Sigman et al., 2010).

In the modern SPNA, surface water nitrate concentration defines two regions characterized by distinctly different regimes (Fig. 5.1). In the eastern SPNA in the southern Norwegian Sea, the main locus of deep water formation, surface nitrate is depleted by the end of summer and thus nutrient consumption in the euphotic zone is complete. To the west, in the Irmiger Sea (south-east of Greenland and south-west of Iceland) unutilized nutrients persist in the surface water throughout the year (Locarnini et al., 2013). The area of annually persistent surface nutrients is congruent with the Subpolar Gyre (SPG), which is driven by winds generated by the Icelandic low pressure system to the North and the Azores high pressure system to the South. A divergent flow of the SPG results from the Ekman transport that works in an opposite sense to the Subtropical Gyres, creating cyclonic rather than anticyclonic dynamics. Surface water transport away from the center drives the upwelling of nutrient rich deep water in the center of the gyre. Apparently, in the eastern SPG, nutrients are supplied by Ekman divergence upwelling faster than biological production is able to consume them, though the exact reasons for the incomplete nutrient consumption are not well understood.

Walker (1928) first described an oscillation of the North Atlantic climate, which influences the strength of the westerlies invading Europe. The North Atlantic Oscillation (NAO) varies on decadal time scales and reflects changes in the strength of the westerly winds across the North Atlantic (Hewitt and Jackson, 2009). Intensified Icelandic low- and enhanced Azores high pressure systems lead to a strengthening of the westerlies over the North Atlantic (NAO index positive). During negative NAO, the pressure gradient between the subtropics and the polar zone is weak, causing the westerlies to dwindle. While the ultimate cause for the decadal oscillation is still unclear, it has been shown that the strength and the position of the SPG is linked to the NAO (Levitus, 1989; Curry and McCartney, 2001). During the periods of positive NAO index, the enhanced westerlies intensify the cyclonic SPG flow and are likely to drive the SPG position eastward. In contrast, weakening of the westerlies and a more western position of the weaker gyre characterize negative NAO states. With regard to the nutrient cycling in the North Atlantic, the region of incomplete surface nutrient consumption is likely to be associated with the gyre center and thus is expected to shift its position along with changes in the SPG position itself. Insights into the development of the SPG and the NAO throughout Earth's recent history would allow for assessing its interactions with the regional and, through teleconnections, global climate and would clarify its role regarding the efficiency of the global biological pump.

The ratio of stable nitrogen isotopes (^{15}N/^{14}N ratio, $\delta^{15}N = (((^{15}N/^{14}N)_{sample}/(^{15}N/^{14}N)_{air}) - 1 * 1000)$ tracks processes in the nitrogen cycle through fractionation between ^{15}N and ^{14}N. Therefore, the δ^{15}N of organic matter can serve as a proxy for nitrogen cycling, indicating the prevalent sources (e.g. N_2 fixation vs. upwelled nitrate), strength of sinks (e.g. denitrification), and/or the nutrient status (completeness of nitrate consumption by phytoplankton). However, within the well ventilated nutrient rich surface water of the SPNA, we do not expect denitrification to occur. The newly fixed low δ^{15}N nitrate from biological N fixation in the low latitude Atlantic surface water is completely consumed in the region of the subtropical gyre and therefore prevented from reaching the high latitude Atlantic, although it does work to lower the δ^{15}N of the subsurface nitrate supply in the SPNA (Marconi et al., 2015). The δ^{15}N export in the SPNA has been shown to be impacted by preferential assimilation of low δ^{15}N nitrate in regimes with incomplete nitrate consumption (Altabet et al., 1991). Preferred assimilation of ^{14}nitrate compared to ^{15}nitrate by primary producers results in formation of organic matter (OM) with lower δ^{15}N than the δ^{15}N of the source nitrate. If the nitrate consumption is incomplete on a seasonal basis, the annually integrated δ^{15}N of OM exported into the subsurface is also lower than the source nitrate. Thus, the δ^{15}N of exported OM contains the information about the degree of nitrate consumption. In this region of the North Atlantic, the degree of nitrate consumption is linked to the strength and the position of the SPG, so it may serve as a proxy for the history of SPG in the past.

Bulk sedimentary δ^{15}N may not faithfully record the δ^{15}N of exported particulate organic matter (POM), being affected by the contribution of allochthonous detrital (e.g. terrigeneous) N input (Schubert and Calvert, 2001) and/or bacterial degradation that alters the original δ^{15}N during diagenesis. These factors may obscure bulk sedimentary records, making paleo-reconstructions unreliable. Over the last few decades, diatom and foraminifera microfossil bound δ^{15}N have been developed as proxies for the δ^{15}N of nitrate assimilated in surface waters (Robinson et al., 2004; Straub et al., 2013a; Martínez-Garcia et al., 2014; Studer et al., 2015). Due to the low organic nitrogen content within foraminifera shells, the low sediment accumulation rate in the SPNA, and effects of bioturbation, of foraminifera-bound δ^{15}N may not be suitable to assess Holocene changes, especially on centennial timescales or shorter (Straub et al., 2013b). Recently, the δ^{15}N of organic matter bound within carbonate (aragonite) skeletons of scleractinian deep sea corals (coral-bound δ^{15}N, or CB-δ^{15}N) has emerged as a new proxy for δ^{15}N export and thus as an additional paleo-archive recording the history of nutrient cycling (Wang et al., 2014).

Here we present results from a groundtruthing study to determine the potential for coral-bound δ^{15}N (CB-δ^{15}N) to record the strength of the SPG and its position within the NAO during the late Holocene (last $\approx$2000 years) by the means of changes in export δ^{15}N. We hypothesize that incomplete nitrate consumption in the center of SPG would generate organic matter with lower δ^{15}N that is recorded by modern deep sea corals. We further surmise that changes in the SPG position/strength accompanying NAO variability should be recorded in changes of CB-δ^{15}N.

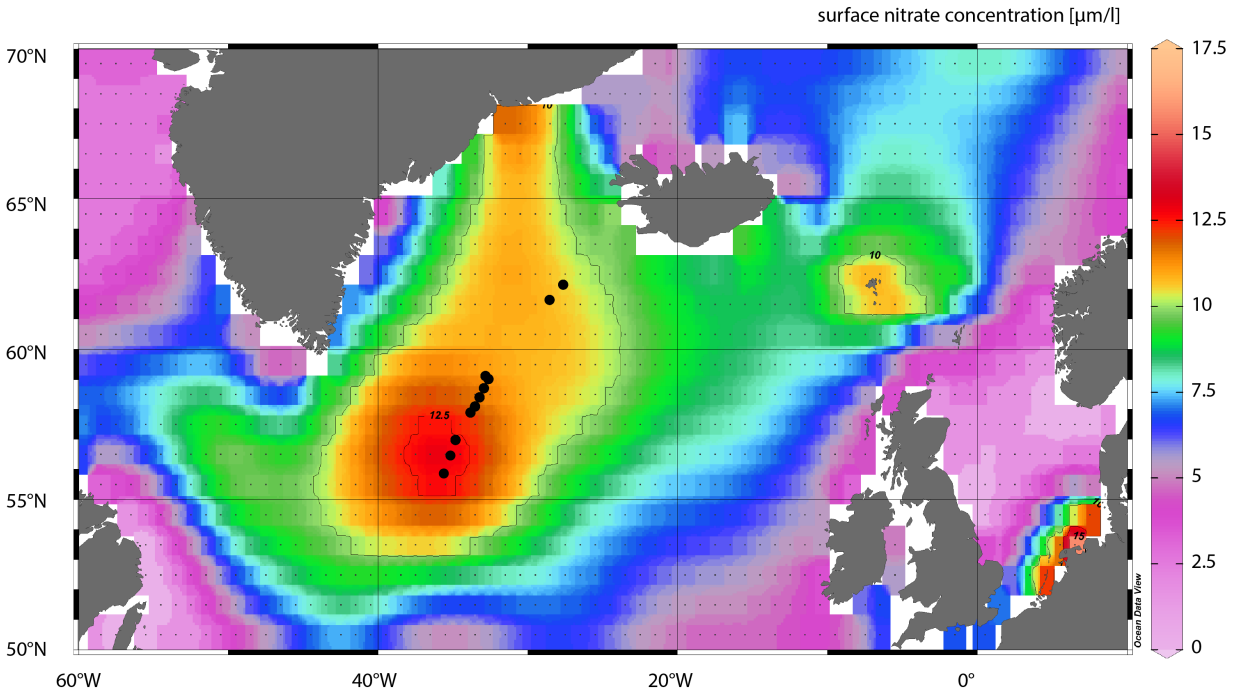

Figure 5.1 – ***Summertime nitrate concentration in the North Atlantic surface ocean*** *by World Ocean Atlas 2013 (WOA13) (Locarnini et al., 2013) with indicated locations of the measured deep sea corals along the Reykjanes Ridge.*

5.2 Samples and Methods

5.2.1 Samples and study site

Measurements were performed on 43 samples of deepsea corals collected from 14 locations in a transect through the North Atlantic SPG along the Reykjanes Ridge (55°N - 62°N and 28°W - 35°W) (Fig. 5.1). The samples were recovered during cruise CE0806 of R/V Celtic Explorer in 2008. In this study, we used in this study *D. dianthus* and colonial corals *Lophelia pertusa* with ^{14}C ages between modern and 2400 yr from depths between 900 and 2000mbsl. Radiocarbon Libby ages of the corals were reported by (Burke, 2012). *Lophelia pertusa* features growth rates of 5-26mm/yr and is likely to reflect proportional δ^{15}N export (Wang et al., 2014). Our study area is the North Atlantic, which features incomplete summertime nitrate consumption. During northern hemisphere winter, the density gradient profile weakens and the mixed layer deepens to 500m. In spring (April/May) increased solar insolation warms the surface water and stabilizes the stratification. Subsequent shoaling of the nutricline to 30-40m leads to an increased biological production during spring bloom. Throughout the production season the nutrients are not consumed completely, leaving 6µmol/l nitrate in the surface ocean by the end of August/beginning of September (Locarnini et al., 2013).

5.2.2 CB-δ^{15}N analysis

The oxidative cleaning was performed according to the persulfate-cleaning protocol of Ren et al 2015. The analytical protocol for CB-δ^{15}N was adapted from foraminifera bound- δ^{15}N studies (Ren et al., 2009, 2012) and previously used in CB-δ^{15}N analysis (Wang et al., 2014) using the denitrifier method

(Sigman et al., 2001). In short, 15-25 mg of clean sample was dissolved with 4 N HCl (ACS grade) to release the organic matter nitrogen into solution. Subsequently the sample nitrogen was oxidized to nitrate by adding an alkaline potassium persulfate reagent. The nitrogen content of the sample was measured by chemiluminescence (Braman and Hendrix, 1989). For bacterial conversion of nitrate into nitrous oxide, denitrifier *P. chlororaphis* were used, which lack the enzyme to convert N_2O into N_2. The N isotopic ratio of the N_2O was measured with a Thermo MAT253 mass spectrometer (analytical precision $< 0.03‰$) following the protocol of Weigand et al. (2016). Obtained δ^{15}N values were referenced to the international nitrate isotope standard (IAEA-NO3, δ^{15}N = 4.7‰). CB-δ^{15}N data were corrected for the contribution of the blank nitrogen (on the order of 1-3%) through parallel analysis of amino-acid standards of known isotopic composition and concentration. Typical $\delta^{15}N_{Blank}$ ranges between 2‰ and 8‰. The samples were analyzed in full procedural replication, resulting in an overall standard deviation of 0.6‰.

5.2.3 Calculation of modern δ^{15}N-export

The expected δ^{15}N of the exported particulate organic Nitrogen (PON) is determined by isotopic fractionation through preferential assimilation of ^{14}N- vs. ^{15}N-containing surface nitrate. In case of incomplete nitrate consumption, the fractionation is expressed as low δ^{15}N in the produced organic matter.

According to isotopic kinetics, the N isotopic composition of the OM exported out of the surface ocean relative to the N supply defines the degree of nutrient consumption. The fractionation models predict that in a progressively consumed reactant pool, the product becomes progressively enriched in ^{15}N, either approaching the source δ^{15}N (in case of an accumulated product scenario) or exceeding the source δ^{15}N (in case of an instantaneously produced organic N product that is continuously removed), as the remaining concentration of the reactant declines (Mariotti et al., 1981; Sigman and Casciotti, 2001). Two models are used to reflect these processes. The Rayleigh model (closed system) describes the isotopic development of a completely consumed reservoir whereas the steady state model (open system) describes a situation where the reactant is replenished while being consumed. Given the kinetic isotope effect ε =5‰ the Rayleigh instantaneous product features a δ^{15}N, which is 5‰ lower than the remaining organic N in the water (reactant). The accumulated product describes the integrated δ^{15}N of OM exported. If the entire pool of reactant is consumed, δ^{15}N of the accumulated product cannot differ from the initial reactant δ^{15}N and no net fractionation occurs.

However, our study region in the North Atlantic cannot be easily categorized into a open or closed Rayleigh system. The nutrient pool within the SPG is recharged seasonally through a deep wintertime mixed layer and partially consumed during spring and summer time. Rayleigh conditions ask for a singular event of nutrient delivery and subsequent isolated consumption. Since it is probable that the gyre features lateral nutrient transport out of the gyre during the productive season, and some more diffuse upwelling away from the very center of the gyre cannot be ruled out, Rayleigh conditions are not fully satisfied. According to the Rayleigh model, lateral transport of elevated δ^{15}N and low Nitrate Concentration ($[NO_3^-]$) into the gyre would lead to an overestimation of δ^{15}N export according to the δ^{15}N-instantaneous (eq. 5.2) and an underestimation compared to the δ^{15}N-accumulated product (eq. 5.3). On the other hand, due to the strong character of seasonal nutrient delivery and production blooms, the steady statemodel is also not completely representative. The lack of continuous supply with low δ^{15}N nitrate causes the δ^{15}N export to be higher than predicted according to the steady state model (eq. 5.4). To calculate the δ^{15}N export within the SPG, we averaged the Rayleigh accumulated product and the Rayleigh instantaneous product (Tab. 5.1). Due to the nutrient transport mechanisms discussed above, this is perhaps an appropriate approximation of the isotope fractionating processes in this region

Table 5.1 – *Calculation of expected δ^{15}N-export*

Long	Lat	[NO_3^-]	f	St.S δ^{15}_{Inst}	R. $\delta^{15}_{reactant}$	R. δ^{15}_{accu}	R. δ^{15}_{inst}	R. δ^{15}_{export}
-24.5	62.5	3.02	0.2	3.99	13.02	2.98	8.02	5.5
-27	61.9	3.52	0.23	3.83	12.25	2.78	7.25	5.01
-27.9	61.4	4.3	0.29	3.57	11.25	2.49	6.25	4.37
-32.2	58.9	6.48	0.43	2.84	9.19	1.81	4.19	3
-32	58.8	6.99	0.47	2.67	8.82	1.67	3.82	2.74
-32.6	58.2	7.42	0.49	2.53	8.52	1.56	3.52	2.54
-32.9	57.9	7.49	0.5	2.5	8.47	1.54	3.47	2.51
-33.2	57.7	7.71	0.51	2.43	8.33	1.48	3.33	2.4
-34.5	56.3	7.19	0.48	2.6	8.68	1.62	3.68	2.65
-35	55.7	5.98	0.4	3.01	9.6	1.95	4.6	3.28
-34.5	55.5	6.01	0.4	3	9.58	1.94	4.58	3.26

$$R.\delta^{15}N_{reactant} = \delta^{15}N_{initial} - \varepsilon[ln(f)] \tag{5.1}$$

$$R.\delta^{15}N_{instantaneous} = \delta^{15}N_{reactant} - \varepsilon \tag{5.2}$$

$$R.\delta^{15}N_{accumulated} = \delta^{15}N_{initial} + \varepsilon[\frac{f}{1-f}]ln(f) \tag{5.3}$$

$$St.S.\delta^{15}N_{instantaneous} = \delta^{15}N_{initial} - \varepsilon(f) \tag{5.4}$$

5.2.4 CB-δ^{15}N as a proxy for SPG position

The impacts the NAO has on the SPG position is not completely known, but the general tendencies can be summarized as follows. During periods of positive NAO index, the enhanced westerlies intensify, the cyclonic SPG flow and are likely to drive the SPG eastwards into a more zonal position. In contrast, during negative NAO states, the weaker westerlies would reduce the cyclonic flow and lead to a more western SPG position with a generally more meridional shape. In general, positive NAO may tend to increase the highest summertime nitrate concentration across the region.

We suggest three possible scenarios linking changes in the SPG dynamics to the variability of δ^{15}N of exported OM recorded in the CB-δ^{15}N of corals along the Reykjanes Ridge (Fig. 5.2):

1. A positive NAO index would shift the center of the gyre eastward away from the Reykjanes Ridge. The whole gyre assumes a more zonal shape with the maximum δ^{15}N export in the eastern SPNA. In this case the whole ensemble of deep sea corals on the Reykjanes Ridge would feature elevated δ^{15}N compared to modern. Since only the southern most corals would cover the region of incomplete nitrate consumption in the SPNA, δ^{15}N export would be uniformly at the subsurface nitrate supply δ^{15}N of 5‰ (Marconi et al., 2015) or slightly lower at the southernmost locations.

2. Intensified gyre flow during a positive NAO index would result in a more zonal position of the gyre and an overall larger region of Ekman divergence within the gyre. The zone of incomplete nitrate consumption would still cover the transect of deep sea corals on the Reykjanes Ridge. In this case we expect a δ^{15}N export pattern with stronger south-to-north δ^{15}N gradient with lower δ^{15}N in the south, while the northern δ^{15}N likely remaining unchanged. Low δ^{15}N is restricted to the center of

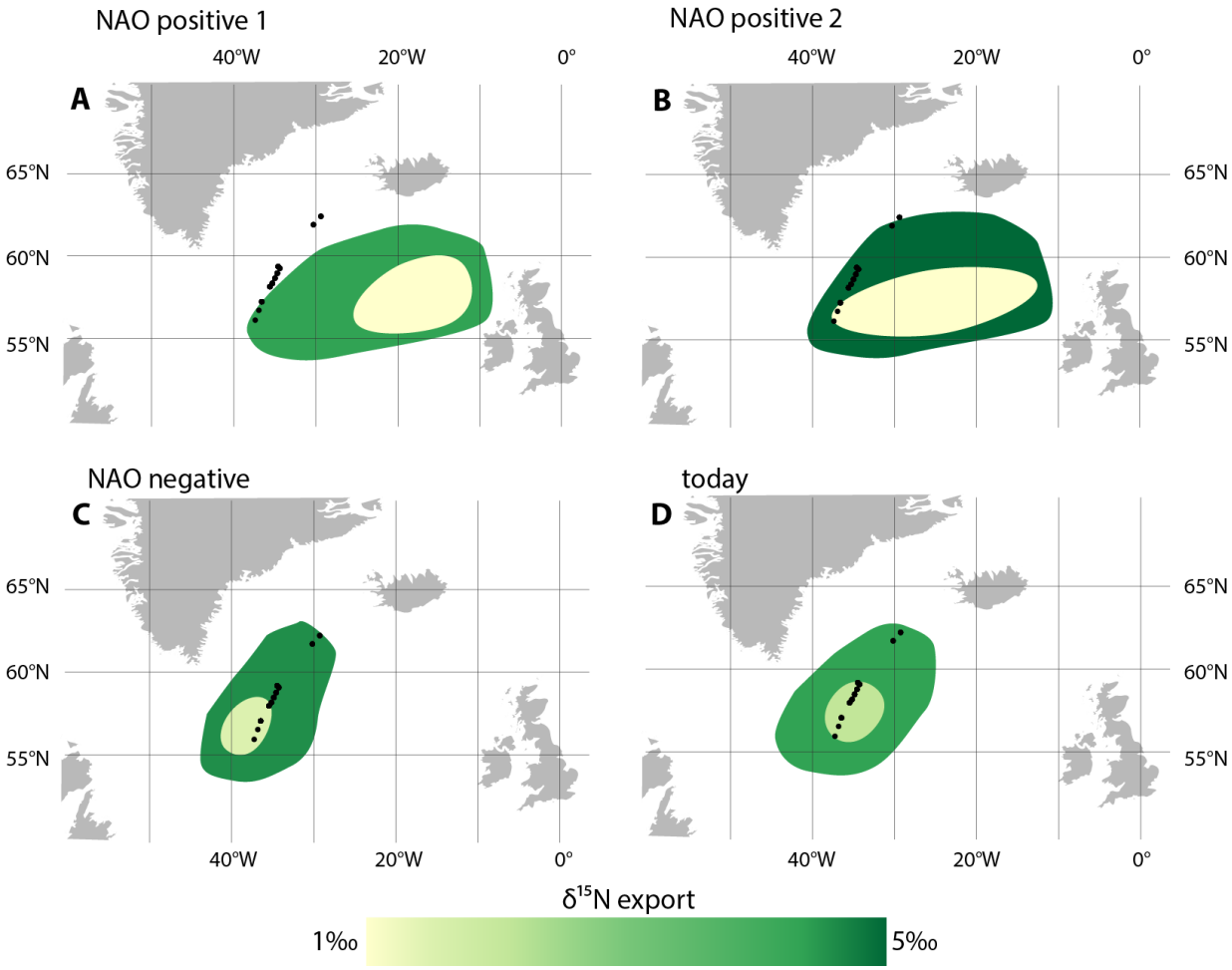

Figure 5.2 – ***Predicted position of the SPG and δ^{15}N export according to the NAO index - A:*** *Positive NAO index option 1 with incomplete nitrate consumption in the eastern SPNA* ***- B:*** *Positive NAO index option 2. Stronger cyclonic flown leads to an elongated gyre and zonal incomplete nitrate consumption* ***- C:*** *Negative NAO index. A weaker cyclonic flow leads to more complete nitrate consumption and generally higher δ^{15}N export* ***- D:*** *modern day situation*

the gyre around 57-58°N. The intermediate locations of the transect 59-60°N would feature elevated δ^{15}N, similar to the most northern locations at 61-62°N.

3. For times with negative NAO we expect a more meridional orientation of the SPG, a more westward position, and weaker cyclonic flow. Lower cyclonic flow would lead to a generally higher level of nitrate consumption in the SPNA and thus higher δ^{15}N export compared to modern throughout the entire transect. We expect the lowest CB-δ^{15}N in the center of the gyre at the southern most positions 57-58°N and, perhaps, lower gradients between all the deep sea corals of the transect.

Reconstructing the position of the SPG and the strength of the NAO would increase our understanding of North Atlantic climate phenomenon in the Holocene like temperature anomalies in Greenland (Appenzeller et al., 1998) or European precipitation patterns (Wirth et al., 2013) and would reveal insight to Holocene climate variations like the Medieval Climate Anomaly or the Little Ice-age.

5.3 Results and Discussion

5.3.1 CB-δ^{15}N as a proxy for sea surface nutrient consumption

The measured CB-δ^{15}N was between 7.8 and 14‰ (Fig. 5.3). CB-δ^{15}N modern varies between 8 and 12‰. The southern most locations (55-57°N) at the southern limb of the gyre feature CB-δ^{15}N between 10.4‰ and 12.6‰. The locations at 57-59°N, which are in the zone of lowest degree of nitrate consumption today feature CB-δ^{15}N of 8.2-9.1‰. CB-δ^{15}N at the northern most corals at 61.4 and 61.9°N is significantly higher, between 10 and 13‰. (Wang et al., 2014) observed a 1‰ variability of δ^{15}N within single polyps of deep sea corals. In comparison, the total variation of CB-δ^{15}N of 6.14‰ is significant.

The observed CB-δ^{15}N of modern corals on the Reykjanes Ridge follows the pattern expected from surface nutrient consumption. In comparison to the predicted δ^{15}N export (Section 5.2.3) (Fig. 5.3), we observe a similar pattern in CB-δ^{15}N of higher δ^{15}N export at the outer regions of the gyre and lower δ^{15}N export in the center. Further we report an absolute offset between δ^{15}N export and CB-δ^{15}N of about 6-7‰, which is consistent with, though somewhat lower, than the average offset of 8.1‰ previously reported for *D. dianthus* (Wang et al., 2014). They concluded from this offset on the primary food source of *D. dianthus* to be mainly suspended POM, which is known to be ≈4-5‰ higher than sinking POM (Saino and Hattori, 1987; Altabet et al., 1991).

One concern regarding the ability of CB-δ^{15}N to reflect sea surface nutrient consumption is the potential dilution and blur of the isotopic signal through lateral movement of the suspended POM. Given the reported characteristics of deep-sea coral habitats with rather vigorous bottom currents (Dorschel et al., 2007; Roberts et al., 2009), they may record the δ^{15}N of POM that has been imported laterally from regions with different biogeochemical conditions in the surface waters (Wang et al., 2014). However, the offset of the CB-δ^{15}N from the estimated δ^{15}N export of around 6-8‰ is similar to the offset observed in regions with less potential for lateral transport effects (Wang et al., 2014), representing one argument against a major effect in this region. In an environment with low δ^{15}N export surrounded by regions with higher δ^{15}N export as the SPG, the δ^{15}N of laterally transported OM in to the center of the gyre would originate from regions with more complete nutrient consumption and would thus tend to raise CB-δ^{15}N in the center of the gyre. In contrast, if anything, the SPG corals from the center of the gyre are slightly lower than predicted from previous work, in which a δ^{15}N offset of ≈8‰ was observed on average between N export and *D. dianthus*. Moreover, the spatial pattern in CB-δ^{15}N for *Lophelia* (for which there are the most data) appears consistent with the expected δ^{15}N gradient through the SPG (Fig. 5.3A).

5.3.2 Holocene development of the Subpolar Gyre

To assess the potential for CB-δ^{15}N as a proxy for the position and the strength of the SPG over time, we measured deep sea corals (*D. dianthus* and *Lophelia*) of ages spanning the last 2000 years. The ages were determined by radiocarbon dating, resulting in Libby ages from 0 to about 2400 years BP. To evaluate the variability of CB-δ^{15}N through time, measured CB-δ^{15}N was normalized against modern values (<100 years in Libby age) (Fig. 5.4). The standard deviation of replicated CB-δ^{15}N is 0.6‰, which results in an error bar for the normalized CB-δ^{15}N of 5-7.5%.

As discussed above, CB-δ^{15}N reflects the incomplete surface nutrient consumption within the SPG. Therefore, a position change of the SPG through time would be reflected in the CB-δ^{15}N measured. Since the SPG is likely to shift its position according to the NAO in decadal timescales, our temporal resolution is too sparse for a detailed reconstruction of the SPG position. Nevertheless, before 1500 yr BP the northern most point of the transect features a 20% higher CB-δ^{15}N. At 500 yr BP the corals at latitude 57.7°N and 56.3-56.8°N feature 20% higher CB-δ^{15}N and at 600 BP the southern most group of corals (55.7°N) is

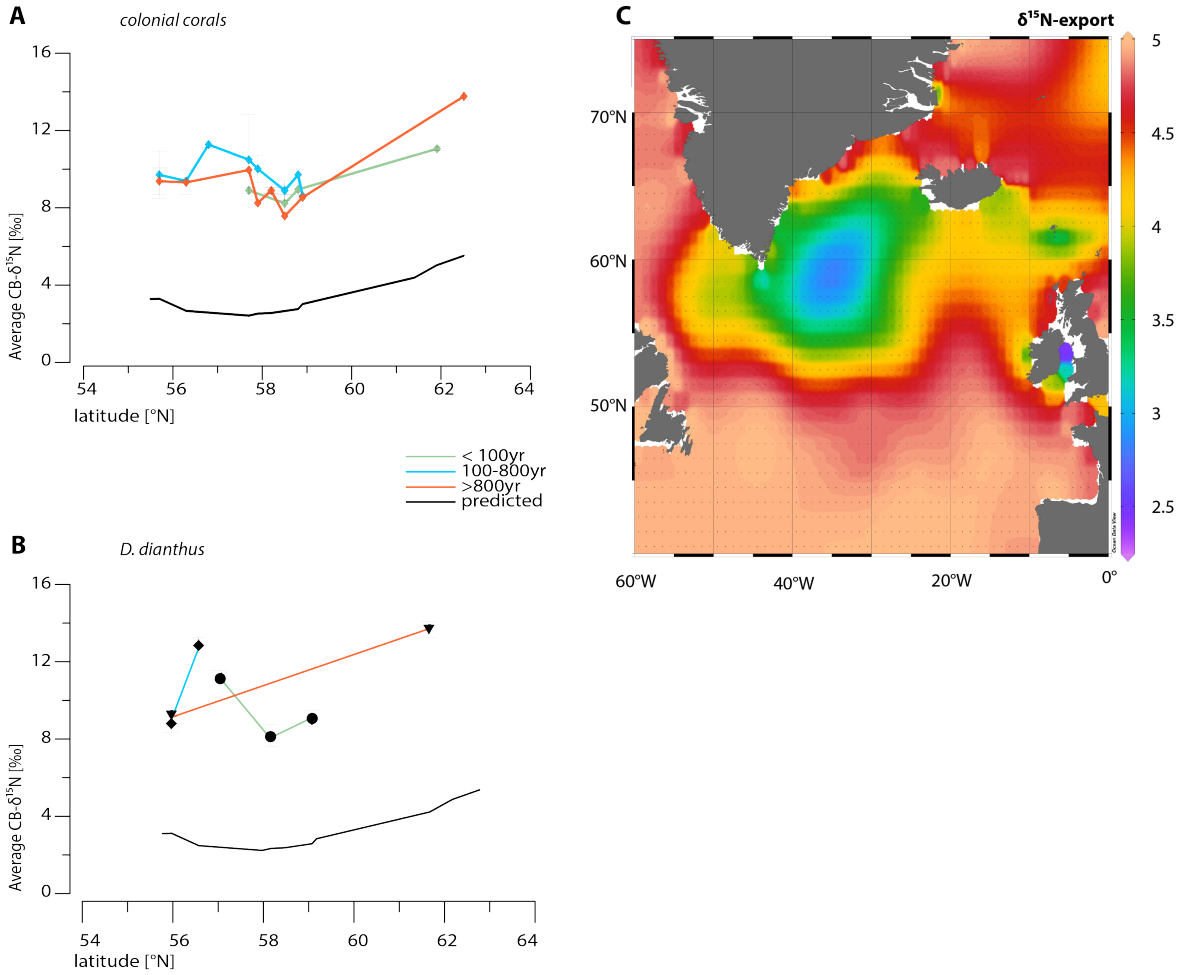

Figure 5.3 – ***CB-δ^{15}N of North Atlantic Corals compared to estimated δ^{15}N export - A:*** *CB-δ^{15}N [‰] from colonial corals Lophelia show a clear off-set of 6-8‰ to the estimated δ^{15}N export (black) -* ***B:*** *CB-δ^{15}N [‰] of D. dianthus with the estimated δ^{15}N of export (black) feature an offset of 6-10‰ -* ***C:*** *Map of estimated export δ^{15}N in the North Atlantic. Calculated as average between Rayleigh and Steady State model from [NO_3^-] data in from WOA13, plotted with Ocean Data View (Locarnini et al., 2013).*

significantly lower (-30% compared to modern). A possible change of the SPG is likely to have a bigger impact on the regions of its outer limits (southern most and northern most points). The two peaks at 1500 yr BP and 600 yr BP are good candidates to reflect a shift of the SPG. The observed δ^{15}N export changes at around 500 yr BP correspond to the predicted δ^{15}N export during NAO positive option2 (Fig. 5.2B). The lower CB-δ^{15}N of the southern most corals can be interpreted as less complete nitrate consumption during that time. An intensified cyclonic flow would increase the nutrient supply to the surface in the center of the gyre and lead to an increase of the δ^{15}N export gradient between the inner and the outer gyre. A southern position and a more zonal shape of the SPG would diminish its influence on the δ^{15}N export at the northern most locations. The southern most corals would enter the center of the gyre. This would lead to a decrease of CB-δ^{15}N of the southern most corals and higher CB-δ^{15}N for the other locations. This proposed shift of the NAO from strongly positive before 500 yr BP to variable-negative NAO afterwards is supported by lake sediment analysis from Greenland (Olsen et al., 2012) and compiled global proxy data by Trouet et al. (2009). The existing NAO proxies show a substantial change in the NAO around the end of the Holocene Thermal Maximum and the beginning of the Little Ice Age (around 600-500 yr BP). Additionally, the Holocene record of flooding events in the European Alps, which are associated with the

NAO, shows a trend of negative NAO index at 500-600 yr BP as well (Wirth et al., 2013).

5.4 Conclusion

To determine the potential for CB-δ^{15}N as a proxy for the level of surface nitrate consumption, we measured δ^{15}N of organic nitrogen incorporated into the scleractinian structure of deep sea corals from the SPNA. 43 coral samples with Libby ages from 0 to 2000 years located along a transect through the SPG on the Reykjanes Ridge were measured. The CB-δ^{15}N was compared to Rayleigh model predicted δ^{15}N export calculated from modern sea surface [NO_3^-] (WOA13). The measured CB-δ^{15}N appears consistent with the δ^{15}N of N export predicted by isotope kinetics but show a mostly constant offset from the δ^{15}N of N export of 6-8‰, which is comparable to the offset observed at previous studies (Wang et al., 2014). We surmise that changes in the SPG position reflecting NAO variability should be recorded in changes in CB-δ^{15}N.

Our data suggests potential for the use of CB-δ^{15}N as a proxy of SPG position in the North Atlantic and the state of NAO. We distinguished a period with probably positive NAO around 500 yr BP. During that time the SPG most probably had a more eastern position and a more zonal shape due to an intensified gyre flow (Fig. 5.2B) consistent with emerging evidence based on other proxies (Trouet et al., 2009). This would explain a decline in CB-δ^{15}N at the southern most point of the transect. However, the existing data represent simply a preliminary effort, and much more work is needed. The interpretation of the CB-δ^{15}N data is limited by the lack of suitable temporal resolution.

Funding Acknowledgment

We acknowledge the partial support for this research by NSF under award number MGG-1234664 to M. Prokopenko.

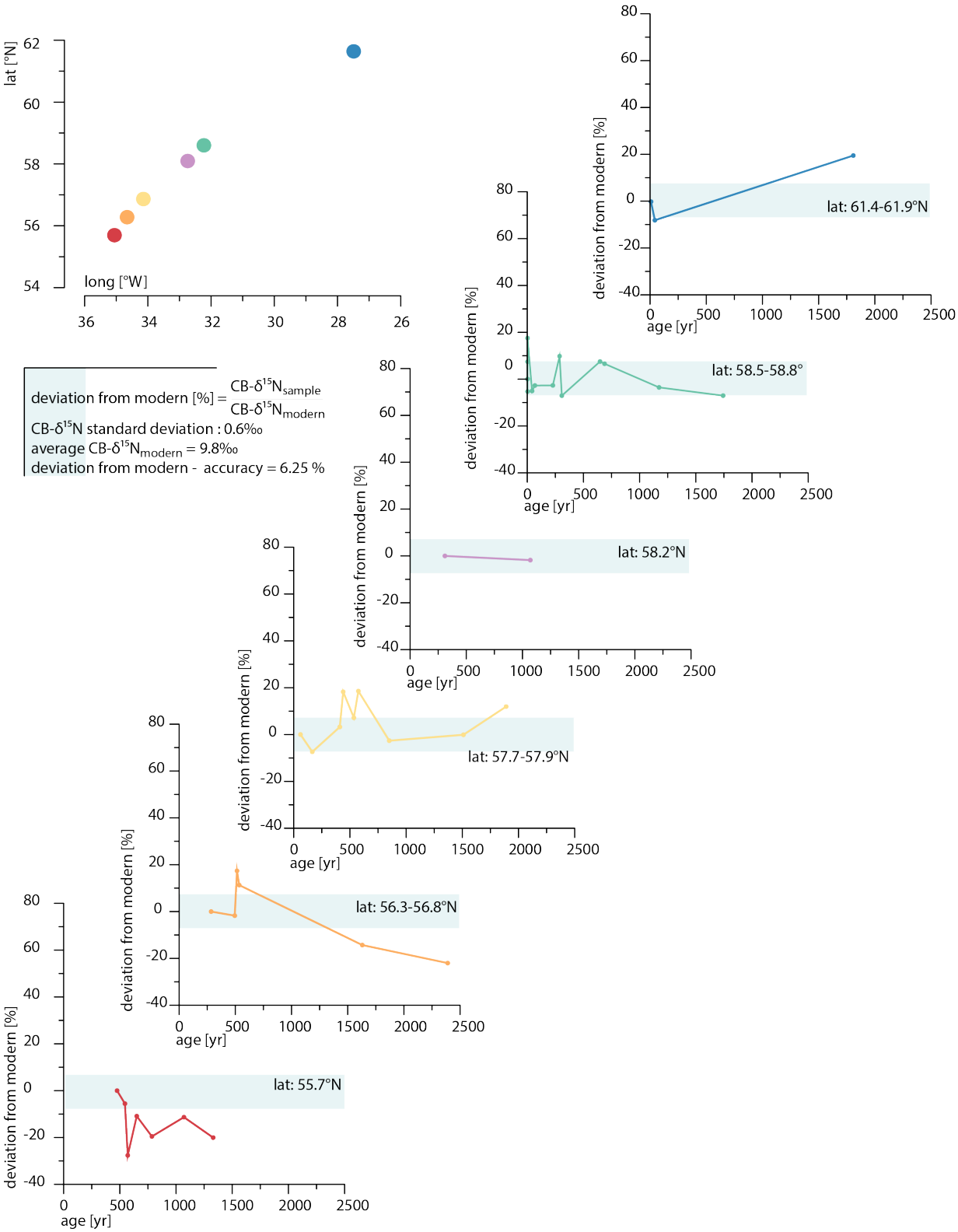

Figure 5.4 – ***Holocene evolution of North Atlantic CB-$\delta^{15}N$*** *- CB-$\delta^{15}N$ deviation from modern [%] on different latitudes. Represented by different colors, from warmer for the southern to colder for the northern latitudes.*

6
Conclusions and Outlook

Lukas E. Oesch[1]

[1]Geological Institute, Department of Earth Sciences, ETH Zürich, Zürich, Switzerland

6.1 Chapter summaries

6.1.1 Late Pleistocene nitrate-δ^{15}N changes in the equatorial Atlantic (Chapter 3)

We measured foraminifera-bound δ^{15}N (FB-δ^{15}N) on the two foraminifera species *Globigerinoides sacculifer* (*Gsacc*) and *Neogloboquadrina dutertrei* (*Ndut*) from sediments from the Ocean Drilling Program (ODP) Site 662 in the Eastern Equatorial Atlantic (EEA) back to the penultimate glacial maximum (160 kyr BP). We found a fairly stable background FB-δ^{15}N of 7-7.3‰ interrupted by three short termed (5-8 kyr) maxima at each of the terminations and one close to the Marine Isotope Stage (MIS) 5b/5a transition (82 kyr BP). We interpret the three prominent maxima observed in FB-δ^{15}N to reflect changes in δ^{15}N of preformed nitrate within Subantarctic Mode Water (SAMW) originating the Southern Ocean (SO).

SO nutrient consumption during the last 160 kyr features a clear pattern of high level of nitrate consumption during glacials and low level of nitrate consumption during interglacials (Martínez-Garcia et al., 2014; Sigman et al., 2004, 2010; Studer et al., 2015). We present a mechanism how those changes in SO nitrate consumption lead to short termed excursions of low latitude thermocline nitrate δ^{15}N. During the northwards flow of intermediate waters, sparse mixing with deep water (low δ^{15}N nitrate and high nitrate concentration) is continuously diluting the δ^{15}N signal of the SO. This mixing is more effective the lower the nitrate concentration in SAMW leaving the SO. According to Rayleigh dynamics, water with the lowest nitrate concentration features the highest δ^{15}N of nitrate. During times of intermediate levels of nutrient consumption in the SO, the residual nitrate concentration is adequately high such that the elevated δ^{15}N signal reaches the low latitudes.

6.1.2 Incomplete Nitrate consumption in the Equatorial Atlantic (Chapter 4)

We reconstructed δ^{15}N of thermocline nitrate in the EEA around the Plio-Pleistocene transition (2.9 Million years Before Present (Myr BP) and 2.4 Myr BP) by the means of FB-δ^{15}N of two species of planktonic foraminifera *Gsacc* and *Ndut* in the sediment of Site 662.

We observe an onset of 41 kyr cycles in FB-δ^{15}N at 2.65 Myr BP with low FB-δ^{15}N during highly productive glacials, which we interpret as periods of incomplete nitrate consumption in the EEA. Although the eolian input to the EEA was higher during the more productive glacials, productivity was most likely limited by iron. From the incomplete nitrate consumption during times with peaking productivity, we can conclude on nitrate supply to the surface EEA during those periods being greatly enhanced. This periodically high nutrient supply is most easily explained by the conceptual model of a contracting Atlantic warm pool proposed by Lawrence et al. (2013). In the Pliocene an increased density gradient between SAMW and the Atlantic surface water as well as an extended Atlantic warm pool lead to a deeper nutricline at the Atlantic equator compared to modern. Global cooling during the Pliocene caused increasing meridional temperature gradients and an equatorward shift of the locus of Ekman divergence in the high latitudes. The resulting contraction of the Atlantic warm pool shoaled the nutricline at the equator (Brierley et al., 2009).

The FB-δ^{15}N maxima during the interglacials are likely to reflect the undisturbed nitrate δ^{15}N in the EEA. The low level of nutrient consumption in the SO during early Pleistocene (Martínez-Garcia et al., 2011) can explain the observed difference of 1-1.5‰ in δ^{15}N of the nitrate supplied to ODP662 during the last glacial cycle compared to early Pliocene. Unlike the situation in the late Pleistocene, during early Pleistocene the productivity in the Subantarctic Zone (SAZ) was weak, which lead to SAMW with higher nutrient content than today being upwelled at the equator.

6.1.3 Coral-bound nitrogen isotopes as an archive for Holocene North Atlantic Nutrient utilization(Chapter 5)

We analyzed coral-bound δ^{15}N on deep sea corals from the subpolar North Atlantic for its potential as a proxy for the δ^{15}N export production and thus the position of the Subpolar Gyre over time. We predict the δ^{15}N export by the means of Rayleigh dynamics and compare to measured CB-δ^{15}N. We found good coherence, with higher CB-δ^{15}N in regions with more complete nitrate consumption and vice versa. An absolute offset between CB-δ^{15}N and δ^{15}N export of 6-8‰ was observed, which matches the reported offset of previous studies. Our data suggests potential for the use of coral-bound δ^{15}N (CB-δ^{15}N) as a proxy of Subpolar Gyre (SPG) position in the North Atlantic and the state of North Atlantic Oscillation (NAO). We distinguished a period with probably positive NAO around 500 yr BP. During that time the SPG most probably had a more eastern position and a more zonal shape due to an intensified gyre flow (Fig. 5.2B) consistent with emerging evidence based on other proxies (Trouet et al., 2009). This would explain a decline in CB-δ^{15}N at the southern most point of the transect. However, the existing data represent simply a preliminary effort, and much more work is needed. The interpretation of the CB-δ^{15}N data is limited by the lack of suitable temporal resolution.

6.2 Discussion and Outlook

6.2.1 Inferences from varying N content of foraminifera

In Chapter 2, I showed that the N content ($\mu molN/g_{calcite}$) of foraminifera varies among species, depth, and age. It ranges from 3 to 5µmol/g. The two measured species *Gsacc* and *Ndut* show a different temporal pattern of their N content during the Pleistocene. We measured a slight increase in the N content of the symbiotic surface dwelling species *Gsacc* from the early to the late Pleistocene and a strong decrease in N content of the subsurface dwelling non-symbiotic species *Ndut* during the same time frame. Straub (2012) observed a strong increase in N content of surface dwelling symbiotic species *G.ruber* throughout the Pleistocene and a generally higher N content of *Gsacc* in the Caribbean compared to our data from the tropical Atlantic. The mechanisms determining the N content of foraminifera or the factors controlling its variation are unknown. However, the observed significant changes ($\approx 20\%$) in N content throughout the Pleistocene require an explanation. King and Hare (1972) measured the amino acids in plaktonic foraminifera tests. They showed that the specific amino acids incorporated into the walls are characteristic for each species and can be used as taxonomic indicator. They hypothesize further that the concentration of organic matter in the calcite shell is a dissolution artifact rather than a signal of the living organism. Since we do not observe any dissolution effect on the tests (Straub, 2012) or in the isotopic signal of organic N within the tests (Chapter 3 & 4), this seems implausible.

The N content is measured as amount of nitrogen per gram of calcite. An increasing N content could thus be caused either by the foraminifera incorporating more N into the walls of their tests or the buildup of less calcite (e.g. thinner walls).

The mechanisms that could lead to incorporation of more N into the wall are unknown. A connection of the N content to the concentration of bio-available N in the surrounding water seems plausible. However, regarding the measured N content and FB-δ^{15}N from the early Pleistocene at Site 662 (Chapter 4), a simple correlation between N content of the shell and N concentration in the water can be ruled out. The N content of the planktonic foraminifera does not trace the observed peaks in nutrient concentration and incomplete nitrate consumption observed (Fig. 6.1).

The other possible cause for varying N content is an attenuated calcite production of the foraminifera. In the early Pleistocene atmospheric CO_2 was about 100-150ppm higher compared to preindustrial (Martínez-Botí et al., 2015). This lead to an enrichment of dissolved inorganic carbon in seawater and thus a lower pH. Even with a slight pH change, it would be more difficult for organisms to build up calcite walls. It thus seams reasonable that the foraminifera from this time would have thinner walls. Assuming that the nitrogen incorporation would not be affected by pH changes, the N content of the foraminifera test would increase with decreasing seawater pH. The observed N content of *Ndut* during the Plio-Pleistocene transition (Fig. 6.1) shows a sharp decrease between 2.75 Myr BP and 2.65 Myr BP. However, the N content of *Gsacc* shows no such decline. To explain the different observations within the different species *Gsacc* and *Ndut*, we have to take into account that we picked *Gsacc* from the coarse (>350µm) and medium (125µm - 350µm) size fraction, whereas *Ndut* was mostly selected from the coarse fraction. The slight change in the N:calcite ratio could thus be an artifact of measuring different size fractions and thus stages of life cycle of the foraminifera. To test this hypothesis, further research is needed. The N content of preferably single foraminifera of well defined size fractions during different time spans and at various latitudes have to be analyzed and interpreted and could be complemented by culture studies. If this hypothesis withstands further investigations, variations in N content could be a potential proxy for pH or even for atmospheric CO_2.

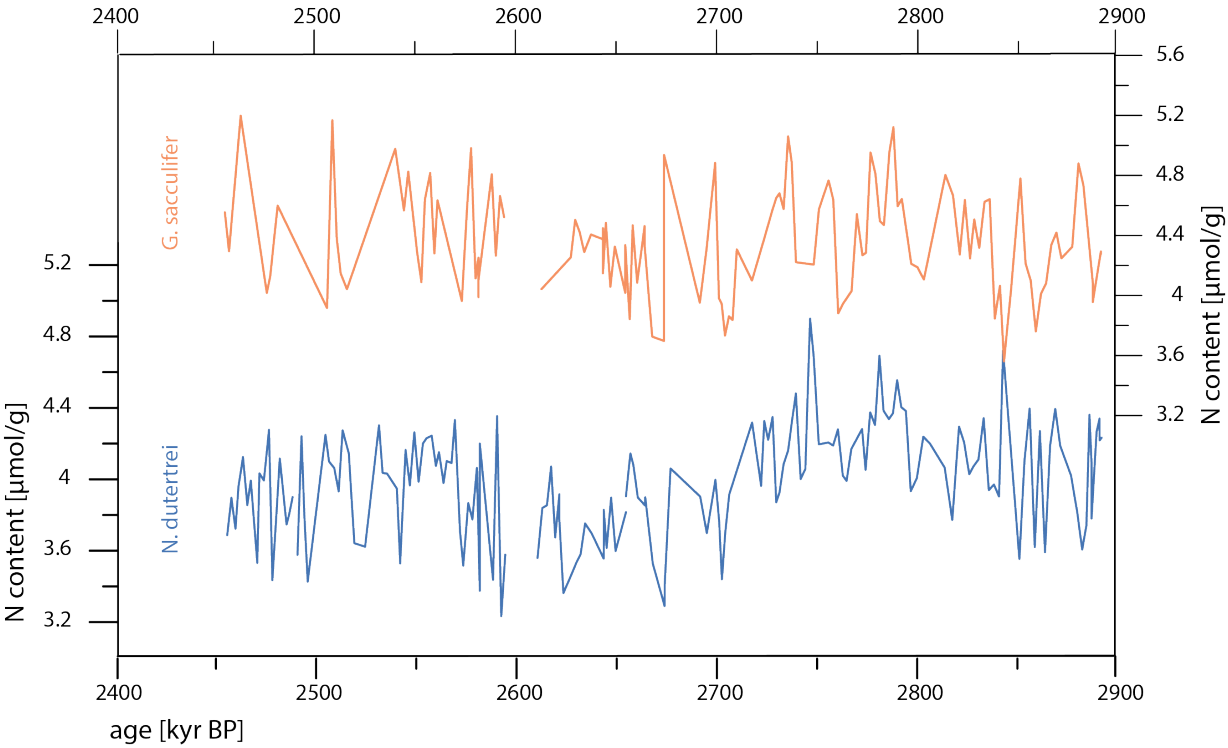

Figure 6.1 – ***N content of planktonic foraminifera Ndut and Gsacc during the late Plio- early Pleistocene***

6.2.2 Implications for the Southern Ocean influence on the low latitude Atlantic

Our data show that nitrogen cycling in the EEA is linked to SO nitrogen consumption. The FB-δ^{15}N from Site 662 during the last 160 kyr (Chapter 3) implies that nitrate consumption was complete in the EEA during this time. In this situation, the δ^{15}N of thermocline nitrate appears to be controlled by SO nutrient consumption only. The proposed mechanism of elevated nitrate δ^{15}N during times with intermediate levels of nitrate consumption in the SO fits the observations. It is very likely that the same mechanism not only applies for the EEA. Since SAMW spreads on nearly the entire intermediate depths (Sarmiento et al., 2004; Robinson et al., 2007), it fuels the nutrient supply to most of the oceans low- to midlatitude upwelling systems. With regard to the known changes in SO nutrient consumption and productivity (Martínez-Garcia et al., 2011; Lawrence et al., 2013; Martínez-Garcia et al., 2014; Studer et al., 2015) during the Pleistocene, possible teleconnections to equatorial upwelling systems in the Eastern Equatorial Pacific (EEP) and coastal upwelling systems on South America and Africa emerge.

Our data could be used for assessing nitrate dynamics in those regions as well. Disentangling the different fractionation processes contributing to FB-δ^{15}N in the EEP and coastal upwelling system is difficult due to the various δ^{15}N fractionation processes in those regions and the unknown δ^{15}N of the source nitrate. Extensive denitrification zones, partial nitrate consumption and changing source nitrate δ^{15}N nitrate are all influencing the measured FB-δ^{15}N. However, it is possible that the δ^{15}N of preformed nitrate is similar within Atlantic SAMW and Pacific SAMW and could thus eliminate one of the uncertainty factors. Nevertheless, the final assessment of partial nitrate consumption and denitrification by the means of FB-δ^{15}N in the tropical Pacific will still be difficult.

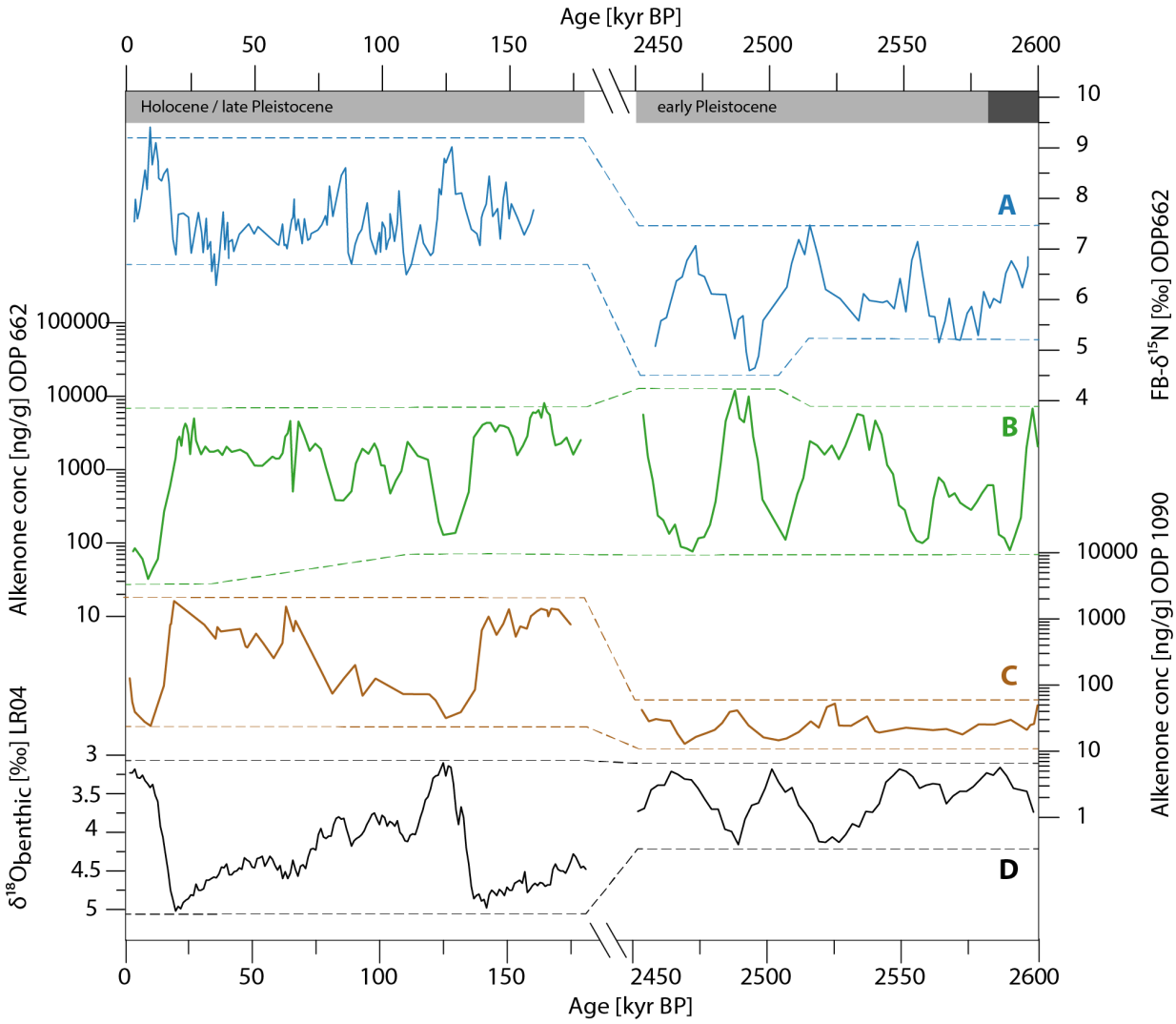

Figure 6.2 – ***Atlantic nutrient dynamics during the Pleistocene - A:*** *FB-$\delta^{15}N$ from EEA Site 662 (Chapter 3 & 4)* ***- B:*** *Alkenone MAR from EEA Site 662 (Lawrence et al., 2013)* ***- C:*** *Alkenone MAR from Southern Ocean Site 1090 (Lawrence et al., 2013)* ***- D:*** *Benthic $\delta^{18}O$ stack (Lisiecki and Raymo, 2005).*

6.2.3 Equatorial Atlantic nutrient dynamics during the entire Pleistocene

The obtained FB-δ^{15}N data from Site 662 from the early- compared to the late Pleistocene (Chapter 4 and 3) feature significant differences. As discussed in Chapter 4, FB-δ^{15}N of the early Pleistocene is interpreted as cycles of incomplete nitrate consumption in the tropical Atlantic paced by the 41 kyr cycle of Earth's obliquity, whereas the maxima in FB-δ^{15}N from late Pleistocene/Holocene are interpreted to result from both, complete nitrate consumption in the EEA and intermediate nitrate consumption in the SO. This implies that the nutrient dynamics in the EEA between 2.4 Myr BP and 160 kyr BP underwent substantial changes. Besides the observed differences in nitrate consumption the origin of the water upwelled at the equator during the interglacials changed as well. For our record in the early Pleistocene, we interpreted only the glacial, high nutrient bearing water to originate in the SO whereas the water upwelled during interglacials is supposed to originate from the Atlantic warm pool. On the other hand, within our record from the late Pleistocene/Holocene, FB-δ^{15}N is interpreted to reflect the δ^{15}N of preformed nitrate in SAMW during glacials and interglacials. This is consistent with the model of a progressive contract-

ing Atlantic warm pool by Lawrence et al. (2013): With an ongoing equatorward shift of the southern hemisphere westerlies, the zone of Ekman divergence and subduction of SAMW shifts into warmer regions. The decreasing density of SAMW and the reduced volume of the Atlantic warm pool lead to a shoaling of the equatorial nutricline. At 2.65 Myr BP a threshold was overcome and SAMW reached the equatorial surface during glacials. This resulted in the high productivity pulses with incomplete nitrate consumption observed. Due to the warming during the interglacials, the nutricline deepened again and SAMW was prevented from reaching the surface. The ongoing long term cooling throughout the Pleistocene (Herbert et al., 2010) lead to a situation in the late Pleistocene where the interglacial warming did not suffice to deepen the nutricline adequately to inhibit SAMW outcropping at the surface.

However the precise sequence of those changes between the early and the late Pleistocene are unknown. Elaborating the history of nutrient dynamics in the Atlantic would be of great interest to clarify the nature of these transitions. Further research could address questions about the precise timing of the individual changes, whether they were simultaneous and whether it was a gradual change or a sudden transition. The enhanced SO productivity upon 1.3 Myr BP (Martínez-Garcia et al., 2009; Lawrence et al., 2013) most likely caused a decline in nutrient concentration in SAMW. The lower nutrient concentration together with the observed higher terrestrial flux into the EEA during the late Pleistocene(de Menocal et al., 1993) serves as an explanation for the complete nitrate consumption at Site 662 during the last 160 kyr BP. A possible period where this change may have occured would be the Early- to Mid-Pleistocene transition (1200 - 700 kyr BP) when the global glacial cycles changed period from 41 kyr to 100 kyr (Lisiecki and Raymo, 2005). A FB-δ^{15}N record from the EEA during the time when SO productivity suddenly peaked (1.3 Myr BP) could help to characterize the temporal coherence. In a low latitude productivity regime that is predominantly controlled by the nutrient concentration within SAMW, we would expect the cycles of incomplete nitrate consumption to stop simultaneously with the emergence of high productivity in the SO.

6.2.4 Assessment of permanent El Niño like conditions during the Pliocene

The Pacific climate during the Pliocene was quite different than today. It has been observed that the Sea Surface Temperatures (SST) gradient between the eastern and the western Pacific as well as between the tropical and the mid latitude Pacific was weaker during the Pliocene (Fedorov et al., 2006; Dekens et al., 2007) similar to the observed patterns in the Atlantic (Herbert et al., 2010). This resulted in a climate similar to modern day El-Niño conditions, the so called permanent El-Niño like state (Molnar and Cane, 2002). Contemporary with the contraction of the tropical warm pool in the Atlantic, the temperature gradients within the Pacific strengthened (Herbert et al., 2010). Pliocene general circulation climate models with atmosphere-ocean coupling show an increased Hadley cell circulation with increasing SST gradients in the Pleistocene compared to Pliocene (Brierley et al., 2009).

The El Niño Southern Oscillation (ENSO) has an impact on regional to large scale climate patterns around the Pacific, directly influencing the precipitation patterns of regions with roughly half the world's population. Since the Pliocene is often considered as the closest analog to what Earth is facing in the near future (Robinson et al., 2008; Fedorov et al., 2013; Brigham-Grette et al., 2013), the development of this large scale climate system in the past and its reaction to the contemporary climate change associated with increasing atmospheric CO_2 concentration (Ciais et al., 2013) is highly important.

The mechanisms leading to a switch from a proposed permanent El Niño like state during the high CO_2-Pliocene, to the Holocene ENSO climate are unclear (Watanabe et al., 2011). Fedorov et al. (2006) observed that the SST difference between western- and eastern Pacific was very small prior to $\approx$1.8 Myr BP and increased thereafter.

Productivity data by Lawrence et al. (2013) from the EEP show a similar pattern of sudden rising productivity around the Plio-Pleistocene transition (2.9 - 2.5 Myr BP) as observed in the tropical Atlantic

(Chapter 4). Pliocene climate models show weak meridional temperature gradients (Brierley et al., 2009) to result in weak equatorial upwelling and an expanded tropical warm pool, which in turn lead to low surface nutrient concentration and low productivity. With the contracting tropical warm pool, the nutricline shoaled similar to the one observed in the Atlantic (Lawrence et al., 2013), which granted substantial nutrient supply to the euphotic zone. A record of thermocline nitrate δ^{15}N from the western tropical pacific should allow for conclusions on the upwelled nutrients and the thermocline depth. I expect FB-δ^{15}N of the EEP to reflect complete nitrate consumption prior to the upwelling of nutrient rich water. In contrast to the tropical Atlantic, the productivity in the western tropical Pacific decreases again suddenly at around 1.8 Myr BP. It is unlikely that the nutricline deepend again. The concept of a progressively contracting tropical warm pool (Lawrence et al., 2013) and the observed low SST (Fedorov et al., 2013) suggest the upwelling of nutrient rich deep water to continue and possibly even to increase. The significant decrease in productivity could be explained by a crash in the level of nutrient consumption or by changing water supply to the EEP upwelling.

Modern day EEP productivity is limited by a lack of iron (Pennington et al., 2006). The high productivity suggests that this was not the case during early Pleistocene (2.7 - 1.8 Myr BP). Sufficient iron supply to the EEP surface would result in an overall enhanced productivity as observed. Accordingly, the observed decrease in productivity (Lawrence et al., 2013) at around 1.8 Myr BP could be explained by a decreased iron supply and therefore a decreased level of nutrient consumption. This could explain how productivity decreased while equatorial upwelling could have increased in order to overcome the permanent El Niño like state.

Alternatively, the reduced productivity after 1.8 Myr BP could be a result of reduced nutrient supply to the euphotic zone of the EEP. A reconstruction of the nutrient dynamics in the EEP in the course of the Pleistocene could resolve whether the nitrate consumption was complete from 2.7 - 1.8 Myr BP. We could disentangle the different processes and may reconstruct how the climate system could switch from a permanent El Niño like state to a modern day ENSO.

A
Appendix

FB-δ^{15}N Data from ODP662 during late Pleistocene/Holocene (Chapter3)
FB-δ^{15}N Data from ODP662 during Plio-Pleistocene transition (Chapter4)
CB-δ^{15}N Data from deep sea corals North Atlantic (Chapter5)

A.1 Data: FB-δ^{15}N from ODP 662

Label Sample description

depth Composite depth [mCD] according to Ruddiman et al. (1988)

age Age of the sample [kyr BP] according to Herbert et al. (2010)

FB-δ^{15}N Average of replicated FB-δ^{15}N corrected for the contribution of δ^{15}_{Blank} for the two species *N.Dutertrei* and *G. Sacculifer*

stdev standard deviation between replicated measurements

FB-δ^{15}N$_{TC}$ Thermocline-FB-δ^{15}N, combined FB-δ^{15}N from *Ndut* and *Gsacc*

A.1.1 Late Pleistocene (Chapter 3)

Label	depth[mcd]	age[ka]	FB-δ^{15}N$_{Ndut}$	stdev$_{Ndut}$	FB-δ^{15}N$_{Gsacc}$	stdev$_{Gsacc}$	FB-δ^{15}N$_{TC}$
662/A1H1 11	0.11	0.79			7.54	0.19	7.54
662/A1H1 17	0.17	1.22	8.5	0.23	8.46	0.04	7.98
662/A1H1 28	0.28	2	8.76	0	7.43		7.6
662/A1H1 31	0.31	2.9	9.33	0.41	7.26		7.8
662/A1H1 38	0.38	5	9.88	0.66	8.24	0	8.56
662/A1H1 42	0.42	5.8	9.33	0.12	8.02	0.07	8.18
662/A1H1 48	0.48	7	9.98	0.52	9.84	0.06	9.41
662/A1H1 52	0.52	7.8	9.73	0.16	8.6	0.07	8.66
662/A1H1 59	0.59	9.23	9.81	0.34	9.39	0.35	9.1
662/A1H1 63	0.63	10.13	10.35	0.33	8.1		8.73
662/A1H1 64	0.64	10.35	9.14	0.07	8.65	0.17	8.4
662/A1H1 69	0.69	11.48	9.45	0.24	8.24	0.11	8.35
662/A1H1 73	0.73	12.38	10.14	0.4	7.82	0.14	8.48
662/A1H1 79	0.79	13.73	9.57	0.27	8.59	0.15	8.59
662/A1H1 82	0.82	14.4	9.16	0.37	8.45	0.17	8.31
662/A1H1 89	0.89	15.98	8.15	0.07	7.22	0.12	7.19
662/A1H1 94	0.94	17.1	7.88				6.88
662/A1H1 99	0.99	18.08	8.81	0.22	7.55	0.09	7.68
662/A1H1 124	1.24	19.98	8.71		7.7		7.71
662/A1H2 1	1.51	22.04	8.62				7.63
662/A1H2 15	1.65	23.11	7.91				6.92
662/A1H2 52	2.02	25.92	9		7.44		7.72
662/A1H2 59	2.09	27.2	8.01		7.64		7.33
662/A1H2 62	2.12	27.8	7.92	0.2			6.93
662/A1H2 69	2.19	29	8.3	0.31	7.91	0.1	7.61
662/A1H2 72	2.22	29.5	8.06	0.4	6.92		6.99
662/A1H2 79	2.29	30.67			7.15		7.15
662/A1H2 82	2.32	31.16	7.55	0.28			6.56
662/A1H2 88	2.38	32.17	7.73	0.12	7.07	0.15	6.9
662/A1H2 92	2.42	32.83	7.28	0.08			6.28
662/A1H2 99	2.49	34	7.78	0.03			6.78
662/A1H2 109	2.59	35.67	8.93	0.08	7.53		7.73
662/A1H2 113	2.63	36.33	7.98				6.99
662/A1H2 119	2.69	37.33	8.78	0.11	7.26	0.25	7.53
662/A1H2 122	2.72	37.83	7.81	0.22			6.81
662/B1H2 47	2.72	37.83	8.13	0.13			7.14
662/A1H2 129	2.79	39.2			7.19		7.19
662/A1H2 132	2.82	39.8	7.95	0.2			6.95
662/A1H2 139	2.89	42	8.21		7.37	0.21	7.29
662/A1H2 142	2.92	43	8.3	0.38	7.39		7.35
662/B1H2 76	3	45.67	9.26		6.73		7.49
662/B1H2 82	3.07	47.8	9.13	0.4	6.46		7.3
662/B1H2 87	3.12	49.3			7.44		7.44
662/A2H1 18	3.38	56.93	8.02	0.09	7.16	0.25	7.09
662/A2H1 22	3.42	57.46	8.19		6.96		7.08

Label	depth[mcd]	age[ka]	FB-$\delta^{15}N_{Ndut}$	stdev$_{Ndut}$	FB-$\delta^{15}N_{Gsacc}$	stdev$_{Gsacc}$	FB-$\delta^{15}N_{TC}$
662/A2H1 33	3.53	58.94	8.88	0.21	7.1		7.49
662/A2H1 38	3.58	59.6	8.05		7.09		7.07
662/A2H1 43	3.63	60.2	8.11	0.15	7.07		7.09
662/A2H1 48	3.68	60.7	8	0.17			7
662/A2H1 66	3.86	62.5	8.48	0.2	7.67	0.13	7.58
662/A2H1 71	3.91	63	9.01		7.23		7.62
662/A2H1 76	3.96	63.5	9.15	0.6	7.82		7.99
662/A2H1 77	3.97	63.6	8.59	0.16	7.78	0.04	7.69
662/A2H1 82	4.02	64.22	8.29		7.45	0.03	7.37
662/A2H1 86	4.06	65.1	8.48	0.24	7.7	0.26	7.59
662/A2H1 89	4.09	65.76	8.37				7.38
662/A2H1 93	4.13	66.64	8.1				7.11
662/A2H1 97	4.17	67.52	8.59				7.6
662/A2H1 100	4.2	68.18	8.2		7.54		7.38
662/A2H1 103	4.23	68.84	8.17				7.17
662/A2H1 107	4.27	69.72	8.23	0.29	7.17		7.21
662/A2H1 109	4.29	70.16			7.3		7.3
662/A2H1 121	4.41	72.8	8.37				7.37
662/A2H1 128	4.48	74.34	8.47				7.48
662/A2H1 135	4.55	75.8	8.45	0.06	7.86		7.66
662/A2H1 138	4.58	76.4	8.47				7.47
662/A2H1 142	4.62	77.33	9.29	0.05	8.2	0.23	8.25
662/A2H1 146	4.66	78.67	8.77	0.14	7.51		7.64
662/A2H2 6	4.76	82	9.58	0.22	8.32	0.41	8.46
662/A2H2 11	4.81	83.67	9.74	0.18	8.47	0.2	8.61
662/A2H2 14	4.84	84.67	7.92	0.15			6.92
662/A2H2 18	4.88	86	7.95	0.37	6.44		6.7
662/A2H2 22	4.92	87.43	8.09	0.11			7.09
662/A2H2 25	4.95	88.71	8.51		7.05		7.28
662/A2H2 28	4.98	90	8.38	0.05			7.39
662/A2H2 33	5.03	92.15	8.91	0.07			7.91
662/A2H2 36	5.06	93.43	8.34		7.08		7.21
662/A2H2 41	5.11	95.57	8.24	0.1	6.54		6.89
662/A2H2 44	5.14	96.28	8.1		7.17		7.14
662/A2H2 49	5.19	96.96	8.32	0.11			7.33
662/A2H2 52	5.22	97.38	8.04		6.83	0.08	6.94
662/A2H2 57	5.27	98.07	8.73	0.03	7.32	0.33	7.53
662/A2H2 65	5.35	99.17	9.06	0.14	6.74		7.41
662/A2H2 68	5.38	99.59	7.91	0	7.07	0.07	6.99
662/A2H2 73	5.43	100.44	8.27	0.04	7.05	0.22	7.16
662/A2H2 76	5.46	101.1	8.26		7.19		7.23
662/A2H2 76	5.46	101.1	8.29	0.11	8.1	0.24	7.7
662/A2H2 81	5.51	102.2	8.42	0.11	7.35	0.4	7.39
662/A2H2 84	5.54	102.86	8.18	0.16	7.12	0.1	7.15
662/A2H2 89	5.59	103.95	8.55	0.13	7.45		7.5
662/A2H2 92	5.62	104.61	9.15	0.27			8.15
662/A2H2 97	5.67	105.71	8.53	0.3	7.21		7.38
662/A2H2 100	5.7	106.37	8.08	0.36	6.76		6.92
662/A2H2 105	5.75	107.47	7.11		6.87		6.49
662/A2H2 113	5.83	109.44	7.84		6.54		6.69
662/A2H2 116	5.86	110.78	7.84		7.13		6.99
662/A2H2 121	5.91	113	8.47	0.14			7.48
662/A2H2 124	5.94	114.2	8.38		6.85		7.12
662/A2H2 131	6.01	117	7.87				6.87
662/A2H2 136	6.06	118	8.22	0.24	6.63		6.93
662/A2H2 139	6.09	118.6	8.2	0.39	7.14	0.2	7.17
662/A2H2 144	6.14	119.6	8.59	0.13			7.59
662/A2H2 148	6.18	120.4	9.31	0.18	8.07		8.19
662/A2H3 2	6.22	121.2	9.41	0.14	7.73	0.21	8.07
662/A2H3 8	6.28	122.4	9.86	0.29	8.71	0.06	8.79
662/A2H3 11	6.31	123	9.94	0.47	8.46	0.09	8.7
662/A2H3 16	6.36	125.38	9.93		9.11	0.23	9.02
662/A2H3 19	6.39	126.81	8.9	0.21	8.26	0.15	8.08

Label	depth[mcd]	age[ka]	FB-$\delta^{15}N_{Ndut}$	stdev$_{Ndut}$	FB-$\delta^{15}N_{Gsacc}$	stdev$_{Gsacc}$	FB-$\delta^{15}N_{TC}$
662/A2H3 24	6.44	129.19			8.11	0.4	8.11
662/A2H3 27	6.47	130.62	8.66		7.94		7.8
662/A2H3 32	6.52	133	8.44	0.18	7.33		7.39
662/A2H3 42	6.62	135.2	8.14		7.46		7.3
662/A2H3 48	6.68	136.4	7.68		7.45		7.07
662/A2H3 51	6.71	137			7.62		7.62
662/A2H3 55	6.75	137.57	8.41		8.04		7.72
662/A2H3 64	6.84	138.86	8.24		8.54		7.89
662/A2H3 72	6.92	140			8.44		8.44
662/A2H3 80	7	141.4	8.65	0.13	7.63	0.41	7.64
662/A2H3 91	7.11	143.31	8.79	0.37			7.8
662/A2H3 97	7.17	144.35	8.19				7.2
662/A2H3 104	7.24	145.56	8.79		8.21		8
662/A2H3 110	7.3	146.61	9.32				8.32
662/A2H3 117	7.37	147.82	8.59	0.15			7.6
662/A2H3 122	7.42	148.69	8.89				7.89
662/A2H3 136	7.56	151.13	8.71	0.55	7.52		7.61
662/A2H4 1	7.71	153.74	8.76	0.28	6.78		7.28
662/A2H4 14	7.84	156	8.7	0.25	7.33		7.52
662/A2H4 27	7.97	157.43	9.14		7.4		7.77

A.1.2 Plio-Pleistocene (Chapter 4)

Label	depth[mcd]	age[ka]	FB-$\delta^{15}N_{Ndut}$	stdev$_{Ndut}$	FB-$\delta^{15}N_{Gsacc}$	stdev$_{Gsacc}$	FB-$\delta^{15}N_{TC}$
662/A17-2 54	148.71	2455.6	5.9	0.29	5.08		5.07
662/A17-2 65	148.82	2457.7	6.58		5.41	0.02	5.58
662/A17-2 75	148.92	2459.77	6.72	0.24	5.4		5.64
662/A17-2 82	148.99	2461.29	6.94	0.07	5.78	0.12	5.94
662/A17-2 92	149.09	2463.47	7.32	0.21	6.25	0.22	6.37
662/A17-2 102	149.19	2465.64	7.3	0.12	6.43	0.01	6.45
662/A17-2 110	149.27	2467.39	7.58	0.12	6.8	0.2	6.77
662/A17-2 125	149.42	2470.65	7.84	0.01	7.13	0.09	7.07
662/A17-2 130	149.47	2471.74	7.19	0.07	6.65	0.04	6.5
662/A17-2 140	149.57	2473.92	7.28	0.13	6.46	0.02	6.45
662/A17-3 2	149.69	2476.51	7.09	0.25	5.96	0.45	6.11
662/A17-3 10	149.77	2478.2	6.92	0	6.13	0.31	6.11
662/A17-3 29	149.96	2481.88	7.03	0.19	6	0.35	6.1
662/A17-3 48	150.15	2485.21	6.05				5.22
662/A17-3 56	150.23	2486.57	6.44				5.6
662/A17-3 66	150.33	2488.28	6.51				5.68
662/A17-3 73	150.4	2489.48	5.8				4.97
662/A17-3 80	150.47	2490.68	5.43				4.59
662/A17-3 92	150.59	2492.72	5.48				4.65
662/A17-3 100	150.67	2494.08	5.72				4.88
662/A17-3 110	150.77	2495.77	6.42				5.59
662/A17-4 2	151.19	2504.64	7.27	0.1	6.06	0.02	6.25
662/A17-4 10	151.27	2506.39	7.71	0.17	6.55		6.71
662/A17-4 22	151.39	2509.05	8.14	0.02	7.06	0.04	7.19
662/A17-4 32	151.49	2511.27	7.98		6.63	0.18	6.89
662/A17-4 40	151.57	2513.18	7.77	0.34	8		7.47
662/A17-4 52	151.69	2516.33	7.53	0.19	6.98		6.84
662/A17-4 62	151.79	2519.07	7.13	0.2	6.1		6.2
662/A17-4 82	151.99	2524.45	6.85				6.02
662/A17-4 112	152.29	2531.4	6.41				5.58
662/A17-4 120	152.37	2533.18	6.95				6.12
662/A17-4 130	152.47	2535.41	6.74		6.05		5.98
662/A17-5 2.5	152.7	2540.31	6.31		6.4		5.94
662/A17-5 10	152.77	2541.97	6.81	0.04			5.97
662/A17-5 22	152.89	2544.6	6.88	0.14	5.59		5.82
662/A17-5 32	152.99	2546.78	7.02	0.06	6.64		6.42
662/A17-5 42	153.09	2548.97	6.59	0.04			5.76
662/A17-5 52	153.19	2551.15	7.55	0.1	6.83	0.17	6.78
662/A17-5 62	153.29	2553.33	7.69	0.03	7.44		7.15
662/A17-5 70	153.37	2555.08	7.5	0.05	6.38	0.32	6.52
662/A17-5 82	153.49	2557.7	6.59	0.37	5.59	0.22	5.67
662/A17-5 92	153.59	2559.75	6.33		5.82	0.36	5.66
662/A17-5 100	153.67	2561.29			5.15		5.15
662/A17-5 112	153.79	2563.57	6.41	0.18			5.58
662/A17-5 120	153.87	2565.14	6.86	0.21			6.02
662/A17-5 132	153.99	2567.57	6.05	0.3			5.21
662/A17-5 140	154.07	2569.22	6.03				5.2
662/A17-6 2	154.19	2571.79	6.56	0.09			5.73
662/A17-6 10	154.27	2573.44	6.03	0.17	6.53		5.86
662/A17-6 22	154.39	2575.9	6.12	0.13			5.29
662/A17-6 32	154.49	2577.96	7	0.12	6.15		6.16
662/A17-6 43	154.6	2580.23	6.73	0.22	5.77		5.84
662/A17-6 50	154.67	2581.67	6.64	0.1	6.23		6.02
662/A17-6 62	154.79	2584.14	6.77	0.28			5.93
662/A17-6 72	154.89	2586.2	7.35	0.3			6.52
662/A17-6 82	154.99	2588.26	7.36	0.33	7.01	0.17	6.77
662/A17-6 92	155.09	2590.31	7.01		6.97	0.22	6.57
662/A17-6 102	155.19	2592.37	7.47	0.36	5.83	0.37	6.23
662/A17-6 112	155.29	2594.43	7.62		6.53	0.14	6.66
662/B9-2 103	155.39	2594.43	7.51	0.02	7.01	0.34	6.85
662/B9-3 3	155.98	2610.48	6.43				5.6
662/B9-3 13	156.08	2612.91	6.41		5.82	0.26	5.7
662/B9-3 23	156.18	2615.19	5.97	0.61			5.14

Label	depth[mcd]	age[ka]	FB-$\delta^{15}N_{Ndut}$	stdev$_{Ndut}$	FB-$\delta^{15}N_{Gsacc}$	stdev$_{Gsacc}$	FB-$\delta^{15}N_{TC}$
662/B9-3 33	156.28	2617.28	6.14	0.02			5.31
662/B9-3 43	156.38	2619.32	6.26	0.14			5.43
662/B9-3 53	156.48	2621.36	6.77				5.94
662/B9-3 63	156.58	2623.4	6.66	0.14			5.83
662/B9-3 73	156.68	2625.44	8.04		7.48		7.34
662/B9-3 83	156.78	2627.55	7.52		6.98	0.03	6.83
662/B9-3 93	156.88	2629.75	7.18	0.01	7.15		6.75
662/B9-3 103	156.98	2631.97	6.91	0.09	7.15	0.02	6.61
662/B9-3 113	157.08	2634.2	6.66	0.13	6.83	0.01	6.33
662/B9-3 123	157.17	2637.61	6.87	0.13	5.87	0.22	5.95
662/B9-3 133	157.2	2641.31	7.26	0.33	6.91	0.24	6.67
662/A18-1 42	157.27	2643.53	6.91	0.18	5.72	0.12	5.9
662/B9-3 143	157.3	2645.01	6.95	0.1	6.01	0.23	6.06
662/A18-1 52	157.37	2647.23	8.02		6.5		6.85
662/B9-4 3	157.4	2649.46	8.19		7.83	0.09	7.59
662/A18-1 62	157.48	2650.94	7.85	0.08	7.27	0.37	7.14
662/B9-4 13	157.5	2653.16	6.95		7.36	0.26	6.74
662/A18-1 72	157.58	2654.64	7.64	0.11	7.41	0.17	7.11
662/B9-4 23	157.6	2656.86	7.32	0.16	6.76		6.63
662/A18-1 82	157.68	2658.34	7.15	0.22	6.65	0.13	6.49
662/B9-4 33	157.7	2660.56	7.27	0.14	6.58	0.01	6.51
662/A18-1 92	157.78	2662.04	7.29	0.26	6.51	0.02	6.48
662/B9-4 43	157.88	2664.26	7.05		6.35	0.13	6.28
662/B9-4 53	157.89	2667.97	7.32		7.11		6.8
662/A18-1 111	157.98	2669.08	6.92	0.17	6	0.04	6.04
662/B9-4 63	158.02	2671.67	6.78	0.21			5.95
662/A18-1 124	158.08	2673.89			6.61		6.61
662/A18-1 132	158.1	2676.85	6.24		5.79		5.6
662/A18-2 2.5	158.31	2684.25					
662/A18-2 22.5	158.51	2691.65	7.15	0.14	5.78	0.02	6.05
662/A18-2 31.5	158.6	2694.99	7.74	0.14	6.86		6.88
662/A18-2 43	158.71	2699.25	7.29	0.29	6.85		6.65
662/A18-2 54	158.82	2701.14	6.97	0.26	5.7	0.01	5.92
662/A18-2 62	158.9	2702.5	6.46		5.25	0.04	5.44
662/A18-2 71.5	159	2704.22	7.34		5.71		6.11
662/A18-2 81.5	159.1	2706.14	7.78		5.8		6.38
662/A18-2 91	159.19	2707.98			6.31		6.31
662/A18-2 101.5	159.3	2710.02			5.89		5.89
662/A18-2 141	159.69	2717.58	6.52	0.41	5.92		5.81
662/A18-3 14	159.92	2722.04	5.82	0.1			4.99
662/A18-3 22	160	2723.6	6.31	0.35	5.52		5.5
662/A18-3 32	160.1	2725.59	6.42	0.07	5.41		5.5
662/A18-3 43	160.21	2727.82	6.89	0.16	5.65		5.85
662/A18-3 52	160.3	2729.64	6.87		5.67		5.85
662/A18-3 60	160.38	2731.26	7.91	0.11	6.86	0.07	6.97
662/A18-3 70	160.48	2733.29	7.5		7.16		6.91
662/A18-3 81	160.59	2735.52	7.66		7	0.06	6.91
662/A18-3 90	160.68	2737.36	7.31	0	6.54	0	6.51
662/A18-3 100	160.78	2739.45	7.25	0.14	6.18		6.3
662/A18-3 111	160.89	2741.78					
662/A18-3 122	161	2744.13	7.14				6.31
662/A18-3 133	161.11	2746.47					
662/A18-3 141	161.19	2748.27			5.95		5.95
662/A18-4 2	161.3	2750.87			6.49		6.49
662/A18-4 12	161.4	2753.26	7.28				6.45
662/A18-4 22	161.5	2755.64	7.11	0.05	6.09		6.18
662/A18-4 32	161.6	2758.03	7.12		5.92	0.08	6.1
662/A18-4 42	161.7	2760.43	7.37	0.07	5.77		6.15
662/A18-4 52	161.8	2762.82	6.95	0	5.85		5.98
662/A18-4 60	161.88	2764.73	6.91	0			6.08
662/A18-4 70	161.98	2767.11	7.3		5.97		6.22
662/A18-4 81	162.09	2769.7	7.41				6.58
662/A18-4 93	162.21	2772.44	7.4		6.34	0.13	6.45

Label	depth[mcd]	age[ka]	FB-$\delta^{15}N_{Ndut}$	stdev$_{Ndut}$	FB-$\delta^{15}N_{Gsacc}$	stdev$_{Gsacc}$	FB-$\delta^{15}N_{TC}$
662/A18-4 101	162.29	2774.23	7.63		7.22		7.01
662/A18-4 111	162.39	2776.46	7.34	0.22	6.37	0.01	6.44
662/A18-4 122	162.5	2778.92	7.23				6.4
662/A18-4 132	162.6	2781.14			5.91	0.03	5.91
662/A18-4 141	162.69	2783.14	7.04	0.01	5.46	0.07	5.83
662/A18-5 4	162.82	2785.87	6.43	0.3	5.98	0.09	5.79
662/A18-5 14	162.92	2787.89	7.22	0.16	6.03	0.13	6.21
662/A18-5 24	163.02	2789.93	7.73		7.26	0.32	7.08
662/A18-5 34	163.12	2792.04	7.37	0.36	6.63	0.12	6.59
662/A18-5 44	163.22	2794.3	6.11	0.02	6.21		5.74
662/A18-5 54	163.32	2796.75	6.63	0.04	6.09	0.03	5.95
662/A18-5 64	163.42	2799.75	7.05	0.01	6.35	0.02	6.28
662/A18-5 74	163.52	2802.99			5.86		5.86
662/A18-5 84	163.62	2806.32	6.49				5.66
662/A18-5 104	163.82	2813.67	6.73	0.25	5.41	0.18	5.65
662/A18-5 114	163.92	2817.48	6.93		5.69		5.89
662/A18-5 124	164.02	2820.84	6.8	0	5.9		5.94
662/A18-5 134	164.12	2823.4	6.47	0.03	6.07	0.17	5.85
662/A18-5 144	164.22	2825.95	6.66		6.22		6.02
662/A18-6 2	164.3	2827.99	7.17	0.2	6.5	0.09	6.42
662/A18-6 12	164.4	2830.55	7.46		6.41	0.07	6.52
662/A18-6 22	164.5	2833.1	7.76		7.02	0.1	6.97
662/A18-6 32	164.6	2835.66	8.05		6.95	0.25	7.08
662/A18-6 42	164.7	2838.22	7.28	0.11			6.45
662/A18-6 52	164.8	2840.77	7.13	0.2	6.48	0.27	6.39
662/A18-6 60	164.88	2842.82	6.83	0.25	6.34		6.17
662/A18-6 74	165.02	2846.39			5.95		5.95
662/A18-6 92	165.2	2850.98	7.11	0.24	5.17		5.72
662/A18-6 102	165.3	2853.53	6.82	0.22	5.51		5.74
662/A18-6 112	165.4	2856.08	7.55		6.35	0.08	6.54
662/A18-6 122	165.5	2858.63	7.25	0.02	5.95	0.14	6.18
662/A18-6 132	165.6	2861.18	7.19		6.01	0.11	6.18
662/A18-6 142	165.7	2863.73	7.19		6.6		6.48
662/A18-7 2	165.8	2866.28	7.46	0.35	6.84	0.17	6.73
662/A18-7 12	165.9	2868.83			6.38	0.22	6.38
662/A18-7 22	166	2871.38	7.32		6.19		6.34
662/B10-4 12	166.33	2876.73	7.37				6.53
662/B10-4 24	166.43	2879.79	6.93	0.15	5.42	0.13	5.76
662/B10-4 34	166.53	2882.34	7.22	0.36	5.35		5.87
662/B10-4 42	166.63	2884.38	6.84		5.49		5.75
662/A19-1 2	166.73	2885.91	6.98	0.1			6.15
662/B10-4 52	166.83	2886.93	7.24	0.22	6.06		6.23
662/B10-4 62	166.93	2889.48	7.56		6.64		6.68
662/A19-1 22	167.03	2891.01	7.43	0.06	6.86	0.16	6.73
662/B10-4 72	167.13	2892.03	6.54		5.67	0.41	5.69
662/B10-4 82	167.42	2894.58	7.41		6.5		6.54
662/B10-4 92	167.62	2897.13	6.86	0.14	6.6		6.31

A.2 Data: Deep sea corals - North Atlantic

Sample ID Sample description, all samples from cruise 806

Age Libby age of the sample [yr BP]

CB-δ^{15}N Average of replicated CB-δ^{15}N corrected for the contribution of $\delta^{15}N_{Blank}$

Longitude/Latitude Location of the sample

Depth Collecting depth [mbsl]

A.2.1 Holocene deep-sea corals (Chapter 5)

SampleID	Age[yr BP]	CB-δ^{15}N	Longitude	Latitude	Depth [mbsl]	Type of corals
IC22-1630	1630	9.71	-34.5	56.3	1290	colonial
IC21-2390	2390	8.84	-34.5	56.3	1290	colonial
IC30-60	60	8.87	-33.2	57.7	1361	colonial
IC31-575	575	10.51	-33.2	57.7	1361	colonial
IC32-1890	1890	9.92	-33.2	57.7	1361	colonial
IC8(b)-410	410	9.15	-32.9	57.9	1680	colonial
IC11-440	440	10.48	-32.9	57.9	1680	colonial
IC14-535	535	9.5	-32.9	57.9	1680	colonial
IC7(b)-850	850	8.63	-32.9	57.9	1680	colonial
IC-9-1510	1510	8.86	-32.9	57.9	1680	colonial
IC4-mod(b)	0	8.82	-32.3	58.5	1369	colonial
IC2-40(b)	40	8.37	-32.3	58.5	1385	colonial
IC3-305	305	8.19	-32.3	58.5	1385	colonial
IC12-310	310	8.94	-32.6	58.2	1284	colonial
IC5-645	645	9.48	-32.3	58.5	1369	colonial
IC1(b)-685	685	9.39	-32.3	58.5	1369	colonial
IC13-1070	1070	8.78	-32.6	58.2	1284	colonial
IC6-1700	1740	8.19	-32.3	58.5	1369	colonial
IC40-mod	0	9.47	-32	58.8	1545	colonial
IC41-65	65	8.57	-32	58.8	1545	colonial
IC42-285	285	9.68	-32	58.8	1545	colonial
IC43-225	225	8.58	-32.2	58.9	1429	colonial
IC44-1170	1170	8.5	-32.2	58.9	1429	colonial
IC37-mod?	0	11.47	-27	61.9	768	colonial
IC36-34U	34	10.57	-27	61.9	768	colonial Madrepora
IC24-475	475	11.08	-35	55.7	2022	
IC27-545	545	10.47	-35	55.7	2022	
IC29-570	570	8.02	-35	55.7	2022	D. dianthus
IC25-650	650	9.88	-35	55.7	2022	D. dianthus
IC26-785	785	8.92	-35	55.7	2022	
IC23-1070	1070	9.83	-35	55.7	2022	D. dianthus
IC28-1330	1330	8.86	-35	55.7	2022	D. dianthus
IC17-285	285	11.34	-34.2	56.8	1464	D. dianthus
IC18-495	495	11.14	-34.2	56.8	1464	D. dianthus
IC19-535	535	12.62	-34.4	56.3	1621	D. dianthus
IC10-165	165	8.21	-32.9	57.9	1680	D. dianthus
IC15-605	605	14.46	-32.9	57.9	1680	D. dianthus
IC38-mod	0	8.35	-32	58.8	1545	D. dianthus
IC39-mod	0	10.36	-32	58.8	1545	D. dianthus
IC34-1800	1800	13.73	-27.9	61.4	994	D. dianthus
IC20-515	515	13.3	-34.5	56.3	1290	D. dianthus

References

Abe-Ouchi, A., Saito, F., Kawamura, K., Raymo, M. E., Okuno, J., Takahashi, K., and Blatter, H. (2013). Insolation-driven 100,000-year glacial cycles and hysteresis of ice-sheet volume. *Nature*, 500(7461):190–3.

Altabet, M., Murray, D., and Prell, W. (1999a). Climatically linked oscillations in Arabian Sea denitrification over the past- Implications for the marine N cycle. *Paleoceanography*, 14(6):732–743.

Altabet, M. A., Deuser, W. G., Honjo, S., and Stienen, C. (1991). Seasonal and depth-related changes in the source of sinking particles in the North Atlantic. *Nature*, 354(6349):136–139.

Altabet, M. A. and Francois, F. (1994). Sedimentary nitrogen isotopic ratio as a recorder for surface ocean ntirate utilization. *Biogeochem. Cycles.*, 8(1):103–116.

Altabet, M. A., Pilskaln, C., Thunell, R., Pride, C., Sigman, D., Chavez, F., and Francois, R. (1999b). The nitrogen isotope biogeochemistry of sinking particles from the margin of the Eastern North Pacific. *Deep Sea Research Part I: Oceanographic Research Papers*, 46(4):655–679.

Appenzeller, C., Schwander, J., Sommer, S., and Stocker, T. F. (1998). The North Atlantic Oscillation and its imprint on precipitation and ice accumulation in Greenland. *Geophysical Research Letters*, 25(11):1939.

Bartoli, G., Hönisch, B., and Zeebe, R. E. (2011). Atmospheric CO 2 decline during the Pliocene intensification of Northern Hemisphere glaciations. *Paleoceanography*, 26(4).

Berger, A. and Loutre, M. F. (1991). Insolation values for the climate of the last 10 million years. *Quaternary Science Reviews*, 10(4):297–317.

Bickert, T. and Wefer, G. (1996). Late Quaternary deep-water circulation in the South Atlantic: reconstruction from carbonate dissolution and benthic stable isotopes. *The South Atlantic: present and past circulation*, pages 599–620.

Bolton, C. T., Lawrence, K. T., Gibbs, S. J., Wilson, P. A., Cleaveland, L. C., and Herbert, T. D. (2010). Glacial-interglacial productivity changes recorded by alkenones and microfossils in late Pliocene eastern equatorial Pacific and Atlantic upwelling zones. *Earth and Planetary Science Letters*, 295(3-4):401–411.

Braman, R. and Hendrix, S. (1989). Nanogram nitrite and nitrate determination in environmental and biological materials by vanadium (III) reduction with chemiluminescence detection. *Analytical Chemistry*, 61(24):2715–2718.

Brandes, J. a., Devol, A. H., Yoshinari, T., Jayakumar, D. a., and Naqvi, S. W. a. (1998). Isotopic composition of nitrate in the central Arabian Sea and eastern tropical North Pacific: A tracer for mixing and nitrogen cycles. *Limnology and Oceanography*, 43(7):1680–1689.

Brierley, C. M., Fedorov, a. V., Liu, Z., Herbert, T. D., Lawrence, K. T., and LaRiviere, J. P. (2009). Greatly Expanded Tropical Warm Pool and Weakened Hadley Circulation in the Early Pliocene. *Science*, 323(5922):1714–1718.

Brigham-Grette, J., Melles, M., Minyuk, P., Andreev, A., Tarasov, P., DeConto, R., Koenig, S., Nowaczyk, N., Wennrich, V., Rosen, P., Haltia, E., Cook, T., Gebhardt, C., Meyer-Jacob, C., Snyder, J., and Herzschuh, U. (2013). Pliocene Warmth, Polar Amplification, and Stepped Pleistocene Cooling Recorded in NE Arctic Russia. *Science*, 340(6139):1421–1427.

Broecker, W. S. (1982). Glacial to interglacial changes in ocean chemistry. *Progress in Oceanography*, 11(2):151–197.

Broecker, W. S. (1984). Terminations. In *Milankovitch and Climate*, pages 687–698. Springer Netherlands, Dordrecht.

Burke, A. (2012). *Constraining Circulation Changes Through the Last Deglaciation with dynamic tracers: Insights from Deep-sea Coral Radiocarbon and Sedimentary Pa/Th*. PhD thesis, Massachusetts Institute of Technology.

Cairns, S. D. (2007). Deep-water corals: An overview with special reference to diversity and distribution of deep-water scleractinian corals. In *Bulletin of Marine Science*, volume 81, pages 311–322.

Cane, M. a. and Molnar, P. (2001). Closing of the Indonesian seaway as a precursor to east African aridification around 3-4 million years ago. *Nature*, 411(6834):157–162.

Capone, D. G. (1997). Trichodesmium, a Globally Significant Marine Cyanobacterium. *Science*, 276(5316):1221–1229.

Capone, D. G., Bronk, D. A., Mulholland, M. R., and Carpenter, E. (2008). *Nitrogen in Marine Environments*. Academic Press, Burlington, MA, USA, 2 edition.

Capone, D. G., Burns, J. A., Montoya, J. P., Subramaniam, A., Mahaffey, C., Gunderson, T., Michaels, A. F., and Carpenter, E. J. (2005). Nitrogen fixation by Trichodesmium spp.: An important source of new nitrogen to the tropical and subtropical North Atlantic Ocean. *Global Biogeochemical Cycles*, 19(2):1–17.

Checkley, D. M. and Miller, C. A. (1989). Nitrogen isotope fractionation by oceanic zooplankton. *Deep Sea Research Part A, Oceanographic Research Papers*, 36(10):1449–1456.

Chiang, J. C. and Friedman, A. R. (2012). Extratropical Cooling, Interhemispheric Thermal Gradients, and Tropical Climate Change. *Annual Review of Earth and Planetary Sciences*, 40(1):383–412.

Christian, J. R. and Murtugudde, R. (2003). Tropical Atlantic variability in a coupled physical-biogeochemical ocean model. *Deep-Sea Research Part II: Topical Studies in Oceanography*, 50(22-26):2947–2969.

Ciais, P., Sabine, C., Bala, G., Bopp, L., Brovkin, V., Canadell, J., Chhabra, A., DeFries, R., Galloway, J., Heimann, M., Jones, C., Quéré, C. L., Myneni, R., Piao, S., and Thornton, P. (2013). The physical science basis. Contribution of working group I to the fifth assessment report of the intergovernmental panel on climate change. *Change, IPCC Climate*, pages 465–570.

Cleaveland, L. C. and Herbert, T. D. (2007). Coherent obliquity band and heterogeneous precession band responses in early Pleistocene tropical sea surface temperatures. *Paleoceanography*, 22(2):1–13.

Curry, R. G. and McCartney, M. S. (2001). Ocean gyre circulation changes associated with the North Atlantic Oscillation. *Journal of Physical Oceanography*, 31(12):3374–3400.

Curry, W. B. and Oppo, D. W. (2005). Glacial water mass geometry and the distribution of δ 13 C of ΣCO 2 in the western Atlantic Ocean. *Paleoceanography*, 20(1).

de Boer, a. M., Toggweiler, J. R., and Sigman, D. M. (2008). Atlantic Dominance of the Meridional Overturning Circulation. *Journal of Physical Oceanography*, 38(2):435–450.

de Menocal, P., Ruddiman, W. F., and Pokras, E. (1993). Influences of high- and low- latitude process on African terrestrial climate: Pleistocene eolian recods from Equatorial Atlantic Ocean drilling Program site 663. *Paleoceanography*, 8(2):209–242.

Dekens, P. S., Ravelo, A. C., and McCarthy, M. D. (2007). Warm upwelling regions in the Pliocene warm period. *Paleoceanography*, 22(3).

Denny, M. (2008). *No How the Ocean Works: An introduction to oceanography*. Princeton University Press, Princeton NJ.

Deplazes, G., Lückge, A., Peterson, L. C., Timmermann, A., Hamann, Y., Hughen, K. A., Röhl, U., Laj, C., Cane, M. A., Sigman, D. M., and Haug, G. H. (2013). Links between tropical rainfall and North Atlantic climate during the last glacial period. *Nature Geoscience*, 6(3):213–217.

Deutsch, C., Gruber, N., Key, R. M., Sarmiento, J. L., and Ganachaud, A. (2001). Denitrification and N2 fixation in the Pacific Ocean. *Global Biogeochemical Cycles*, 15(2):483–506.

Dorschel, B., Hebbeln, D., Foubert, A., White, M., and Wheeler, A. J. (2007). Hydrodynamics and cold-water coral facies distribution related to recent sedimentary processes at Galway Mound west of Ireland. *Marine Geology*, 244(1-4):184–195.

Dowsett, H. J., Chandler, M. A., and Robinson, M. M. (2009). Surface temperatures of the Mid-Pliocene North Atlantic Ocean: implications for future climate. *Philosophical Transactions of the Royal Society A: Mathematical, Physical and Engineering Sciences*, 367(1886):69–84.

Elmore, a. C. and Wright, J. D. (2011). North Atlantic Deep Water and climate variability during the Younger Dryas cold period. *Geology*, 39(2):107–110.

Fedorov, a. V., Brierley, C. M., Lawrence, K. T., Liu, Z., Dekens, P. S., and Ravelo, a. C. (2013). Patterns and mechanisms of early Pliocene warmth. *Nature*, 496(7443):43–9.

Fedorov, a. V., Dekens, P. S., McCarthy, M., Ravelo, a. C., DeMenocal, P. B., Barreiro, M., Pacanowski, R. C., and Philander, S. G. (2006). The Pliocene paradox (mechanisms for a permanent El Niño). *Science*, 312(5779):1485–9.

François, R., Altabet, M., Yu, E., and Sigman, D. (1997). Contribution of Southern Ocean surface-water stratification to low atmospheric CO2 concentrations during the last glacial period. *Nature*, pages 929–935.

Galbraith, E. D., Sigman, D. M., Robinson, R. S., and Pedersen, T. F. (2008). Nitrogen in Past Marine Environments. In *Nitrogen in the Marine Environment*, chapter 34, pages 1497–1535. Elsevier, Amsterdam, 2nd edition.

Ganeshram, R. S., Pedersen, T. F., Calvert, S. E., McNeill, G. W., and Fontugne, M. R. (2000). Glacial-interglacial variability in denitrification in the world's oceans: Causes and consequences. *Paleoceanography*, 15(4):361–376.

Garrison, T. (2009). *Essentials of Oceanography*. Brooks/Cole Cengage, Belmont CA USA, 5 edition.

Gastrich, M. D. (1988). Ultrastructure of a new intracellular symbiotic alga found within planktonic foraminifera. *Journal of Phycology*, 23(4):623–632.

Granger, J., Sigman, D. M., Lehmann, M. F., and Tortell, P. D. (2008). Nitrogen and oxygen isotope fractionation during dissimilatory nitrate reduction by denitrifying bacteria. *Limnology and Oceanography*, 53(6):2533–2545.

Gruber, N. (2008). The Marine Nitrogen Cycle. In *Nitrogen in the Marine Environment*, chapter 1, pages 1–50. Elsevier, Amsterdam, 2nd edition.

Gruber, N. and Galloway, J. N. (2008). An Earth-system perspective of the global nitrogen cycle. *Nature*, 451(7176):293–6.

Hain, M. P., Sigman, D. M., and Haug, G. H. (2010). Carbon dioxide effects of Antarctic stratification, North Atlantic Intermediate Water formation, and subantarctic nutrient drawdown during the last ice age: Diagnosis and synthesis in a geochemical box model. *Global Biogeochemical Cycles*, 24(4).

Hammer, Ø., Harper, D. A. T., and Ryan, P. D. (2001). Paleontological statistics software package for education and data analysis. *Palaeontologia Electronica*, 4(1):9–18.

Haug, G. H., Sigman, D. M., Tiedemann, R., Pedersen, T. F., and Sarnthein, M. (1999). Onset of permanent startification in the subarctic Pacific Ocean. *Nature*, 401(October):779–782.

Haynes, J. R. (1981). *Foraminifera*. Macmillan Publishers Ltd, London.

Hays, J. D., Imbrie, J., and Shackleton, N. J. J. . (1976). Variations in the Earth ' s Orbit : Pacemaker of the Ice Ages. *Science*, 194(4270):1121–1132.

Haywood, A. M., Valdes, P. J., and Sellwood, B. W. (2000). Global scale palaeoclimate reconstruction of the middle Pliocene climate using the UKMO GCM : initial results. *Global and Planetary Change*, 25:239–256.

Hemleben, C., Michael, S., and Roger, A. (1989). *Modern Planktonic Foraminifera*. Springer Verlag, New York.

Herbert, T. D., Peterson, L. C., Lawrence, K. T., and Liu, Z. (2010). Tropical ocean temperatures over the past 3.5 million years. *Science (New York, N.Y.)*, 328(5985):1530–1534.

Hewitt, C. and Jackson, A. (2009). *Atmospheric Science for Environmental Scientists*. John Wiley and Sons, Oxford.

Hönisch, B., Hemming, N. G., Archer, D., Siddall, M., and McManus, J. F. (2009). Atmospheric carbon dioxide concentration across the mid-Pleistocene transition. *Science (New York, N.Y.)*, 324(5934):1551–1554.

Hovland, M. (2008). *Deep-Water Coral Reefs - Unique biodiversity Hot-spots*. Praxis Publishing Ltd., Chichester UK.

Howell, P. (2001). ARAND Time Series and Spectral Analysis Package for the Macintosh, Brown University, IGBP PAGES/World Data Center Paleoclimatol. *Data Contribution*.

Hulth, S., Aller, R. C., Canfield, D. E., Dalsgaard, T., Engström, P., Gilbert, F., Sundbäck, K., and Thamdrup, B. (2005). Nitrogen removal in marine environments: recent findings and future research challenges. *Marine Chemistry*, 94(1-4):125–145.

Hurrell, J. W., Delworth, T., Danabasoglu, G., Drange, H., Griffies, S., Holbrook, N., Kirtman, B., Keenlyside, N., Latif, M., and Marotzke, J. (2010). Decadal climate prediction: Opportunities and challenges. *OceanObs' 09: Sustained Ocean Observations and Information for Society*, pages 521–533.

Imbrie, J. (1982). Astronomical theory of the Pleistocene ice ages: A brief historical review. *Icarus*, 50(2-3):408–422.

Imbrie, J., Berger, A., Boyle, E. A., Clemens, S. C., Duffy, A., Howard, W. R., Kukla, G., Kutzbach, J., Martinson, D. G., McIntyre, A., Mix, A. C., Molfino, B., Morley, J. J., Peterson, L. C., Pisias, N. G., Prell, W. L., Raymo, M. E., Shackleton, N. J., and Toggweiler, J. R. (1993). On the structure and origin of major glaciation cycles 2. The 100,000-year cycle. *Paleoceanography*, 8(6):699–735.

IOC, SCOR, and IAPSO (2010). The international thermodynamic equation of seawater - 2010: Calculation and use of thermodynamic properties. Technical report, Intergovernmental Oceanographic Commission, Manual and Guides No. 56.

Jouzel, J., Masson-Delmotte, V., Cattani, O., Dreyfus, G., Falourd, S., Hoffmann, G., Minster, B., Nouet, J., Barnola, J. M., Chappellaz, J., Fischer, H., Gallet, J. C., Johnsen, S., Leuenberger, M., Loulergue, L., Luethi, D., Oerter, H., Parrenin, F., Raisbeck, G., Raynaud, D., Schilt, a., Schwander, J., Selmo, E., Souchez, R., Spahni, R., Stauffer, B., Steffensen, J. P., Stenni, B., Stocker, T. F., Tison, J. L., Werner, M., and Wolff, E. W. (2007). Orbital and millennial Antarctic climate variability over the past 800,000 years. *Science (New York, N.Y.)*, 317(5839):793–796.

Karlin, K., Ruddiman, F., and McIntyre, A. (1989). 13. Comparison of late Pliocene and late Pleistocene sea-surface temperatures of the Equatorial Atlantic divergence. In *Proceedings of the Ocean Drilling Program*, volume 108, pages 187–210. Ocean Drilling Program.

Keigwin, L. D. (1982). Isotopic Paleoceanography of the Caribbean and East Pacific: Role of Panama Uplift in Late Neogene Time. *Science*, 217(4457):350–353.

King, K. and Hare, P. E. (1972). Amino Acid Composition of the Test as a Taxonomic Character for Living and Fossil Planktonic Foraminifera. *Micropaleontology*, 18(3):285.

Kipp, N. G. (1976). New Transfer Function for Estimating Past Sea-Surface Conditions from Sea-Bed Distribution of Planktonic Foraminiferal Assemblages in the North Atlantic. In *Investigation of Late Quaternary Paleoceanography and Paleoclimatology*, volume 145 of *Geological Society of America Memoirs*, chapter 1, pages 3–42. Geological Society of America.

Knapp, A. N., Dekaezemacker, J., Bonnet, S., Sohm, J. A., and Capone, D. G. (2012). Sensitivity of Trichodesmium erythraeum and Crocosphaera watsonii abundance and N2 fixation rates to varying NO3 - and PO4 3- concentrations in batch cultures. *Aquatic Microbial Ecology*, 66(3):223–236.

Knapp, A. N., DiFiore, P. J., Deutsch, C., Sigman, D. M., and Lipschultz, F. (2008). Nitrate isotopic composition between Bermuda and Puerto Rico: Implications for N 2 fixation in the Atlantic Ocean. *Global Biogeochemical Cycles*, 22(3).

Knox, F. and McElroy, M. (1984). Changes in atmospheric CO2: Influence of the marine biota at high latitude. *Journal of Geophysical Research*, 89:4629–4637.

Kohfeld, K. E., Harrison, S. P., Que, C. L., and Anderson, R. F. (2005). Role of Marine Biology in. *Oceans*, 308(2005):74–78.

Kürschner, W. M., Burgh, J. V. D., Visscher, H., and Dilcher, D. L. (1996). Oak leaves as biosensors of late Neogene and early Pleistocene paleoatmospheric CO2 concentrations. *Marine Micropaleontology*, 27:299–312.

Laskar, J., Robutel, P., Joutel, F., Gastineau, M., Correia, a. C. M., and Levrard, B. (2004). A long-term numerical solution for the insolation quantities of the Earth. *Astronomy and Astrophysics*, 428(1):261–285.

Lawrence, K. T., Liu, Z., and Herbert, T. D. (2006). Evolution of the Eastern Tropical Pacific Through Plio-Pleistocene Glaciation. *Science*, 312(5770):79–83.

Lawrence, K. T., Sigman, D. M., Herbert, T. D., Riihimaki, C. a., Bolton, C. T., Martínez-Garcia, A., Rosell-Mele, A., and Haug, G. H. (2013). Time-transgressive North Atlantic productivity changes upon Northern Hemisphere glaciation. *Paleoceanography*, 28(4):740–751.

Levitus, S. (1989). Interpentadal variability of temperature and salinity in the upper 150m of the North Atlantic Ocean, 1970–1974 versus 1955–1959. *J. Geophys. Res.*, 94:9679–9685.

Lisiecki, L. E. and Raymo, M. E. (2005). A Pliocene-Pleistocene stack of 57 globally distributed benthic d 18 O records. *Paleoceanography*, 20(1):n/a–n/a.

Lisiecki, L. E. and Raymo, M. E. (2007). Plio-Pleistocene climate evolution: trends and transitions in glacial cycle dynamics. *Quaternary Science Reviews*, 26(1-2):56–69.

Liu, Z., Altabet, M. a., and Herbert, T. D. (2005). Glacial-interglacial modulation of eastern tropical North Pacific denitrification over the last 1.8-Myr. *Geophysical Research Letters*, 32(23):L23607.

Locarnini, R. A., Mishonov, A. V., Antonov, J. I., Boyer, T. P., Garcia, H. E., Baranova, M. M., Zweng, M. M., Paver, C. R., Reagan, J. R., Johnson, D. R., Hamilton, M., and Seidov, D. (2013). World Ocean Atlas 2013.

Lüthi, D., Le Floch, M., Bereiter, B., Blunier, T., Barnola, J.-M., Siegenthaler, U., Raynaud, D., Jouzel, J., Fischer, H., Kawamura, K., and Stocker, T. F. (2008). High-resolution carbon dioxide concentration record 650,000-800,000 years before present. *Nature*, 453(7193):379–382.

Lynch-Stieglitz, J., Adkins, J. F., Curry, W. B., Dokken, T., Hall, I. R., Herguera, J. C., Hirschi, J. J.-M. J.-M., Ivanova, E. V., Kissel, C., Marchal, O., Marchitto, T. M., McCave, I. N., McManus, J. F., Mulitza, S., Ninnemann, U., Peeters, F., Yu, E.-F., and Zahn, R. (2007). Atlantic meridional overturning circulation during the Last Glacial Maximum. *Science*, 316(5821):66–9.

Marchitto, T. M. and Broecker, W. S. (2006). Deep water mass geometry in the glacial Atlantic Ocean: A review of constraints from the paleonutrient proxy Cd/Ca. *Geochemistry, Geophysics, Geosystems*, 7(12).

Marconi, D., Weigand, M. A., Rafter, P. A., Mcilvin, M. R., Forbes, M., Casciotti, K. L., and Sigman, D. M. (2015). Nitrate isotope distributions on the US GEOTRACES North Atlantic cross-basin section : Signals of polar nitrate sources and low latitude nitrogen cycling. *Marine Chemistry*, 177:143–156.

Marinov, I., Follows, M., Gnanadesikan, A., Sarmiento, J. L., and Slater, R. D. (2008). How does ocean biology affect atmospheric p CO 2 ? Theory and models. *Journal of Geophysical Research*, 113(C7):C07032.

Mariotti, A., Germon, J. C., Hubert, P., Kaiser, P., Letolle, R., Tardieux, A., and Tardieux, P. (1981). Experimental determination of nitrogen kinetic isotope fractionation: Some principles; illustration for the denitrification and nitrification processes. *Plant and Soil*, 62(3):413–430.

Martin, J. H. (1990). Glacial-interglacial CO 2 change: The Iron Hypothesis. *Paleoceanography*, 5(1):1–13.

Martin, J. H. and Fitzwater, S. E. (1988). Iron deficiency limits phytoplankton growth in the north-east Pacific subarctic. *Nature*, 331(6154):341–343.

Martínez-Botí, M. a., Foster, G. L., Chalk, T. B., Rohling, E. J., Sexton, P. F., Lunt, D. J., Pancost, R. D., Badger, M. P. S., and Schmidt, D. N. (2015). Plio-Pleistocene climate sensitivity evaluated using high-resolution CO2 records. *Nature*, 518(7537):49–54.

Martínez-Garcia, A., Rosell-Melé, A., Geibert, W., Gersonde, R., Masqué, P., Gaspari, V., and Barbante, C. (2009). Links between iron supply, marine productivity, sea surface temperature, and CO 2 over the last 1.1 Ma. *Paleoceanography*, 24(1).

Martínez-Garcia, A., Rosell-Melé, A., Jaccard, S. L., Geibert, W., Sigman, D. M., and Haug, G. H. (2011). Southern Ocean dust-climate coupling over the past four million years. *Nature*, 476(7360):312–315.

Martínez-Garcia, A., Sigman, D. M., Ren, H., Anderson, R. F., Straub, M., Hodell, D. a., Jaccard, S. L., Eglinton, T. I., and Haug, G. H. (2014). Iron Fertilization of the Subantarctic Ocean During the Last Ice Age. *Science*, 343(6177):1347–1350.

Mc Intyre, A. and Ruddiman, W. (1989). Surface water response of the Equatorial Atlantic ocean to orbital forcing. *Paleoceanography*, 4(1):19–55.

Meckler, a. N., Haug, G. H., Sigman, D. N., Plessen, B., Peterson, L. C., and Thierstein, H. R. (2007). Detailed sedimentary N isotope records from Cariaco Basin for terminations I and V: Local and global implications. *Global Biogeochemical Cycles*, 21(4).

Meckler, a. N., Ren, H., Sigman, D. M., Gruber, N., Plessen, B., Schubert, C. J., and Haug, G. H. (2011). Deglacial nitrogen isotope changes in the Gulf of Mexico: Evidence from bulk sedimentary and foraminifera-bound nitrogen in Orca Basin sediments. *Paleoceanography*, 26(4).

Meckler, A. N., Sigman, D. M., Gibson, K. a., François, R., Martínez-García, A., Jaccard, S. L., Röhl, U., Peterson, L. C., Tiedemann, R., and Haug, G. H. (2013). Deglacial pulses of deep-ocean silicate into the subtropical North Atlantic Ocean. *Nature*, 495(7442):495–498.

Milankovitch, M. (1920). *Théorie Mathématique des Phénomènes Thermiques produits par la Radiation Solaire*. Gauthier-Villars, Paris.

Miyake, Y. and Wada, E. (1971). The isotope effect on the nitrogen in biochemical, oxidation-reduction reactions. *Records of oceanographic works in Japan*, 11(1):1–6.

Molfino, B. and McIntyre, A. (1990). Precessional forcing of nutricline dynamics in the equatorial atlantic. *Science (New York, N.Y.)*, 249(4970):766–769.

Molnar, P. and Cane, M. (2002). El Nino's tropical climate and teleconnections as a blueprint for pre-Ice Age climates. *Paleoceanography*, 17(2).

Montoya, J. P. (2009). Old New Nitrogen. *Science (New York, N.Y.)*, 323(January):219–220.

Montoya, J. P., Carpenter, E. J., and Capone, D. G. (2002). Nitrogen fixation and nitrogen isotope abundances in zooplankton of the oligotrophic North Atlantic. *Limnol. Oceanogr.*, 47(6):1617–1628.

Nürnberg, D., Müller, A., and Schneider, R. R. (2000). Paleo-sea surface temperature calculations in the equatorial east Atlantic from Mg/Ca ratios in planktic foraminifera: A comparison to sea surface temperature estimates from U 37 , oxygen isotopes, and foraminiferal transfer function. *Paleoceanography*, 15(1):124–134.

Olsen, J., Anderson, N. J., and Knudsen, M. F. (2012). Variability of the North Atlantic Oscillation over the past 5,200 years. *Nature Geoscience*, 5(11):808–812.

Pennington, J. T., Mahoney, K. L., Kuwahara, V. S., Kolber, D. D., Calienes, R., and Chavez, F. P. (2006). Primary production in the eastern tropical Pacific: A review. *Progress in Oceanography*, 69(2-4):285–317.

Pérez, V., Fernández, E., Marañón, E., Serret, P., and García-Soto, C. (2005). Seasonal and interannual variability of chlorophyll a and primary production in the Equatorial Atlantic: In situ and remote sensing observations. *Journal of Plankton Research*, 27(2):189–197.

Peterson, R. G. and Stramma, L. (1991). Upper-level circulation in the South Atlantic Ocean. *Progress in Oceanography*, 26(1):1–73.

Petit, J. R., Raynaud, D., Basile, I., Chappellaz, J., Ritz, C., Delmotte, M., Legrand, M., Lorius, C., and Pe, L. (1999). Climate and atmospheric history of the past 420 , 000 years from the Vostok ice core. *Nature*, 399.

Philander, S. G. and Fedorov, A. V. (2003). Role of tropics in changing the response to Milankovich forcing some three million years ago. *Paleoceanography*, 18(2).

Philander, S. G. H., Gu, D., Halpern, D., Lambert, G., Lau, N. C., Li, T., and Pacanowski, R. C. (1996). Why the ITCZ is mostly north of the equator. *Journal of Climate*, 9(12):2958–2972.

Raymo, M. E. (1997). The timing of major climate terminations. *Paleoceanography*, 12(4):577–585.

Raymo, M. E., Grant, B., Horowitz, M., and Rau, G. H. (1996). Mid-Pliocene warmth : stronger greenhouse and stronger conveyor. *Marine Micropaleontology*, 27(1987):313–326.

Raymo, M. E., Ruddiman, W. F., and Froelich, P. (1988). Influence of late Cenozoic mountain building on ocean geochemical cycles. *Geology*, 16:649–653.

Redfield, A. C. (1934). *On the proportions of organic derivatives in sea water and their relation to the composition of plankton*. University Press of Liverpool, Liverpool.

Ren, H. (2010). *Development and paleoceanographic application of planktonic foraminifera-bound nitrogen isotopes*. PhD thesis, Princeton University.

Ren, H., Sigman, D. M., Meckler, a. N., Plessen, B., Robinson, R. S., Rosenthal, Y., and Haug, G. H. (2009). Foraminiferal isotope evidence of reduced nitrogen fixation in the ice age Atlantic Ocean. *Science (New York, N.Y.)*, 323(5911):244–248.

Ren, H., Sigman, D. M., Thunell, R. C., and Prokopenko, M. G. (2012). Nitrogen isotopic composition of planktonic foraminifera from the modern ocean and recent sediments. *Limnology and Oceanography*, 57(4):1011–1024.

Ren, H., Studer, A. S., Serno, S., Sigman, D. M., Winckler, G., Anderson, R. F., Oleynik, S., Gersonde, R., and Haug, G. H. (2015). Glacial-to-interglacial changes in nitrate supply and consumption in the subarctic North Pacific from microfossil-bound N isotopes at two trophic levels. *Paleoceanography*, 30(9):1217–1232.

Rhein, M., Kieke, D., Hüttl-Kabus, S., Roessler, A., Mertens, C., Meissner, R., Klein, B., Böning, C. W., and Yashayaev, I. (2011). Deep water formation, the subpolar gyre, and the meridional overturning circulation in the subpolar North Atlantic. *Deep Sea Research Part II: Topical Studies in Oceanography*, 58(17-18):1819–1832.

Rhein, M., Rintoul, S. R., Aoki, S., Campos, E., Chambers, D., Feely, R., Gulev, S., Johnson, G., Josey, S., Kostianoy, A., Mauritzen, C., Roemmich, D., Talley, L. D., and Wang, F. (2013). Observations: Ocean Pages. In Intergovernmental Panel on Climate Change, editor, *Climate Change 2013 - The Physical Science Basis*, chapter 3, pages 255–316. Cambridge University Press, Cambridge.

Rickaby, R. E. M. and Elderfield, H. (2005). Evidence from the high-latitude North Atlantic for variations in Antarctic Intermediate water flow during the last deglaciation. *Geochemistry, Geophysics, Geosystems*, 6(5).

Roberts, J., Wheeler, A. J., Freiwald, A., and Cairns, S. D. (2009). *Cold-water Corals The Biology and Geology of Deep-Sea Habitats*. Cambridge University Press, Cambridge.

Robinson, M. M., Dowsett, H. J., and Chandler, M. A. (2008). Pliocene Role in Assessing Future Climate Impacts. *Eos, Transactions American Geophysical Union*, 89(49):501–512.

Robinson, R. S., Brunelle, B. G., and Sigman, D. M. (2004). Revisiting nutrient utilization in the glacial Antarctic: Evidence from a new method for diatom-bound N isotopic analysis. *Paleoceanography*, 19(3).

Robinson, R. S., Mix, A., and Martinez, P. (2007). Southern Ocean control on the extent of denitrification in the southeast Pacific over the last 70 ka. *Quaternary Science Reviews*, 26(1-2):201–212.

Robinson, R. S. and Sigman, D. M. (2008). Nitrogen isotopic evidence for a poleward decrease in surface nitrate within the ice age Antarctic. *Quaternary Science Reviews*, 27(9-10):1076–1090.

Rogelj, J. and Knutti, R. (2016). Geosciences after Paris. *Nature Geoscience*, 9(3):187–189.

Ruddiman, W. (2008). *Earth's Climate - Past and Future*. W.H. Freeman and Company, New York.

Ruddiman, W., Sarnthein, M., and Baldauf, J. (1988). Site 662. In *Proceedings of the Ocean Drilling Program, 108 Initial Reports*. Ocean Drilling Program.

Ruddiman, W. F. and Janecek, T. R. (1989). Pliocene-Pleistocene biogenic and terrigenous fluxes at equatorial Atlantic sites 662, 663, and 664. *Proceedings of the Ocean Drilling Program, Scientific Results*, 108:211–240.

Saino, T. and Hattori, A. (1987). Geographical variation of the water column distrubution of suspended particulate organic nitrogen and its 15N natural abundance in the Pacific and its marginal seas. *Deep Sea Research Part A, Oceanographic Research Papers*, 34(5-6):807–827.

Saito, T., Thompson, P., and Breger, D. (1981). *Systematic Index of Recent and Pleistocene Planktonic Foraminifera*. University of Tokyo Press, Tokyo.

Sarmiento, J. L., Gruber, N., Brzezinski, M. A., and Dunne, J. P. (2004). High-latitude controls of thermocline nutrients and low latitude biological productivity. *Nature*, 427(6969):56–60.

Sarmiento, J. L. and Toggweiler, J. R. (1984). A new model for the role of the oceans in determining atmospheric PCO2. *Nature*, 308(5960):621–624.

Schiebel, R. and Hemleben, C. (2001). Protozoa, planktonic foraminifera. In Speel, E., Thorpe, S., and Turekian, K., editors, *Encyclopedia of Ocean Sciences*. Academic Press.

Schmittner, A. and Galbraith, E. D. (2008). Glacial greenhouse-gas fluctuations controlled by ocean circulation changes. *Nature*, 456(7220):373–376.

Schneider, T., Bischoff, T., and Haug, G. H. (2014). Migrations and dynamics of the intertropical convergence zone. *Nature*, 513(7516):45–53.

Schubert, C. J. and Calvert, S. E. (2001). Nitrogen and carbon isotopic composition of marine and terrestrial organic matter in Arctic Ocean sediments:. *Deep Sea Research Part I: Oceanographic Research Papers*, 48(3):789–810.

Schuster, U. and Watson, A. J. (2007). A variable and decreasing sink for atmospheric CO 2 in the North Atlantic. *Journal of Geophysical Research*, 112(C11):C11006.

Seki, O., Foster, G. L., Schmidt, D. N., Mackensen, A., Kawamura, K., and Pancost, R. D. (2010). Alkenone and boron-based Pliocene pCO2 records. *Earth and Planetary Science Letters*, 292(1-2):201–211.

Siegenthaler, U. and Wenk, T. (1984). Rapid atmospheric CO2 variations and ocean circulation. *Nature*, 308(5960):624–626.

Sigman, D. and Casciotti, K. (2001). Nitrogen Isotopes in the Ocean. In Steele, J., Turekian, K., and Thorpe, S., editors, *Encyclopedia of Ocean Sciences*, number 1997, pages 1884–1894. Elsevier, London.

Sigman, D. M. and Boyle, E. A. (2000). Glacial/interglacial variations in atmospheric carbon dioxide. *Nature*, 407(6806):859–869.

Sigman, D. M., Casciotti, K. L., Andreani, M., Barford, C., Galanter, M., and Böhlke, J. K. (2001). A bacterial method for the nitrogen isotopic analysis of nitrate in seawater and freshwater. *Analytical Chemistry*, 73(17):4145–4153.

Sigman, D. M., Hain, M. P., and Haug, G. H. (2010). The polar ocean and glacial cycles in atmospheric CO2 concentration. *Nature*, 466(7302):47–55.

Sigman, D. M., Jaccard, S. L., and Haug, G. H. (2004). Polar ocean strati cation in a cold climate. *Nature*, 428(March):59–63.

Sigman, D. M., M. a, A., McCorkle, D. C., Francois, R., and Fischer, G. (1999). The d15N of nitrate in the Southern Ocean: Nitrate consumption in surface waters. *Global Biogeochemical Cycles*, 13(4):1149–1166.

Steph, S., Regenberg, M., Tiedemann, R., Mulitza, S., and Nürnberg, D. (2009). Stable isotopes of planktonic foraminifera from tropical Atlantic/Caribbean core-tops: Implications for reconstructing upper ocean stratification. *Marine Micropaleontology*, 71(1-2):1–19.

Stetson, T. R., Squires, D. F., and Pratt, R. M. (1962). Coral banks occurring in deep water on the Blake Plateau. *Amer Mus Novitates*, 2114:1–39.

Straub, M. (2012). *Application of Foraminifera-bound Nitrogen Isotopes to Atlantic Paleoceanography*. PhD thesis, ETH Zürich.

Straub, M., Sigman, D. M., Ren, H., Martínez-García, A., Meckler, a. N., Hain, M. P., and Haug, G. H. (2013a). Changes in North Atlantic nitrogen fixation controlled by ocean circulation. *Nature*, 501:200–3.

Straub, M., Tremblay, M., Sigman, D., Studer, A., Ren, H., Toggweiler, J., and Haug, G. (2013b). Nutrient conditions in the subpolar North Atlantic during the last glacial period reconstructed from foraminifera-bound nitrogen isotopes. *Paleoceanography*, 28.

Studer, A. S., Sigman, D. M., Martínez-Garcia, A., Benz, V., Winckler, G., Gersonde, R., and Haug, G. H. (2015). Antarctic Zone nutrient conditions during the last two glacial cycles. *Paleoceanography*, 30:845–862.

Subramaniam, A., Mahaffey, C., Johns, W., and Mahowald, N. (2013). Equatorial upwelling enhances nitrogen fixation in the Atlantic Ocean. *Geophysical Research Letters*, 40(9):1766–1771.

Toggweiler, J. R. (1999). Variation of atmospheric CO 2 by ventilation of the ocean's deepest water. *Paleoceanography*, 14(5):571–588.

Toggweiler, J. R., Dixon, K., and Broecker, W. S. (1991). The Peru upwelling and the ventilation of the South-Pacific thermocline. *Journal of Geophysical Research-Oceans*, 96(C11):20467–20497.

Trouet, V., Esper, J., Graham, N. E., Baker, A., Scourse, J. D., and Frank, D. C. (2009). Persistent Positive North Atlantic Oscillation Mode Dominated the Medieval Climate Anomaly. *Science*, 324(5923):78–80.

Waliser, D. E. and Gautier, C. (1993). A satellite-derived climatology of the ITCZ.

Walker, G. (1928). World weather. *Quarterly Journal of the Royal Meteorological Society*, 54(226):79–87.

Wang, X. T., Prokopenko, M. G., Sigman, D. M., Adkins, J. F., Robinson, L. F., Ren, H., Oleynik, S., Williams, B., and Haug, G. H. (2014). Isotopic composition of carbonate-bound organic nitrogen in deep-sea scleractinian corals: A new window into past biogeochemical change. *Earth and Planetary Science Letters*, 400:243–250.

Wang, Z., Mysak, L. A., and McManus, J. F. (2002). Response of the thermohaline circulation to cold climates. *Paleoceanography*, 17(1):6–1–6–14.

Watanabe, T., Suzuki, A., Minobe, S., Kawashima, T., Kameo, K., Minoshima, K., Aguilar, Y. M., Wani, R., Kawahata, H., Sowa, K., Nagai, T., and Kase, T. (2011). Permanent El Niño during the Pliocene warm period not supported by coral evidence. *Nature*, 471(7337):209–11.

Weigand, M. A., Foriel, J., Barnett, B., Oleynik, S., and Sigman, D. M. (2016). Updates to instrumentation and protocols for isotopic analysis of nitrate by the denitrifier method. *Rapid Communications in Mass Spectrometry*, 30(12):1365–1383.

Winton, M. (1997). The Effect of Cold Climate upon North Atlantic Deep Water Formation in a Simple Ocean-Atmosphere Model. *Journal of Climate*, 10(1):37–51.

Wirth, S. B., Glur, L., Gilli, A., and Anselmetti, F. S. (2013). Holocene flood frequency across the Central Alps - solar forcing and evidence for variations in North Atlantic atmospheric circulation. *Quaternary Science Reviews*, 80:112–128.

Acknowledgement

I would like to thank:

My supervisors **Gerald Haug** and **Daniel Sigman** for giving me the wonderful opportunity to work on this great topic. Thanks a lot for all the advice and motivation over the years. Thanks a lot to Danny for opening up his lab for me and giving me the freedom to work in an extraordinary setting.

My external examiner **Peter de Menocal** and the additional expert, **Timothy Eglinton** for being in my committee. Thanks a lot for your time, your advises and your constructive comments. And thanks alot to Tim for the countless Gipfelis over the years.

Anja, for all the help, assistance and guidance, for the introduction to the world of foram-bound nitrogen in Princeton, for the scientific discussions and especially the countless reviews of all the chapters. Thank you very much!

Masha, for your helpful revisions, your coral insights, your constructive inputs and your advise and for sacrificing your advent celebration for the sake of my thesis.

Alexa, **Sergey** for their technical support and help in the lab and for rescuing my samples repeatedly.

Adam, **Utsav** and **Tessa** for being awesome office mates, for all the scientific and not so scientific discussions, for all the coffee- and beer-breaks, for enduring my nagging, for all the good memories, for all the Birthdays and the fake ones, and for your help and your friendship.

The ETH-guys: Anna, Fränzi, Kathrina, Ursi, Adi, Reto, Michi, Steward and **the Princetonian-Sigmoids**: Emma, Torri, Jess, Tony and Dario for being good colleagues and friends in Zürich and Princeton. You made those four years appreciable and contributed that it became a wonderful time.

My good friend **Chris** for showing me the American way of life and **Irene** for the uncomplicated and friendly hosting in Princeton.

Babette, **Andi**, **Dodo**, **Patrizia**, **Michi** and **Beni** for silently tolerating my stressed-out behavior during the last few months.

Meret and **Adi** for the helpful design advises.

My parents, for raising me with a moral compass and teaching me the endurance to act accordingly.

My sister for her unabated support and continuous help whatever I'm doing.

Joy, for your unconditional support, your caring and your understanding, for encouraging and advising me, for taking my side even if you don't know the other, for listening to my ideas and for distracting me from them, for keeping me grounded and for just being there and making me laugh every day.